LONG-TERM BIOCATALYST PERFORMANCE VIA HEURISTIC AND RIGOROUS MODELING APPROACHES

A Dissertation
Presented to
The Academic Faculty

by

Thomas A. Rogers

In Partial Fulfillment
of the Requirements for the Degree
Doctor of Philosophy in the
School of Chemical and Biomolecular Engineering

Georgia Institute of Technology
December 2010

LONG-TERM BIOCATALYST PERFORMANCE VIA HEURISTIC AND RIGOROUS MODELING APPROACHES

Approved by:

Dr. Andreas S. Bommarius, Advisor
School of Chemical and Biomolecular Engineering
Georgia Institute of Technology

Dr. Athanassios Sambanis
School of Chemical and Biomolecular Engineering
Georgia Institute of Technology

Dr. Thomas M. Orlando
School of Chemistry and Biochemistry
Georgia Institute of Technology

Dr. Amyn S. Teja
School of Chemical and Biomolecular Engineering
Georgia Institute of Technology

Dr. Roy M. Daniel
Department of Biological Sciences
University of Waikato – New Zealand

Date Approved: August 11, 2010

ACKNOWLEDGEMENTS

First and foremost, I wish to thank my family for their continued love and support through all of the trials and tribulations of my graduate school experience. I am eternally indebted to my parents, James and Christine, for instilling in me just the right balance of patience, diligence, skepticism, and individuality required to succeed as a researcher. I truly could not have reached this pinnacle in my academic life without their unconditional support, valuable wisdom, and unparalleled compassion. I can only hope my accomplishments make them as proud to be my parents as I am to be their son. I would like to thank my brother, Jon, for always being there as a trusted friend and providing me with a healthy level of competition in all things, academic and otherwise, from the day we were toddlers.

My advisor, Andy Bommarius, has been a positively indispensable resource during the course of my graduate studies. I thank him for granting me the independence to pursue different avenues in my research and for always offering sound, expert advice when I needed it most. Andy has been the model of a good mentor: offering encouragement at times when I feared I had reached a proverbial dead end, always providing me with opportunities to pursue interesting side projects, and constantly encouraging his students to maintain a healthy and balanced life with facets extending well beyond the walls of the lab. I am truly fortunate to have found an advisor whose managerial philosophy meshes well with my personal goals and my working style, and I am glad to now be a branch on his "academic family tree."

I would like to thank my thesis committee members here at Georgia Tech, Dr. Amyn Teja (for serving not only as my committee member but also as an outstanding professor in my graduate thermodynamics course), Dr. Athanassios Sambanis, and Dr. Thomas Orlando, for their advice and feedback during the course of my thesis work. I would like to give special thanks to Roy Daniel, my committee member on the other side of the world, for agreeing to host me in his lab to learn the inner workings of the Equilibrium Model. The time I spent in New Zealand was one of the high points of my graduate studies, both in terms of being exposed to cutting-edge progress in the field of enzyme stability and of visiting a beautiful country I had never before seen. I must also thank Colin Monk, the very bright and helpful technician in the Daniel lab, both for helping me sort out details of the mathematical modeling and for being a great tour guide.

I extend thanks to my fellow graduate students in the Bommarius lab. Janna Blum has proven to be an immensely helpful and skilled co-worker and a good friend since the day we arrived here together. Prabuddha Bansal, our resident math guru, has offered me good insight on mathematical modeling techniques. Yanto Yanto, Mike Abrahamson, and Andria Deaguero have been great colleagues: always willing to help out in the lab, share war stories, or go forget about research for a while. I also thank a few key past members of the lab, Javier Chaparro-Riggers for helping me tremendously with molecular biology work during the early stages, Phil Gibbs and Tracey Thaler for being the inaugural members of the lab and laying the foundations for my temperature ramp and polarimetry work, and James Broering for his guidance and patience in training me on instrumentation when I first arrived. There are many other members of the lab, past and present, and I thank them all for creating a cooperative and fun working environment.

I also want to thank all of the students whom I have had the privilege of mentoring over the past few years. Christian Albert, who visited us from Technische Universität München, was instrumental in our initial experimental efforts related to β-lactamase deactivation. Hong Chang and Emilie Warren, both undergraduates at Georgia Tech, have been helpful and hard-working contributors to our forthcoming results involving β-lactamase stability in salt solutions. It has been a pleasure working with these three gifted young students, even on the days when we realized jointly that frustration is just a necessary component of research.

Finally, I would like to thank all of my family, friends, and colleagues whom I have not named personally. While only one person receives the diploma at the end of the day, it is his network of supporters that makes it all possible; even the smallest bits of advice and encouragement can truly make all the difference.

TABLE OF CONTENTS

Page

ACKNOWLEDGEMENTS iii

LIST OF TABLES ix

LIST OF FIGURES x

LIST OF SYMBOLS xii

LIST OF ABBREVIATIONS xv

SUMMARY xvi

CHAPTER

1 INTRODUCTION 1
References 6

2 BACKGROUND 7
2.1 Classical and Recent Models of Protein Stability 7
2.2 Kinetic vs. Thermodynamic Stability of Enzymes 10
2.2.1 Measurements of Enzyme Stability 11
2.2.2 Operational Stability and the Total Turnover Number 14
2.3 TEM-1 β-Lactamase 16
2.3.1 Enzyme Characteristics 17
2.3.2 Choosing TEM-1 as a Test Case 19
2.3.3 Expression and Purification 20
2.3.4 Activity Assays 23
2.4 Enzyme Membrane Reactor 29
2.4.1 Theory of CSTR Operation 31
2.4.2 Control Measures 32
2.4.3 Reactor Timescale Considerations 34
2.5 References 38

3 DEACTIVATION OF TEM-1 BETA-LACTAMASE INVESTIGATED BY ISOTHERMAL BATCH AND NON-ISOTHERMAL CONTINUOUS ENZYME MEMBRANE REACTOR METHODS 42
3.1 Introduction 42
3.1.1 The Equilibrium Model and Isothermal Applications 42
3.1.2 The “Molten Globule” Method and Temperature Ramps 45
3.1.3 Functional Comparison of Methods/Models 48

3.2 Experimental Section 49
3.2.1 Materials 49
3.2.2 Batch-mode Experimental Setup 49
3.2.3 Continuous-mode EMR Experimental Setup 51
3.3 Results and Discussion 52
3.3.1 Batch-mode Results 52
3.3.2 Continuous-mode EMR Results 53
3.3.3 Comparison to Direct TTN Measurement 54
3.3.4 Physical Significance of Parameters 57
3.4 Conclusions 59
3.5 Publication Information 62
3.6 References 63

4 UTILIZING SIMPLE BIOCHEMICAL MEASUREMENTS TO PREDICT LIFETIME OUTPUT OF BIOCATALYSTS IN CONTINUOUS ISOTHERMAL PROCESSES 66
4.1 Introduction 66
4.1.1 Stability Considerations for Industrial Biocatalysts 67
4.1.2 Total Turnover Number as a Productivity Indicator 68
4.2 Methods 70
4.2.1 Observed Enzyme Activity in an Isothermal Process 70
4.2.2 Generalizable Model for Long-term Enzyme Deactivation 71
4.2.3 Progress of Enzyme Deactivation During an Isothermal Process 74
4.3 Results and Discussion 76
4.3.1 Total Turnover Number Expression from Stability Model 76
4.3.2 Estimation of TTN from Activity and Deactivation Data 77
4.3.3 Strengths and Limitations of the TTN Method 80
4.4 Conclusions 82
4.5 Publication Information 83
4.6 References 84

5 VALIDATION OF HEURISTIC AND ACCELERATED MODELING APPROACHES FOR ESTIMATING BIOCATALYST TOTAL TURNOVER NUMBER 87
5.1 Introduction 87
5.2 Experimental Methods 89
5.2.1 Batch-mode Experiments 89
5.2.2 EMR Temperature Ramps 91
5.2.3 Direct Isothermal Measurement 92
5.2.4 Timescale Considerations 93
5.2.5 Modeling Analysis 93
5.3 Results and Discussion 98
5.3.1 Heuristic TTN Estimation 98
5.3.2 Accelerated TTN Estimation 100
5.3.3 Comparison to Direct TTN Measurement 107
5.4 Conclusions 111

5.5 Publication Information 112
5.6 References 113

6 CONCLUSIONS AND RECOMMENDATIONS 114
References 118

APPENDIX A: RIGOROUS MATHEMATICAL DERIVATION OF THE HEURISTIC TOTAL TURNOVER NUMBER ESTIMATION METHOD 119

APPENDIX B: SAMPLE CALCULATION: MICROSOFT EXCEL CODE 123

APPENDIX C: TEMPERATURE RAMP MODELING RESULTS: FIVE MODELS, ALL RAMP RATES 126

VITA 137

LIST OF TABLES

		Page
Table 3.1:	Estimation of deactivation parameters	55
Table 4.1:	*TTN* Estimates for several representative biocatalysts	79
Table 5.1:	Relevant timescales for TEM-1 β-lactamase deactivation study in EMR	94
Table 5.2:	Expressions for differential change in reaction rate	97
Table 5.3:	*TTN* estimation from 37-57°C using the heuristic approach	99
Table 5.4:	Average percentage error of fit for five models, all ramp rates	101
Table 5.5:	Fitting parameters obtained from five models, all ramp rates	105
Table 5.6:	*TTN* prediction from 37-54°C for five models, 4 K/h ramp rate	108
Table 5.7:	*TTN* prediction from 37-54°C for all ramp rates, model 3	109
Table 5.8:	Comparison of heuristic and modeling *TTN* estimations to directly measured *TTN* values at selected temperatures	110

LIST OF FIGURES

		Page
Figure 2.1:	First-order kinetic deactivation of enzyme from residual activity plot	11
Figure 2.2:	Experimental measurement of thermodynamic stability parameters	13
Figure 2.3:	Instantaneous temperature optimum	15
Figure 2.4:	Optimum process temperature of a biocatalyst	16
Figure 2.5:	Enzymatic hydrolysis of penicillin G	17
Figure 2.6:	Crystal structure of wild-type TEM-1 β-lactamase from *E. coli* with active site details shown	18
Figure 2.7:	Protein sequence of mature TEM-1 β-lactamase from *E. coli*	18
Figure 2.8:	SDS-PAGE analysis of TEM-1 β-lactamase purification	22
Figure 2.9:	Chemical structure of CENTA β-lactamase substrate	24
Figure 2.10:	Polarimetric assay calibration curve	28
Figure 2.11:	Enzyme membrane reactor (EMR) diagram	30
Figure 2.12:	Experimental setup for EMR deactivation studies	30
Figure 2.13:	Results of BSA addition to prevent catalyst adsorption to membrane	33
Figure 2.14:	Reactor jacket temperature vs. water bath set point, 12 K/h ramp	34
Figure 2.15:	Deviation of reactor temperature from water bath set point, all ramp rates	35
Figure 3.1:	Equilibrium Model	43
Figure 3.2:	“Molten globule” model	46
Figure 3.3:	Isothermal batch-mode results	53
Figure 3.4:	Continuous temperature ramp results	54
Figure 4.1:	Lumry-Eyring model	72
Figure 4.2:	Equilibrium Model with associated constants	72

Figure 4.3: Extended Lumry-Eyring model 73

Figure 4.4: Multiple-intermediate model 73

Figure 4.5: Multiple intermediate model with direct denaturation pathways 74

Figure 5.1: Five models of deactivation applied to non-isothermal experiments 95

Figure 5.2: Comparison of slow and fast temperature ramp rates, model 3 102

Figure 5.3: Comparison of selected three- and four-state models, 4 K/h ramp 102

Figure 5.4: Relative inflexibility of model 1 in capturing two deactivation regimes 104

LIST OF SYMBOLS

A	pre-exponential of Arrhenius equation, heat transfer contact area
A_{280}	absorbance at 280 nm
C	concentration
C_p	heat capacity
ΔC_p	heat capacity difference
D	denatured enzyme state, impeller diameter
E_a	activation energy
E_{act}	active enzyme state (Equilibrium Model)
E_{inact}	reversibly inactivated enzyme state (Equilibrium Model)
E_0	initial enzyme concentration
$E(t)$	residence-time distribution function
g	gravitational force unit
ΔG_{cat}	Gibbs free energy of chemical reaction
$\Delta G_{D,n}$	Gibbs free energy of deactivation from nth intermediate state
ΔG_{inact}	Gibbs free energy of inactivation
ΔG_u	Gibbs free energy of unfolding
h	Planck's constant, heat transfer coefficient
ΔH_{eq}	enthalpy change (Equilibrium Model)
ΔH_m	enthalpy change upon unfolding
I_n	nth inactive intermediate enzyme state
K_{eq}	equilibrium constant between active and inactive states
K_M	Michaelis constant

K_{mg}	equilibrium constant between unfolded and molten globule states
K_n	equilibrium constant for nth intermediate transition
k	general kinetic rate constant, thermal conductivity
k_B	Boltzmann constant
k_{cat}	enzyme catalytic constant
$k_{cat,obs}$	observed catalytic constant
k_D	deactivation rate constant
$k_{D,obs}$	observed deactivation rate constant
$k_{D,n}$	rate constant for direct denaturation from nth intermediate
k_{inact}	rate constant of inactivation
M	molten globule enzyme state
m	temperature ramp heating rate
N	native enzyme state, impeller rotation number
OD_{600}	optical density measured at 600 nm
Q	flow rate
R	universal gas constant
R^2	coefficient of determination for linear fit
r	rate of chemical reaction
$[S]_0$	substrate concentration in feed stream
T	temperature
T_{eq}	midpoint temperature of reversible deactivation (Equilibrium Model)
T_m	melting temperature
T_{mg}	midpoint temperature of molten globule transition
$T_{m,n}$	melting temperature for nth transition
T_{opt}	instantaneous temperature optimum

TTN	total turnover number
t	time
$t_{1/2}$	half-life
t_{ss}	time required to reach steady state
Δt	length of time step
U	unfolded enzyme state, overall heat transfer coefficient
V	volume
V_{max}	maximum rate of reaction
X	denatured enzyme state (Equilibrium Model), substrate conversion
x_W	wall thickness
ε	molar extinction coefficient
$\Delta\varepsilon$	change in extinction coefficient
$[\alpha]$	specific optical rotation
θ	optical rotation
ν	volumetric flow rate
ρ	density
τ	reactor residence time
τ_{ht}	characteristic time for heat transport
τ_{rxn}	characteristic time for chemical reaction
τ_{mix}	characteristic time for mixing
τ_{flow}	characteristic time for reactor flow

LIST OF ABBREVIATIONS

AA	amino acid
AU	absorbance unit
BSA	bovine serum albumin
CD	circular dichroism
DNA	deoxyribonucleic acid
DSC	differential scanning calorimetry
EMR	enzyme membrane reactor
ID	inner diameter
MWCO	molecular weight cutoff
PTFE	polytetrafluoroethylene
SDS-PAGE	sodium dodecyl sulfate polyacrylamide gel electrophoresis
UV	ultraviolet

SUMMARY

The experiments which are required to directly assess the operational stability of thermostable biocatalysts can be time-consuming, troublesome, and, in the context of industry, expensive. In the present work, we develop and validate two methods for quickly estimating the total turnover number (a useful indicator of lifetime productivity) of a biocatalyst for any desired operating temperature. The first method is a heuristic approach, built upon a complete mathematical derivation from first principles, in which the total turnover number can be calculated from two simple biochemical measurements. The second method relies on a single non-isothermal, continuous-mode experiment in conjunction with mathematical modeling to determine the intrinsic deactivation parameters of the biocatalyst. Both methods provide estimates of the total turnover number which are well within one order of magnitude of the values measured directly via isothermal aging tests and therefore are extremely valuable tools in terms of the amount of experimental time eliminated.

CHAPTER 1

INTRODUCTION

Biocatalysts are powerful tools. A wide variety of commercially pertinent chemicals including pharmaceutical intermediates and specialty chemicals can be produced more quickly and efficiently, with fewer process steps to an extremely pure product, and with less environmental impact, when enzymes are used as catalysts. Enzymes are highly complex and specific molecules, either found in nature or borrowed as a template from nature, which typically offer better substrate specificity and enantioselectivity than almost any corresponding organic synthesis approach. Recent developments such as high throughput screening and directed evolution have made it easier to identify enzymes which have activity toward a substrate of interest, and then to fine-tune their specificity.

For all of the advantages that biocatalysts can offer, they are still only used in a relatively modest number of large-scale applications. One of the dominant limiting factors against their widespread application is concern about their operational stability.[1] Enzymes have evolved over time to function most effectively in conditions resembling physiological systems (which is part of their appeal from an environmental standpoint). However, the high concentrations of solvents, extreme pH, and elevated temperatures that are often used to improve the efficiency of a chemical process can have deleterious effects on an enzyme's ability to properly catalyze the desired reaction. Therefore, efforts toward understanding and improving enzyme stability are of utmost importance.

A review of the theory and methodology relevant to the study of biocatalyst operational stability is presented in Chapter 2. Especially important is the discussion of both the kinetic and thermodynamic stability of enzymes, since previous attempts to quantify the concept of enzyme thermostability all too often focus only on one of these two concepts. Classical models of protein stability, as well as more recent improved models, are examined in the context of bioprocess productivity and some strategies for measuring the parameters pertinent to these models are discussed. Details of the test case enzyme, TEM-1 β-lactamase, and the enzyme membrane reactor (EMR) - both of which were used in several phases of our work - are also presented.

In Chapter 3, two different approaches (in terms of experimental technique, mathematical modeling procedure, and proposed stability model) are applied to the measurement of the intrinsic stability parameters of TEM-1 β-lactamase.[2] The first approach, which uses an array of batch-mode isothermal deactivation experiments to generate a rate/temperature/time "landscape", incorporates the firmly established Equilibrium Model theory of enzyme deactivation.[3] This model, co-pioneered in 2001 by our collaborator Roy M. Daniel, has been used to successfully fit approximately 50 experimental data sets from nearly 30 tested enzymes.[4] Since the model had never been tested on TEM-1 β-lactamase, Prof. Daniel kindly hosted me in his lab at the University of Waikato in New Zealand in December 2008 so that I could learn first-hand how to apply the computational 3-D fitting procedure and to collect data in a manner consistent with his previous studies. At Georgia Tech, I used the same stock of TEM-1 β-lactamase to study the enzyme's stability via a single non-isothermal experiment designed to identify the same intrinsic stability parameters as the experiments in New Zealand. The

non-isothermal approach builds upon previous studies by our group on immobilized glucose isomerase,[5] but i.) adds improvements to the mathematical modeling which better reflect the history-dependent aspect of the data ii.) incorporates an enzyme membrane reactor (EMR) for the study of soluble (i.e. non-immobilized) biocatalysts and iii.) explores the requirement in the case of TEM-1 β-lactamase for a four-state enzyme deactivation model versus a three-state model.

A heuristic method for quickly estimating the lifetime productivity of a biocatalyst at a chosen process temperature is developed in Chapter 4. A simple expression for the total turnover number (*TTN*), a dimensionless number which is equal to the number of moles of product generated by one mole of biocatalyst during its lifetime, is rigorously derived from a theoretical framework which assumes no prior knowledge of the enzyme's specific mechanism of deactivation.[6] The *TTN* is perhaps the most useful indicator of biocatalyst performance as it can be used to compare lifetime productivity across different classes of catalytic technologies (biological, homogeneous, heterogeneous). The only data required for the application of our heuristic *TTN* estimation may either be obtained from simple biochemical measurements, or calculated from published specific activity and half-life values (provided these two are measured under the same conditions, including temperature). The utility of this method is demonstrated by comparing published data for selected enzymes with several similarly stable mutants, and predicting how their *TTN*s will differ. For the protein engineer who must quickly screen several promising enzymes and identify the most cost-effective candidate through minimal experimental labor, the heuristic approach is a valuable tool.

The non-isothermal modeling approach in an EMR is tested for five stability models, each with a different number of potential thermodynamic and/or kinetic deactivation routes, with TEM-1 β-lactamase as a test case in Chapter 5. The newly developed heuristic *TTN* estimation approach is simultaneously applied to this enzyme, and the relative strengths of the two methods are compared. Both methods proved to yield reasonable estimates of *TTN* (well within one order of magnitude) at every point within the uppermost 10°C of the enzyme's effective operating range. Comparison of the five models shows that a four-state stability model with only one kinetically-controlled denaturation pathway (from the enzyme's unfolded state) fits the experimental data better than any of the three-state models and just as well as any four-state model with extra direct denaturation pathways allowed (i.e. more parameters). We also establish guidelines which simplify the verification of proper reactor design in these non-isothermal continuous-mode deactivation studies, first by examining the physical timescales relevant to the system and then by evaluating the effects of the temperature scan rate on the modeled parameters.

We conclude in Chapter 6 by considering the overall impact of these two new techniques for *TTN* estimation, and by highlighting some of the future opportunities to improve these methods or expand their scope. In particular, we note that the modeling analysis of the continuous non-isothermal experiments could be performed with advanced techniques including nonlinear state estimation (to address the issue that reaction rate data is actually a proxy for the non-observable concentration of native enzyme in our reactor) and these results could be compared to our Euler-type numerical approximation in terms of accuracy and computational efficiency. Furthermore, both the heuristic and

modeling methods should be tested on a variety of enzymes, including ones with known two- and three-state deactivation mechanisms, to verify the accuracy of the heuristic method across deactivation schemes and to assess the power of the accelerated modeling method as a diagnostic tool for identifying the appropriate deactivation mechanism in cases where it is not known *a priori*.

The principal contribution of this work to the scientific and engineering community is that we establish and verify two methods for quickly predicting (within one order of magnitude or better) the total lifetime output of a biocatalyst. One method, which is derived from first principles and theoretically independent of the particular deactivation mechanism, requires only two simple biochemical measurements: the evaluation of the enzyme's apparent turnover number and of its observed first-order deactivation rate constant (which may already be available in the form of specific activity and half-life data). The second method uses a single, non-isothermal, continuous experiment to estimate physical parameters associated with the enzyme's activity and unfolding via mathematical modeling: parameters which can then be used to predict the total lifetime output of the enzyme at any desired temperature without any further experimentation. Both methods eliminate the need for potentially lengthy, expensive, and difficult experiments to directly measure the biocatalyst's yield, under simulated process conditions, for the entire useful life of the enzyme. Overall, this work employs the well-practiced framework in chemical engineering of developing a kinetic representation of a system, based on a physical model, and applies it to the study of enzyme deactivation in both isothermal and non-isothermal cases.

References

1. Schoemaker, H.E., Mink, D., and Wubbolts, M.G., *Dispelling the Myths - Biocatalysis in Industrial Synthesis*. Science, 2003. **299**(5613): 1694-1697.

2. Rogers, T.A., Daniel, R.M., and Bommarius, A.S., *Deactivation of TEM-1 β-Lactamase Investigated by Isothermal Batch and Non-Isothermal Continuous Enzyme Membrane Reactor Methods*. ChemCatChem, 2009. **1**(1): 131-137.

3. Daniel, R.M., Danson, M.J., and Eisenthal, R., *The temperature optima of enzymes; a new perspective on an old phenomenon*. Trends in Biochemical Sciences, 2001. **26**: 223-225.

4. Daniel, R.M. and Danson, M.J., *A new understanding of how temperature affects the catalytic activity of enzymes.* Trends in Biochemical Sciences, 2010. (in press)

5. Gibbs, P.R., Uehara, C.S., Neunert, U., and Bommarius, A.S., *Accelerated Biocatalyst Stability Testing for Process Optimization.* Biotechnology Progress, 2005. **21**(3): 762–774.

6. Rogers, T.A. and Bommarius, A.S., *Utilizing simple biochemical measurements to predict lifetime output of biocatalysts in continuous isothermal processes*. Chemical Engineering Science, 2010. **65**(6): 2118-2124.

CHAPTER 2

BACKGROUND: OPERATIONAL STABILITY, ENZYME MEMBRANE REACTORS, AND TEM-1 BETA-LACTAMASE

2.1 Classical and Recent Models of Protein Stability

The simplest view of an enzyme is that of a "lock-and-key" which will accommodate certain substrates due to its own specific shape. If the enzyme's conformation is altered significantly, to the point where the active site residues do not properly interact with the substrate molecule, the enzyme can no longer perform its function as a catalyst. The same end result will occur if the enzyme's active site residues become irreversibly bound to an inhibitory agent or if a vital cofactor molecule becomes dislodged from the enzyme. In any case, the enzyme can only be described in one of two ways: functional or permanently non-functional. In this "all-or-nothing" scheme, the enzyme is considered to maintain its native state, *N*, until it becomes denatured (*D*).

$$N \rightarrow D \qquad [2\text{-}1]$$

Many decades of observation have shown that some events, particularly protein unfolding, which would cause activity to cease may have a reversible character.[1-3] When the transition to a reversibly unfolded state, *U*, is the primary cause of deactivation, the scheme shown in Equation 2-2 applies.

$$N \rightleftharpoons U \qquad [2\text{-}2]$$

Deactivation in general, however, does not necessarily need to be fully reversible. Once an enzyme has become unfolded, it may refold to a state which is different, and possibly more thermodynamically favorable, than the native conformation. Furthermore, proteins which are held under denaturing conditions for longer periods of time have a diminished ability to recover their activity. The stability model set forth by Lumry and Eyring in 1954, shown in Equation 2-3, accounts for partial, time-dependent reversibility of unfolding.[4]

$$N \rightleftharpoons U \rightarrow D \qquad [2\text{-}3]$$

Importantly, the Lumry-Eyring model captures the notion that the stability of an enzyme depends on both thermodynamically-controlled equilibrium (unfolding) and kinetically-controlled permanent alterations of the protein's structure based on continued exposure to heat (denaturation).

Through the past two decades, additional consideration has been given to the idea that enzymes can be rendered inactive by events other than unfolding *per se*. Even before reaching the temperature at which there is a significant degree of unfolded enzyme, as evidenced by the loss of secondary structural elements such as α-helices and β-sheets, some enzymes exhibit a reversible decrease in apparent activity: a phenomenon which cannot be attributed to either of the state transitions in the Lumry-Eyring model.[14] The consequence is that enzymes can exhibit a temperature optimum which is considerably lower than the melting temperature, T_m, associated with unfolding. To this end, Daniel et al. proposed the Equilibrium Model (Equation 2-4), which recognizes that a thermodynamic equilibrium may exist between an enzyme's catalytically active state,

E_{act}, and an inactive (though not necessarily unfolded) state, E_{inact}, which can then proceed to a permanently denatured state, X.[15]

$$E_{act} \rightleftharpoons E_{inact} \rightarrow X \qquad [2\text{-}4]$$

The next logical extension of this theory is that E_{act} and E_{inact} do not necessarily each represent a single state, but possibly an ensemble of states. The literature shows that several proteins including α-chymotrypsin,[16] hen egg white lysozyme,[17] glutamate dehydrogenase,[18] β-lactamase,[19] and many others exhibit partially unfolded or "molten globule" states which maintain a native-like tertiary structure but may or may not be catalytically active.[20] These folding intermediates have been observed in experiments where either heat, pH changes, or agents such as sodium dodecyl sulfate or guanidinium hydrochloride were responsible for denaturation. Treating the molten globule state, M, as being in thermodynamic equilibrium with the native state, the corresponding stability model is represented by Equation 2-5.

$$N \rightleftharpoons M \rightleftharpoons U \rightarrow D \qquad [2\text{-}5]$$

Theoretically, there is no limit to the number of stable intermediates which have obtained different degrees of unfolding, and so the multiple intermediate model (Equation 2-6) presented by Freire et al. may be required in complex cases.[21] This model can be extended even farther by allowing permanent denaturation pathways from states other than the least-structured inactive state, I_n (to be fully discussed in Chapter 4). However, from the modeling standpoint, the scheme with the fewest intermediates which can still accurately reflect experimental observations for a particular enzyme should always be selected. The inclusion of additional states adds extraneous parameters to the model,

which is universally expected to improve the quality of fit but could potentially undermine the physical significance of the results.

$$N \rightleftharpoons I_1 \rightleftharpoons I_2 \cdots \rightleftharpoons I_{n-1} \rightleftharpoons I_n \rightarrow D$$

[2-6]

2.2 Kinetic vs. Thermodynamic Stability of Enzymes

Enzymes show an enormous potential for use in biotransformations due largely to their specificity and environmentally positive attributes. However, the limiting factor in their application continues to be their relatively low tolerance to conditions which are found in many industrial processes (i.e. high temperatures, extreme pH, certain solvents and salts). For the majority of biocatalytic processes, thermal deactivation remains the most dominant concern since there are many good reasons to operate at high temperatures when possible. These reasons include, but are not limited to, acceleration of the catalyzed reaction, reduction of bacterial contaminants, and higher solubility of key reaction components.[10] Hence, several strategies have been employed to develop stable enzymes which can withstand high temperatures for days or weeks at a time[11-13]. As noted in Section 2.1, the kinetic stability of an enzyme (ability to maintain near-constant specific activity level for long time periods in a given process) does not necessarily guarantee its thermodynamic stability (integrity of the active site which directly affects the maximum reaction rate), or vice versa, and so factors which affect both types of stability must be considered.

2.2.1 Measurements of Enzyme Stability

To assess the intrinsic parameters of deactivation for a particular enzyme, transition state theory is often used to describe both the reversible and irreversible changes to the enzyme's conformation. The kinetic deactivation can be described by an Arrhenius Rate Law, shown in Equation 2-7, in which the parameter of interest, E_a, is a representation of activation energy of the process which results in irreversible activity loss.

$$k = Ae^{-E_a / RT} \qquad [2\text{-}7]$$

The most straight-forward manner to calculate E_a experimentally is to conduct an array of isothermal deactivation experiments at several different temperatures. Provided the deactivation follows an overall first-order behavior with respect to time, the value of k (here termed k_D) can be determined at each temperature; a typical experimental result is shown in Figure 2-1.

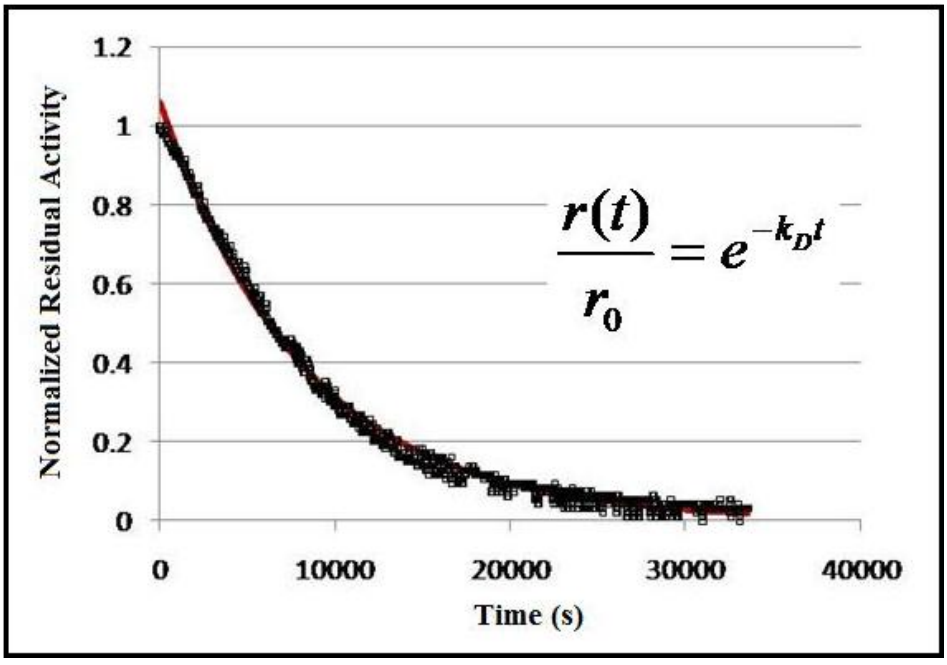

Figure 2.1 First-order kinetic deactivation of enzyme from residual activity plot.

From a sufficient number of isothermal experiments, one can construct an Arrhenius plot (ln k vs. $1/T$) which has a slope of - E_a/R, where R is the gas constant. The main limitation of this approach is that the collection of deactivation data at several low temperatures, which is necessary to construct a proper Arrhenius plot, can require experiments of very long duration. Also (and most importantly from the standpoint of our studies) the observed k_D at each different temperature in the Arrhenius plot could be affected by the degree of thermodynamic unfolding of the enzyme, and would thus need to be corrected by the associated equilibrium constants, which are not always immediately available.

There are also some established experimental techniques for estimating the thermodynamic unfolding parameters of an enzyme, most notably differential scanning calorimetry (DSC) and circular dichroism (CD) spectroscopy. The unfolding behavior of an enzyme can be described by Equation 2-8, derived from the Gibbs-Helmholtz equation.[32]

$$\Delta G_u(T) = \Delta H_m (1 - T/T_m) + \Delta C_p[T - T_m - T \ln (T/T_m)] \quad [2\text{-}8]$$

The parameters of Equation 2-8 include the enzyme's melting temperature, T_m, the enthalpy change associated with the unfolding transition, ΔH_m, and the change in heat capacity between the native and unfolded forms of the protein, ΔC_p. The values of these parameters can be measured via DSC, which operates by independently heating two sample cells (one with enzyme and one with empty buffer) such that their temperature remains identical, and measuring the difference in power input to the two cells. A typical DSC scan is shown in Figure 2.2.

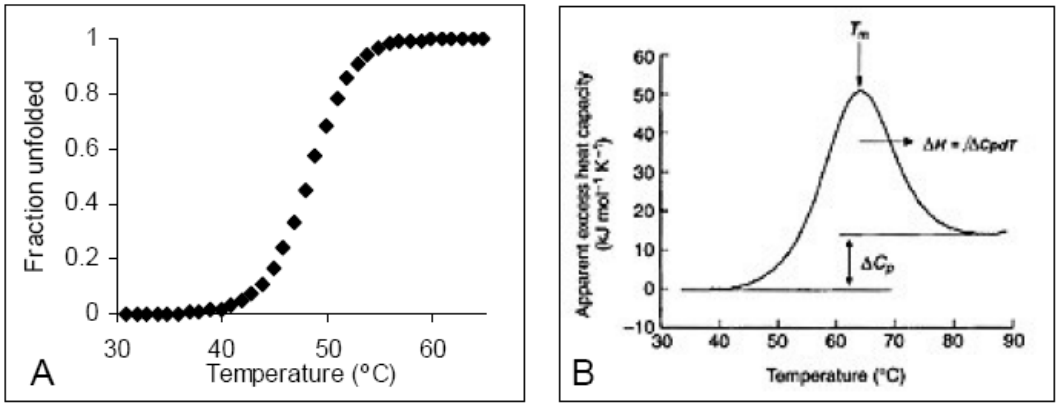

Figure 2.2 Experimental measurement of thermodynamic stability parameters. (A) Unfolding progress curve derived from CD data. (B) Use of differential scanning calorimetry to study unfolding.[36]

The melting temperature, T_m, can also be estimated through the use of CD, which detects the change in ellipticity at the specific wavelengths associated with protein secondary structures (for example, 222 nm for α-helices) as a sample is continuously heated. The ellipticity data can be used to determine the degree to which secondary structure has been lost at any point during the temperature scan, such that the fraction of enzyme which has unfolded may be plotted against temperature (Figure 2.2). The T_m is found at the midpoint of the transition, corresponding to 50% unfolded enzyme.

Both DSC and CD are useful for determining the intrinsic unfolding parameters of enzymes, but they both carry certain limitations with regards to predicting the complete operational stability of an enzyme. Both methods only give information related to the unfolding, and to reiterate, not all enzymes maintain active site integrity up to the point of unfolding. Small changes in the tertiary structure, which would be difficult or impossible to detect by either CD or DSC, can change the orientation of active site residues such that catalytic activity is lost. A direct correlation between unfolding and activity cannot be

made unless the enzyme unfolds in a highly cooperative manner. Furthermore, the observed parameter values from both DSC and CD exhibit dependence upon the temperature scan rate of experiments, as different degrees of cumulative denaturation during the course of the scan can affect the results. This once again reinforces the notion that both thermodynamic and kinetic phenomena must be considered in any proper discussion of enzyme stability.

2.2.2 Operational Stability and the Total Turnover Number

The Arrhenius Rate Law (Equation 2-7) applies not only to deactivation phenomena, but also to the dependence of the enzyme-catalyzed reaction rate on temperature. Theoretically, an increase in temperature will be accompanied by an exponential increase in the rate of the desired reaction, yet that same temperature increase will render the enzyme itself less stable. Therefore, there are two competing effects which dictate the productivity of the enzyme. In terms of process design, each biocatalyst will have an optimum temperature at which the heightened specific activity and the present degree of enzyme deactivation result in the maximum substrate turnover. The "optimum temperature", T_{opt}, typically refers to the point at which the instantaneously measured activity reaches its maximum value. Figure 2.3 illustrates the typical instantaneous temperature optimum of an enzyme, with a steady increase in activity until the enzyme reaches its melting temperature, T_m, after which the observed activity decreases sharply. This conceptualization only considers the thermodynamic stability of the enzyme.

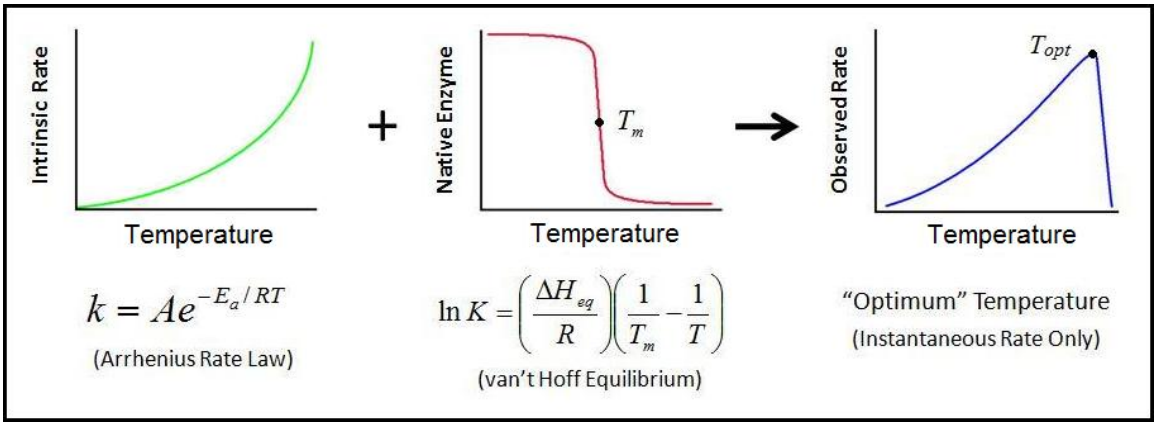

Figure 2.3 Instantaneous temperature optimum.

In a process lasting days or weeks, kinetically-controlled mechanisms of deactivation become highly important. The temperature which produces the highest specific activity will not necessarily result in the highest yield over the lifetime of the enzyme. In fact, our recent work indicates that as temperature is decreased, the total output of the enzyme will continue to increase even though the reaction rate becomes much slower. At some point, minimum rate requirements must be imposed to achieve an economical process. Therefore, when considering the conditions and the duration of a given process, the true temperature optimum (in terms of yield) will occur at a temperature lower than the instantaneous T_{opt}, as seen in Figure 2.4.

One particularly useful indicator of the lifetime productivity of a biocatalyst is the total turnover number (*TTN*) which is mentioned frequently in the following chapters. The *TTN*, by definition, is the number of catalytic events which a single molecule of biocatalyst conducts during its entire lifetime (i.e. until it is irreversibly inactivated). An alternative, macroscopic definition is that *TTN* equals the number of moles of product yielded by one mole of biocatalyst before it becomes depleted. Either definition results

in *TTN* being a dimensionless number. Experimentally, *TTN* can be defined as the area under the curve of a reaction rate vs. time plot for a given biocatalyst, divided by the initial concentration of enzyme placed into the system.

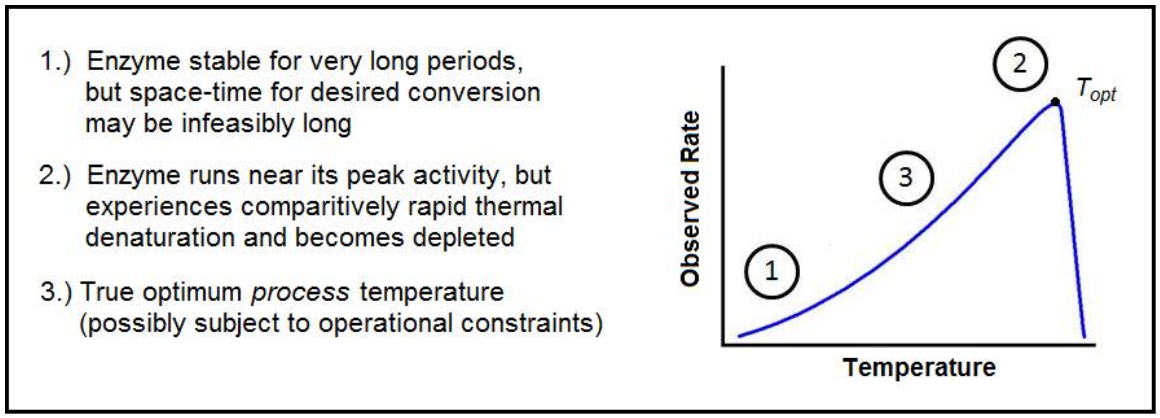

Figure 2.4 Optimum process temperature of a biocatalyst.

The use of *TTN* as a productivity indicator has two key advantages. Firstly, it is very straightforward to implement *TTN* in costing estimations as it directly scales the operating cost of enzyme consumption to the revenue from the product. Secondly, *TTN* can be used to compare lifetime productivity across different classes of catalytic technologies (biological, homogeneous, heterogeneous).

2.3 TEM-1 β-Lactamase

The enzyme chosen as a test case for the present study was the TEM-1 form of the well-studied enzyme, β-lactamase. The β-lactamases are well-known for their role in bacterial resistance to β-lactam antibiotics and their clinical importance has led to thorough study of their structure and mechanisms over nearly 75 years.[5] Though there are presently no large-scale industrial bioprocess applications for this enzyme, it was selected for our deactivation studies due to a variety of reasons to be discussed in this section.

2.3.1 Characteristics

The β-lactamases are a family of enzymes which, as their name implies, demonstrate activity toward hydrolysis of the β-lactam bond found in the core structure of penicillin-based antibiotics. The reaction scheme involving a well-known antibiotic molecule, penicillin G (benzylpenicillin) is shown in Figure 2.5.

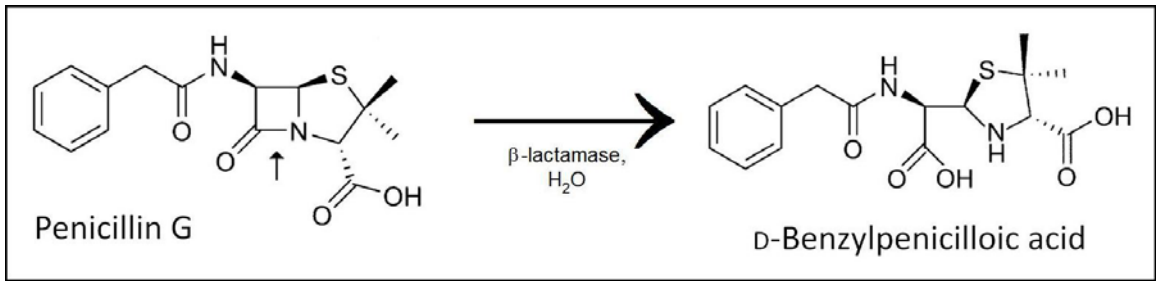

Figure 2.5 Enzymatic hydrolysis of penicillin G. β-lactam bond indicated by small arrow on substrate.

Three of the four classes of β-lactamases (A, C, and D) are serine proteases, while Class B metallo-β-lactamases (which are few in number) require a Zn^{++} cofactor. TEM-1 β-lactamase (E.C. 3.5.2.6) is a Class A β-lactamase with a sequence length of 286 AA and a molecular mass of 31,515 Da. It is the most common plasmid-mediated β-lactamase found in gram-negative bacteria; its designation as a Class A β-lactamase means that it shows activity toward penicillin and is inhibited by clavulanic acid.[22,23] The catalytic pathway of TEM-1 involves acylation of the active serine (Ser-70) followed by the hydrolysis of the resulting ester bond and proton transfer to the carboxylate group of Glu-166 either directly or via a water molecule.[24] The crystal structure of TEM-1 β-lactamase at 1.55Å resolution[25] (PDB: 1ZG4) along with a detailed view of the active

site[26] is shown in Figure 2.6 and the protein sequence (UniProt Knowledge Base, accession number P62593) of TEM-1 is shown in Figure 2.7.

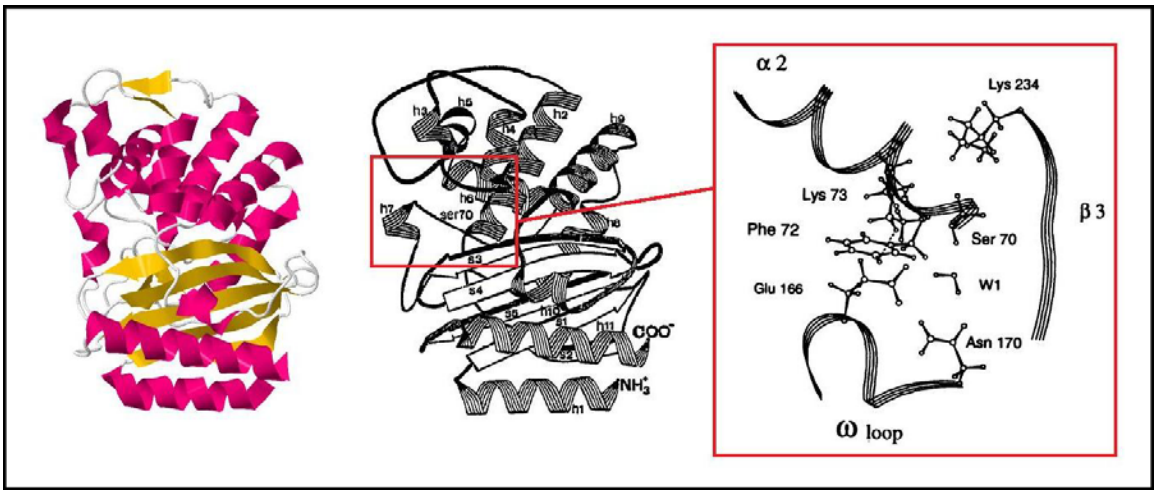

Figure 2.6 Crystal structure of wild-type TEM-1 β-lactamase from *E. coli* with active site details shown.

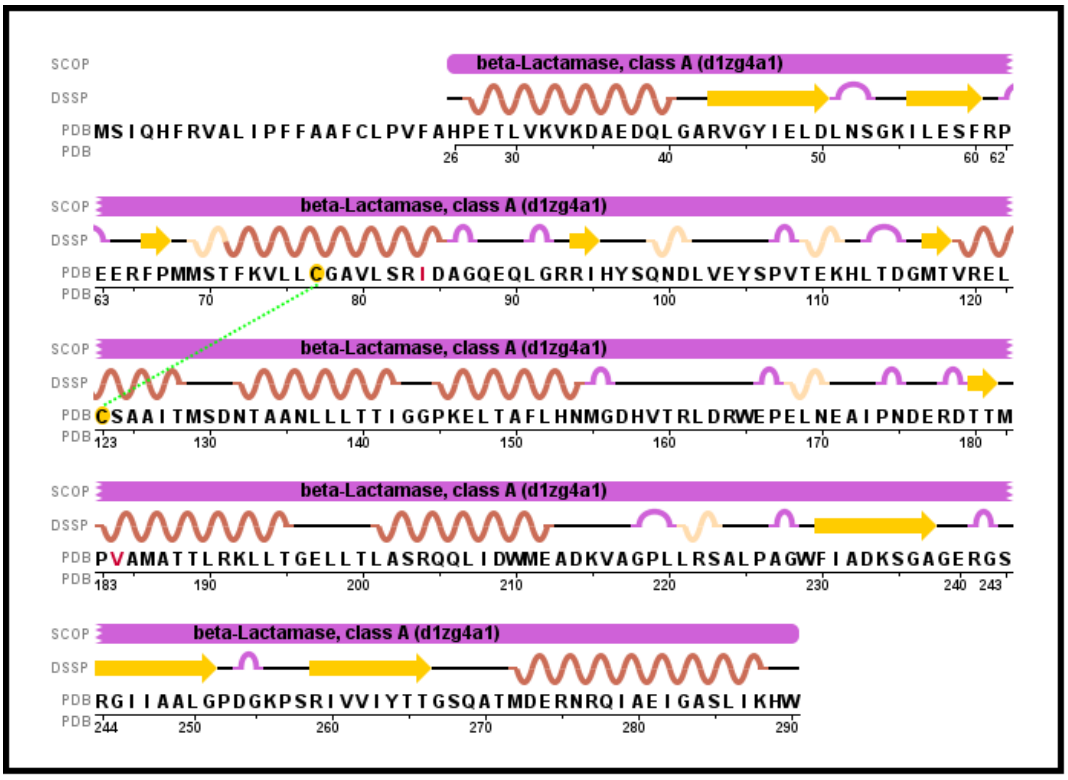

Figure 2.7 Protein sequence of mature TEM-1 β-lactamase from *E. coli*.

TEM-1 β-lactamase has evolved to function under physiological conditions of 37°C but shows limited stability at higher temperatures. Its published melting temperature, T_m, as indicated by CD spectroscopy, is 51°C.[27] Toward the natural substrate penicillin G, TEM-1 β-lactamase is considered to be a relatively efficient catalyst, with a published k_{cat}/K_M ratio of 9.24 x 10^6 M^{-1} s^{-1} at 25°C, pH 7.0 in 50 mM potassium phosphate buffer.[28] The diffusion-controlled limit for enzyme-catalyzed reactions in aqueous solution is approximately 10^9 M^{-1} s^{-1}.

2.3.2 Choosing TEM-1 as a Test Case

For the purposes of our thermal deactivation studies, TEM-1 β-lactamase was chosen as the test case for a multitude of reasons. The fact that it is a monomeric enzyme eliminated concerns about the effects of subunit dissociation on the observed activity and stability upon heating. There are no required cofactors in the catalytic action of TEM-1 β-lactamase, so the experimental design was not complicated by cofactor concerns. Many cofactors are quite expensive and it would have been highly impractical to use an enzyme which requires one in our long-term continuous studies. Furthermore, any potential changes in cofactor binding at elevated temperatures would need to be addressed, which would compound the complexity of the non-isothermal modeling analysis. The availability and low price of the enzyme's natural substrate, penicillin G, was also a clear benefit.

The mesophilic character (moderate thermal stability) of the wild-type TEM-1 β-lactamase made it more practical for use in the accelerated *TTN* modeling approach. Though the modeling approach should work equally well for a hyperthermophilic

enzyme (and indeed should be the approach of choice in such cases), the corroboration of the models by direct measurement becomes exceedingly difficult with an engineered commercial biocatalyst which is stable for weeks or months even at temperatures in the vicinity of 90°C, as noted in previous work.[33]

Our early observations indicated that TEM-1 β-lactamase unequivocally obeys a stability model other than the simple two-state mechanism shown in Equation 2-1, as partial recovery of activity was observed after subsequent heating and cooling. We also noted that the enzyme activity versus temperature profile did not increase exponentially at moderate-to-low temperatures, which led us to believe that the active site was somehow becoming compromised far below the published T_m and that the application of the Equilibrium Model should be considered.[15] TEM-1 and other Class A β-lactamases has been shown to exhibit four-state unfolding behavior in chemical denaturation studies with guanidinium hydrochloride - having a stable "molten globule" intermediate which precedes the completely unfolded state.[19,34,35] Therefore, this enzyme presented an interesting case with which to analyze models of different complexity in a complete operational stability study.

2.3.3 Expression and Purification

The DNA sequence encoding wild-type TEM-1 β-lactamase was cloned into the pET-27b(+) vector (EMD Biosciences - Gibbstown, NJ) and used to transform an aliquot of *E. coli* BL21 (DE3) competent cells. The cells were incubated for 24 h at 30°C on a kanamycin-infused agar plate and a single colony was picked to generate a stock of transformed cells. A 1-mL sample of the transformed cell stock was used to inoculate

200 mL of the expression medium, which consisted of LB-Miller broth with 0.3 M sorbitol and 2.5 mM betaine (osmolytes to enhance medium secretion)[7] and 35 μg/mL kanamycin sulfate. The culture was incubated at 37°C in a 1.0 L Erlenmeyer flask, agitated at 120 rpm, until an OD_{600} of 0.8 was reached; at this point over-expression was induced by the addition of 0.3 mM isopropyl β-D-1-thiogalactopyranoside (IPTG). The induced culture was incubated for 16 h at 25°C, with 120 rpm agitation, after which the cell debris was removed by centrifugation at 5100 *g* for 30 minutes (Model J6M centrifuge, Beckman-Coulter - Brea, CA). The resulting yield of cells (dry cell weight) was 2.2 g/L.

The clarified medium (supernatant) was chilled to 4°C and mixed with saturated ammonium sulfate solution (also at 4°C) to a final salt level of 55% saturation (2.16 M). After incubation for 1 h at 4°C, the precipitated solids were removed by centrifugation at 5100 *g* for 60 minutes and discarded. The supernatant was brought to 90% ammonium sulfate saturation (3.55 M) by addition of more salt solution, and incubated for 1 h at 4°C. The precipitated solids were collected by centrifugation at 5100 *g* for 60 minutes and resuspended in 10 mL of 20 mM Tris-HCl buffer at pH 8.2; the recovered fraction was dialyzed for 16 h at 4°C in 3 L of the same Tris-HCl buffer using Spectra/Por® cellulose tubing (Spectrum Labs - Rancho Dominguez, CA) with a MWCO of 3.5 kDa. After dialysis, the retained protein sample was passed through a 0.2 μm sterile polyethersulfone syringe filter (VWR - West Chester, PA).

The filtered sample was purified by anion exchange chromatography using an ÄKTAexplorer™ 100 system (GE Healthcare - Piscataway, NJ) equipped with a 5-mL Q Sepharose™ XL column; 20 mM Tris-HCl buffer at pH 8.2 was used as the running

buffer and a linear gradient of 0-0.5M NaCl was applied over 50 column volumes. The resulting fractions were assayed for activity using the CENTA assay (see Subsection 2.3.4.1) and the single 5-mL eluted fraction with the highest specific activity was collected and used for further study. Immediately following purification, the enzyme showed a specific activity of 118 U/mg toward the CENTA chromogenic substrate (assay conditions are 25°C, pH 7.0, 50 mM sodium phosphate buffer). Multiple batches of enzyme were used throughout the course of these studies, but the initial activity of the purified enzyme never differed from this value by +/- 10%, or else the protein was discarded and the purification repeated.

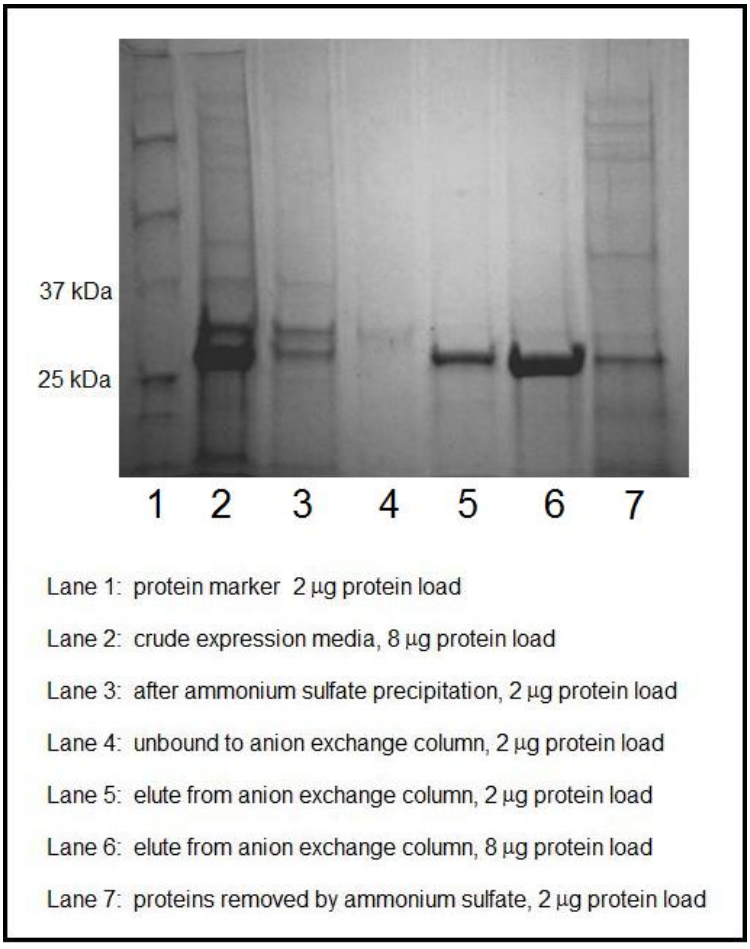

Figure 2.8 SDS-PAGE analysis of TEM-1 β-lactamase purification.

The ammonium sulfate precipitation and anion exchange chromatography steps had activity yields of 87.6% and 40.2%, respectively. The expression level in the media before any purification steps was 7.3 U/mL (83.8 U/mg) for a final purification level of 1.41-fold and an overall yield of 35.2%. The use of SDS-PAGE confirmed the high level of purity of the final protein sample, as shown in Figure 2.8, using a Precise™ 12% Protein Gel (Pierce - Rockford, IL) and an unstained Precision Plus™ protein standard marker (Bio-Rad - Hercules, CA). The gel was stained with GelCode Blue™ solution (Thermo Scientific - Rockford, IL). The initial (crude expression media) and final (purified fraction) lanes were overloaded to more clearly show the change in purity.

2.3.4 Activity Assays

2.3.4.1 CENTA

The chromogenic substrate CENTA (CAS # 9073-60-3) is a commercially available substance, derived from the antibiotic cephalothin, used for the screening of β-lactamase activity. The structure is shown in Figure 2.9. The compound has a neutral yellow color in aqueous solution, and upon hydrolysis of the β-lactam ring by the enzyme, changes noticeably to a pale, bright yellow. The literature reports that the change in extinction coefficient of CENTA upon hydrolysis is $\Delta\varepsilon$ = -6400 M^{-1} cm^{-1} at 405 nm and that the K_M value of TEM-1 β-lactamase toward CENTA is 70 μM at 30°C, pH 7.0, in 50 mM sodium phosphate buffer.[6]

A CENTA concentration of 500 μM (in 50 mM sodium phosphate buffer, pH 7.0) was used in the activity assay in order to stay well above the K_M value; unfortunately this resulted in a starting absorbance of over 3 AU. The UV/visible spectrophotometer used

in our study (model DU-800, Beckman-Coulter - Brea, CA) was near the limit of signal saturation at this level, as most similar instruments would be, and the data would have been considered unreliable. Rather than lowering the CENTA concentration and risking an unsaturated condition for the enzyme, we shifted the analytical wavelength to 460 nm where the change in extinction coefficient upon hydrolysis was found to be $\Delta\varepsilon$ = -2370 M^{-1} cm^{-1} (25°C, pH 7.0, 50 mM sodium phosphate buffer) and the starting absorbance was only 1.2 AU. The value of $\Delta\varepsilon_{460}$ was confirmed by performing triplicate dilution series at seven different concentrations; the R^2 value for the linear fit of the absorbance vs. [CENTA] data exceeded 0.999. Using 750 μL of the 500 μM stock solution per assay, along with a 10-μL sample containing approximately 100 ng of enzyme, resulted in pseudo-zero order kinetics and allowed for simple calculation of reaction rate from raw absorbance data.

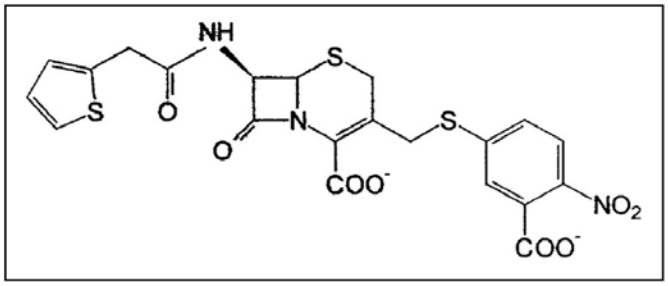

Figure 2.9 Chemical structure of CENTA β-lactamase substrate.

The CENTA assay was very useful in verifying the success of protein purification runs, but was not pursued as a test substrate during the deactivation studies. The primary factors in choosing an alternate substrate were 1.) the significant level of background thermal degradation of CENTA at temperatures above 45°C 2.) the relatively high cost ($7.25/mg) which would have made long-term continuous experiments prohibitively

expensive and 3.) lack of access to an open-loop continuous flow spectrophotometer which could be attached to our reactor. Another commonly used chromogenic substrate, nitrocefin[8] ($18.20/mg), was ruled out for these same reasons.

2.3.4.2 Penicillin G (spectrophotometric)

For the arrays of isothermal deactivation studies performed in conjunction with the Equilibrium Model studies done in New Zealand (see Chapter 3), a spectrophotometric method was developed to measure the activity of TEM-1 β-lactamase toward its natural substrate, penicillin G. As with the CENTA assay described in Subsection 2.3.4.1, the analytical wavelength (and in this case, also the cell path length) was chosen such that a sufficiently high substrate concentration could be used in order to stay well above K_M, without pushing the measured absorbance values above 1.5 AU where the accuracy of the spectrophotometer may be compromised.

The reaction mixture consisted of an aqueous solution of 50 mM sodium phosphate buffer and 4.4 mM penicillin G at pH 7.0. An analytical wavelength of 252 nm was chosen, at which the penicillin G exhibited an extinction coefficient of $\varepsilon_{252} = 682$ M^{-1} cm^{-1} and the fully hydrolyzed mixture exhibited an extinction coefficient of $\varepsilon_{252} = 213$ M^{-1} cm^{-1} as evidenced by the linear fits ($R^2 = 0.995$) of triplicate dilution series from 0-4.4 mM in increments of 0.44 mM. This absorbance difference $\Delta\varepsilon$ of 469 M^{-1} cm^{-1} between the substrate and product remained constant throughout the entire temperature range of the studies. The sample cell was a quartz cuvette with a path length of 0.5 cm, which gave a starting absorbance of 1.5 AU.

2.3.4.3 Penicillin G (polarimetric)

All experiments involving the EMR as well as the batch-mode enzyme activity profiles and deactivation studies performed at Georgia Tech used our novel polarimetric penicillin G assay. The experiments were performed on an Autopol II polarimeter (Rudolph Research Analytical - Hackettstown, NJ) equipped with either a static, temperature-jacketed 8.5-mm ID x 10-cm path length sample cell (for batch-mode experiments) or a flow-through, temperature-jacketed 2.5-mm ID x 10-cm path length sample cell (for continuous-mode experiments).

To achieve a good signal-to-noise ratio from the polarimeter, which had a precision level of +/- 0.01°, the assay was designed to have a starting optical rotation value above 2.0°. The penicillin G substrate exhibited a specific optical rotation $[\alpha]_{589}^{25}$ of 107° M^{-1} at 25°C in 50 mM sodium phosphate buffer, pH 7.0, according to the results of a triplicate dilution series. Hence, a substrate concentration of 20 mM was chosen for the assay solution.

The presence of the hydrolysis product, D-benzylpenicilloic acid, induced significant pH changes after 100% substrate conversion by the enzyme in 50 mM sodium phosphate buffer at pH 7.0. Therefore, the substrate-to-buffer ratio was optimized to maintain a constant pH throughout the range from 0-100% conversion. A solution of 20 mM penicillin G in 200 mM sodium phosphate buffer, with a starting pH of 7.05, was found to maintain a pH of 7.0 +/- 0.1 at all levels of conversion and all temperatures in the range of 20-60°C.

The hydrolysis product is itself chiral and has also been reported to be prone to thermal degradation[9], so its observed optical rotation was expected to be non-zero and possibly variable through our temperature range of interest. A calibration curve was constructed by first flowing substrate solution through the EMR (see Section 2.4 for details of the reactor) at a flow rate of 1 mL/min (for a reactor residence time of 10 minutes) with no enzyme present. The temperature of the reactor was increased from 20°C to 60°C at a rate of 4°C/h and the optical rotation of the reactor effluent was recorded at 25°C to assess the background thermal degradation of the substrate. Next, the EMR was overloaded with 1 mg of enzyme (over 100x the amount needed to observe full conversion at this residence time) and subjected to the same scan from 20°C to 60°C.

Unlike the substrate, which showed only very slight change in optical rotation, the product showed a monotonically decreasing trend as the temperature increased to 55°C. At 55°C, the trend suddenly reversed due to the fact that all of the enzyme had become deactivated, so this curve was truncated at 55°C. The calibration curve is shown in Figure 2.10. As the calibration curve shows, the 0% conversion data could be fitted to a straight line with a very slight negative slope, and the 100% conversion curve could be fitted to a second-order polynomial with temperature as the parameter. Thus, in all continuous EMR experiments, the proportion of substrate conversion, X, could be expressed as the function of optical rotation θ and temperature T (Kelvin) shown in Equation 2-9.

$$X(\theta,T)=\frac{2.05-.000867(T-293)-\theta}{0.99-.0024(T-293)+.0003(T-293)^2} \qquad [2\text{-}9]$$

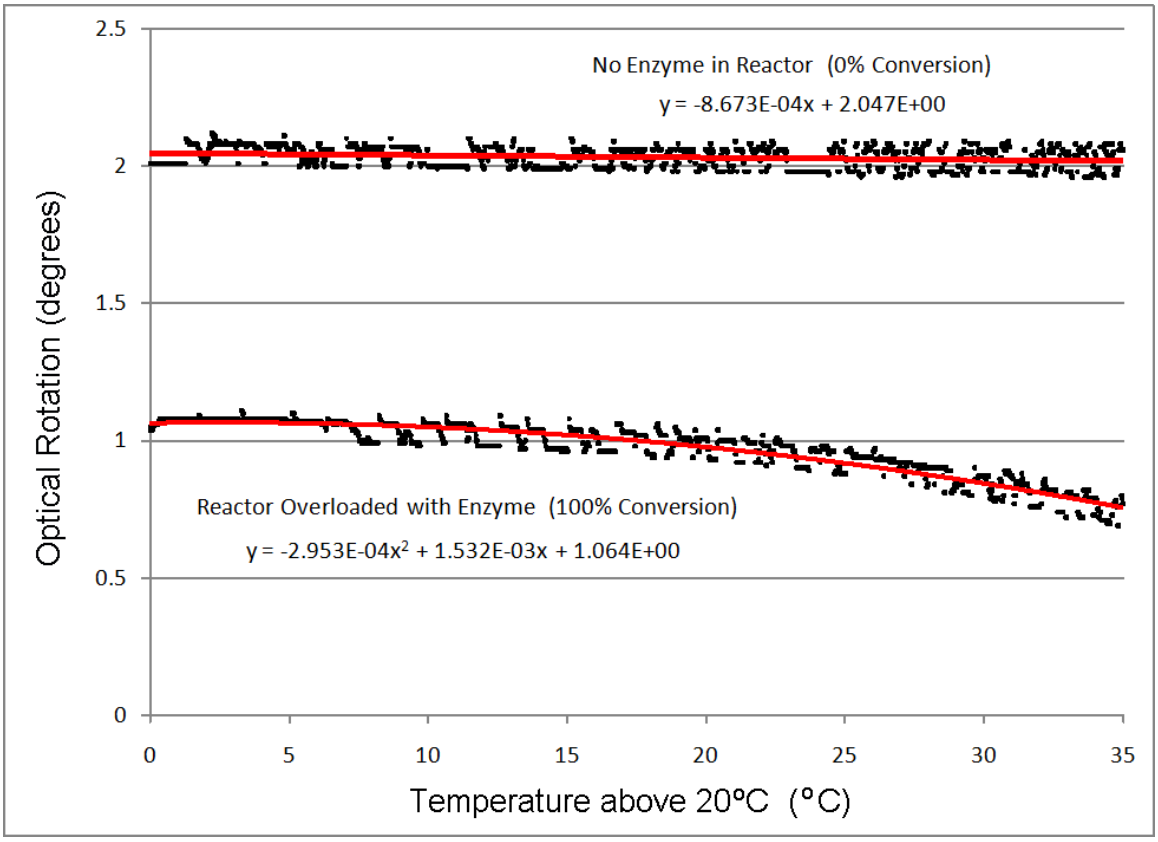

Figure 2.10 Polarimetric assay calibration curve.

The reaction rate in mol L^{-1} s^{-1}, when the reactor is operated as a continuous stirred-tank reactor (CSTR) is given by Equation 2-10, where the substrate concentration in the feed stream, $[S]_0$, feed flow rate, ν, and reactor volume, V, are held constant in all experiments.

$$r(T,t) = \frac{X(T,t)[S]_0 \nu}{V} \qquad [2\text{-}10]$$

Similarly, for batch mode experiments in which the substrate concentration was not held constant in the sample cell (though still in large excess and well above the K_M of the enzyme, i.e. pseudo-zero order), the reaction rate in mol L^{-1} s^{-1} was calculated from the slope of the optical rotation vs. time data at the desired temperature as in Equation 2-11.

$$r(T) = \frac{d\theta}{dt}\left(\frac{0.02}{0.99 - 0.024(T-293) + .0003(T-293)^2}\right) \qquad [2\text{-}11]$$

2.4 Enzyme Membrane Reactor

The enzyme membrane reactor (EMR) used in continuous experiments for this study consisted of a temperature-jacketed stainless steel vessel with built-in temperature jacket (EDS Maschinebau - Linnich, Germany) and an effective volume of 10.0 mL, excluding the internal PTFE-coated magnetic stir disc. The enzyme (with its molecular weight of 32 kDa) was retained in the reactor by an Amicon 63.5-mm diameter polyethersulfone membrane with a MWCO of 5 kDa, while substrate and products were able to pass through to the permeate side of the reactor. This type of membrane was chosen for its favorable temperature and pressure ratings (65°C, 70 psi) and the low protein binding of polyethersulfone as compared to regenerated cellulose or cellulose acetate membranes. The enzyme was used in its soluble form, requiring no immobilization for use in this reactor.

Feed solution was supplied to the reactor from a refrigerated tank via a digitally programmable peristaltic pump with ratcheted pressure control (ISMATEC Model CP 70817-10 - Glattbrugg, Switzerland). The temperatures of the reactor jacket and the polarimeter sample cell were controlled independently by two water baths with built-in programmable digital controllers (Model 1167, PolyScience - Niles, IL). The fluid temperature within the reactor jacket was monitored during experiments with a Traceable® dual channel thermometer (VWR - West Chester, PA) with a Type-K beaded-probe thermocouple, equipped with an RS-232 output for continuous data recording by PC. The total dead volume between the reaction chamber and the

polarimeter sample cell (consisting of the perforations in the membrane support disk and the small-bore outlet tubing) was 300 μL such that there was only a minimal time delay (20 s at the flow rate of 1 mL/min) in the recorded optical rotation data. Schematic diagrams of the reactor vessel and the complete experimental setup are shown in Figures 2-11 and 2-12, respectively.

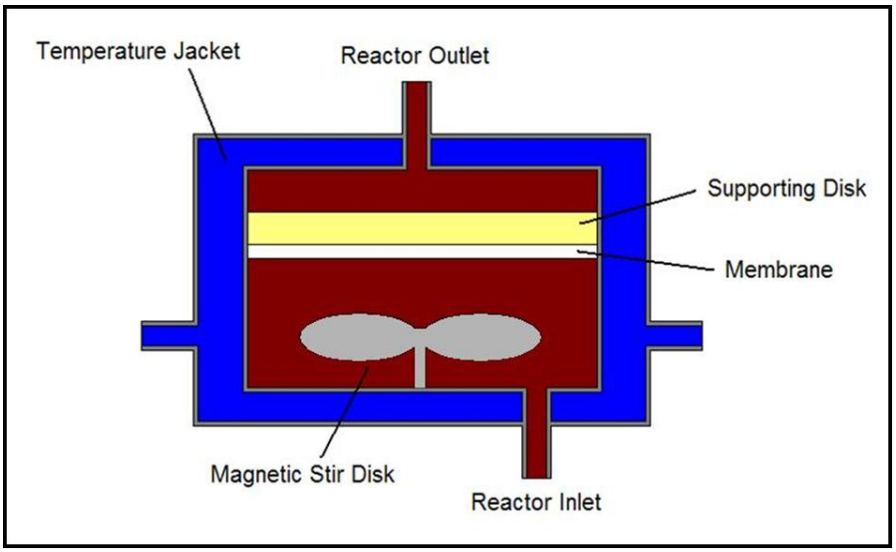

Figure 2.11 Enzyme membrane reactor (EMR) diagram.

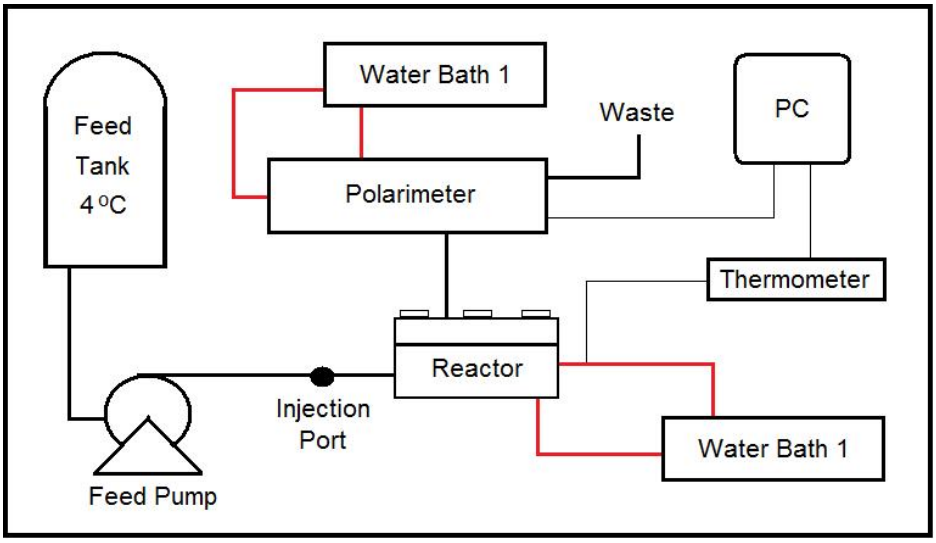

Figure 2.12 Experimental setup for EMR deactivation studies.

2.4.1 Theory of CSTR Operation

The simplest method for extracting reaction rate data from the measured concentration of the reactor effluent stream is to operate the EMR as a continuous stirred-tank reactor (CSTR). Theoretically, an ideal CSTR contains no dead volume, temperature or concentration gradients, or other mixing irregularities and the composition of the effluent stream is identical to that of the (homogeneous) contents of the reactor. In the case of an ideal CSTR, the residence-time distribution function, $E(t)$, which describes how much time fluid elements spend inside the reactor, is given by Equation 2-12.

$$E(t) = \frac{1}{\tau} e^{-t/\tau} \qquad [2\text{-}12]$$

A perfectly-mixed reactor which initially has an initial concentration, C_0, of some observable species and is then subjected to a sudden step change in the feed concentration of that same species will obey Equation 2-13.

$$C(t) = C_0 e^{-t/\tau} \qquad [2\text{-}13]$$

Therefore, a step tracer input test was used to determine whether the EMR in our study can be considered an ideal CSTR. A step input tracer test was conducted, in which the feed (1.0 mL/min flow rate) was instantly switched from 20 mM penicillin G in 200 mM sodium phosphate buffer to a penicillin-free solution of the same buffer (optical rotation of zero). A linearized plot of ln $C(t)/C_0$ vs. time was constructed, and the measured slope (- $1/\tau$) resulted in a calculated reactor volume of 10.02 mL (nearly identical to the measured volume. When these two volumes agree, CSTR behavior is confirmed.

Equation 2-13 can be used to describe the time delay of a CSTR in achieving steady-state composition of the reactor contents. As a general rule of thumb, the time for steady state to be reached, t_{ss}, is equal to five times the calculated residence time of the CSTR. The rule of thumb arises from setting the requirement that the observed change in tracer concentration at the reactor outlet has reached a value that is 99% of the actual step change in the feed stream concentration. At such a point, $C(t)/C_0$ = 0.01 and the associated time calculation is shown in Equation 2-14.

$$t_{ss} = -(\ln 0.01)\,\tau = 4.61\tau \approx 5\tau \qquad [2\text{-}14]$$

2.4.2 Control Measures

Once CSTR behavior was confirmed, certain measures were taken to ensure the smooth operation of the reactor through both the temperature ramp and isothermal experiments. Foremost, it was observed during control runs at 4°C (where no observable kinetic deactivation was found) that the apparent activity of the enzyme consistently fell to undetectable levels within 36 h. The activity decrease exhibited clear first-order behavior with a half-life of approximately 2 h. The membranes were inspected for physical damage and none was found; furthermore, the choice of such a low MWCO rating (the enzyme is six times the size of the nominal cutoff) led us to rule out the likelihood of leakage of the enzyme through the membrane. The stirring speed of the internal Teflon-coated magnetic disc had already been optimized to a range (100-180 rpm, impeller diameter 6.5 cm) where CSTR behavior was maintained but cavitation bubbles were not found to form underneath the membrane (i.e. shear was kept to a minimum).

The adsorption of enzyme to the membrane was implicated as the cause of the apparent deactivation. A test was conducted in which 1 mg/mL of bovine serum albumin (BSA) - a 66 kDa inert protein with zero catalytic activity toward penicillin G - was injected into the reactor and mixed for one hour before the addition of the β-lactamase. The BSA was intended to block the catalyst from adsorbing the membrane surface, and the results in Figure 2.13 show conclusively that this was a necessary measure.

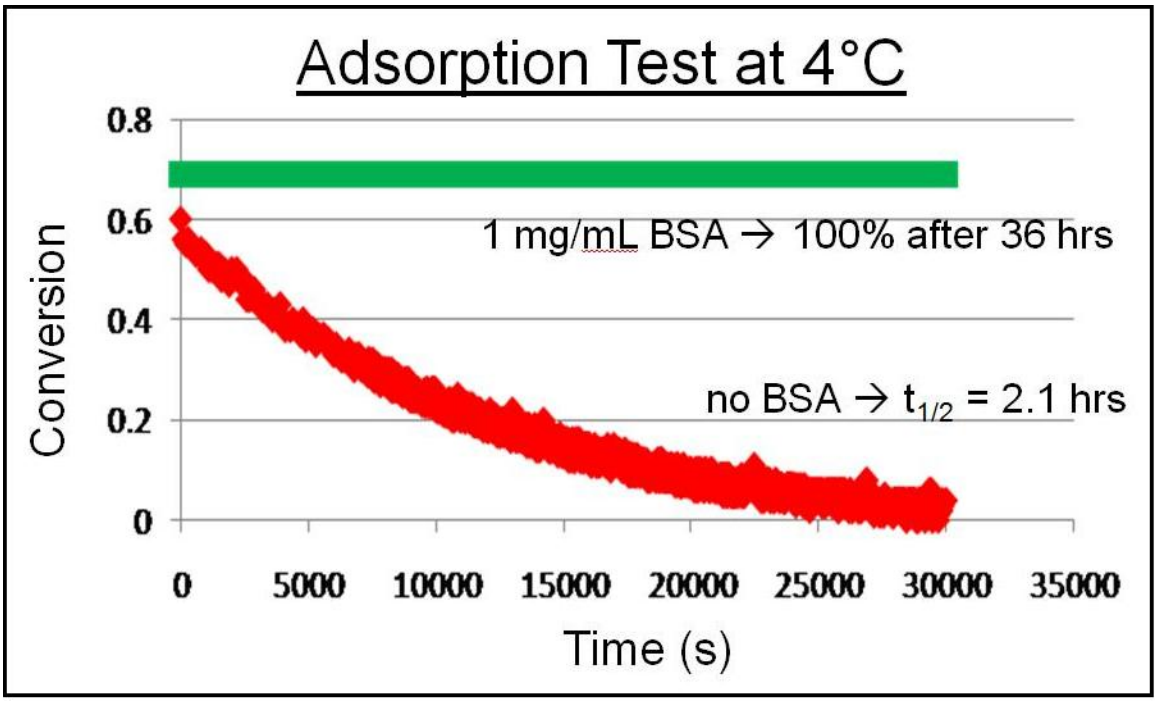

Figure 2.13 Results of BSA addition to prevent catalyst adsorption to membrane.

Though the geometry of the reactor interior with its relatively large heat transfer area ensured a lack of temperature gradient within the reactor (and this is corroborated by the demonstration of ideal CSTR behavior), we observed a slight temperature discrepancy between the programmed set point of the temperature bath and the reactor jacket/interior. This difference was due to heat loss through the stainless steel walls to

the environment, and became larger at temperatures farther from ambient. However, even at the heat transfer timescale of a 12 K/h temperature ramp, the temperature inside the reactor maintained its intended linear profile, as shown in Figure 2.14. The discrepancy between the reactor interior and the programmed set point versus temperature at all ramp rates is shown in Figure 2.15.

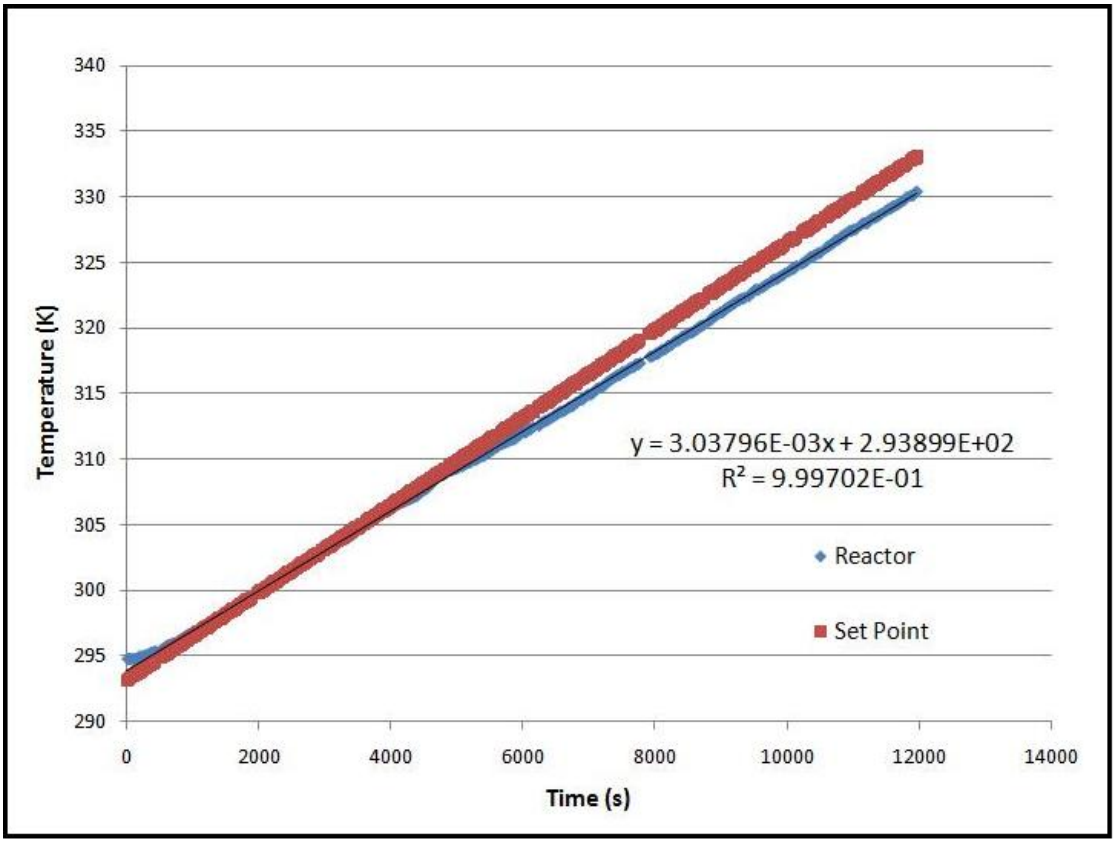

Figure 2.14 Reactor jacket temperature vs. water bath set point, 12 K/h ramp.

2.4.3 Reactor Timescale Considerations

Prior to performing modeling analysis on reaction rate data from the EMR, we considered the relevant timescales that could affect the measured output from the reactor. As a general rule, the phenomenon which is under investigation should always be the

rate-limiting step which controls the observed signal. In the case of enzyme stability testing, the timescale for the deactivation of the enzyme should be the longest one. In the scale-up of reactors used in bioprocesses, some important characteristics times are commonly assessed: diffusion, heat transport, oxygen transport, mixing, flow, microbial growth, chemical reaction, among others. Several of these do not apply to our small-scale reactor with soluble enzyme used in place of live microbes, but four of them potentially do. Heat transport, mixing, flow, and chemical reaction were all identified as phenomena which could impact the performance of the EMR, and so the timescale of each was evaluated using the physical parameters of our system and the published equations for stirred-tank reactors.[30]

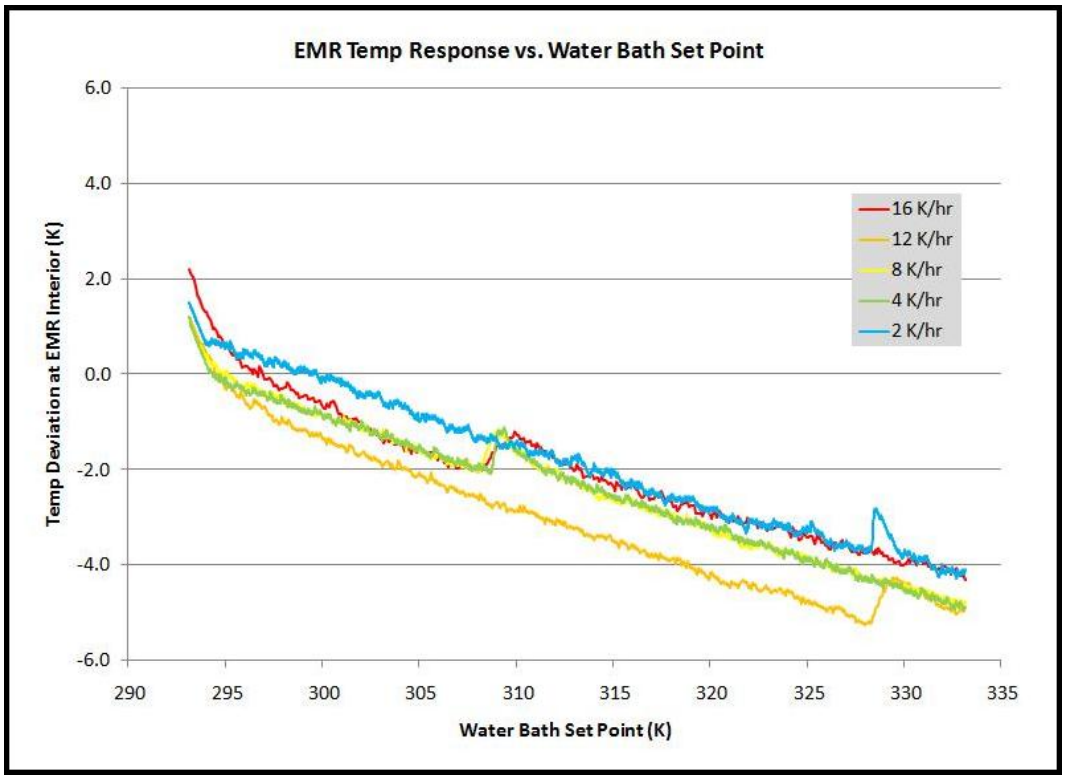

Figure 2.15 Deviation of reactor temperature from water bath set point, all ramp rates.

The chemical reaction timescale was calculated after activity measurements were made on TEM-1 β-lactamase and the value was found to be very small (τ_{rxn} = 48-590 μs) over the experimental temperature range (these results are explained fully in Chapter 5). The characteristic time for the heat transport process in a stirred vessel is given by 2-15, where V is the reactor volume, ρ is the density of the fluid in the reactor, C_p is the heat capacity of the fluid in the reactor, A is the contact area between the temperature jacket and the fluid in the reactor, and U is the overall heat transfer coefficient.

$$\tau_{ht} = \frac{V\rho C_p}{UA} \qquad [2\text{-}15]$$

The value of U was calculated for this system by assuming the values of the heat transfer coefficients for the heating water in the temperature jacket and the stirred contents of the reactor to be h = 500 W/m^{2}K (both are aqueous solutions in the turbulent flow regime). Using the wall thickness of the reactor, x_W = 0.6 cm, and the thermal conductivity of stainless steel, k = 21 W/mK, the value of U was found to be 233 W/m^{2}K according to Equation 2.16.

$$U = \left(\frac{1}{h_A} + \frac{x_W}{k} + \frac{1}{h_B} \right)^{-1} \qquad [2\text{-}16]$$

Hence, with V = 10 mL, ρ = 1 g/mL, C_p = 4186 J/kgK, and the measured contact area of A = 38.5 cm^2, the value of τ_{ht} was found to be 47 s for this system.

The characteristic time for mixing in the stirred vessel, τ_{mix}, is given by Equation 2.17, where V = reactor volume, N = impeller rotation number, and D = impeller

diameter. With V = 10 mL, N = 3 s^{-1} (at the typical 180 rpm setting), and D = 6.5 cm, the timescale of mixing was found to be very short, with a value of τ_{mix} = 0.032 s.

$$\tau_{mix} = \frac{4V}{1.5ND^3} \qquad [2\text{-}17]$$

The timescale for flow in a stirred tank is simply given by $\tau_{flow} = V/\nu$ where ν is the volumetric feed flow rate. In a CSTR, the value of τ_{flow} is, by definition, equal to one reactor residence time. In all of our EMR experiments, V = 10 mL and ν = 1.0 mL/min, hence τ_{flow} = 10 min. Of all the timescales we considered, τ_{flow} was by far the longest and therefore the most likely to interfere with data collection under reactor conditions where enzyme deactivation is rapid. If necessary, this could be remedied by increasing the feed flow rate, thereby shortening the residence time, provided that i.) pressure limitations of the EMR membrane are not exceeded and ii.) τ_{flow} is longer than both τ_{ht} and τ_{mix} (a prerequisite for ideal CSTR behavior).

2.5 References

1. Anson, M.L. and Mirsky, A.E., *The Reversibility of Protein Coagulation*. Journal of Chemistry, 1931. **35**(1): 185-193.

2. Wu, H., *Studies on the Denaturation of Proteins, Xiii. A Theory of Denaturation.* Chinese Journal of Physiology, 1931. **5**: 321-344.

3. Privalov, P.L. and Khechina, N.N., *Thermodynamic Approach to Problem of Stabilization of Globular Protein Structure - Calorimetric Study.* Journal of Molecular Biology, 1974. **86**(3): 665-684.

4. Lumry, R. and Eyring, H., *Conformation Changes of Proteins.* Journal of Physical Chemistry, 1954. **58**(2): 110-120.

5. Abraham E.P. and Chain, E., *An enzyme from bacteria able to destroy penicillin*. Nature, 1940. **146**(3713): 837.

6. Bebrone, C., Moali, C., Mahy, F., Rival, S., Docquier, J.D., Rossolini, G.M., Fastrez, J., Pratt, R.F., Frere, J.M., and Galleni, M., *CENTA as a Chromogenic Substrate for Studying β–Lactamases*. Antimicrobial Agents and Chemotherapy, 2001. **45**(6): 1868-1871.

7. Sosa-Peinado, A., Mustafi, D., and Makinen, M.W., *Overexpression and Biosynthetic Deuterium Enrichment of TEM-1 β-Lactamase for Structural Characterization by Magnetic Resonance Methods*. Protein Expression and Purification, 2000. **19**(2): 235-245.

8. O'Callaghan, C.H., Morris, A., Kirby, S.M., and Shingler, A.H., *Novel Method for Detection of β-Lactamases by Using a Chromogenic Cephalosporin Substrate***.** Antimicrobial Agents and Chemotherapy, 1972. **1**(4): 283-288.

9. Deshpande, A.D., Baheti, K.G., and Chatterjee, N.R., *Degradation of β-lactam antibiotics*. Current Science, 2004. **87**(12): 1684-1695.

10. Klibanov, A.M., "Stabilization of Enzymes Against Thermal Inactivation." in *Advances in Applied Microbiology*, Vol. 29. Published by Academic Press, 1983. pp. 1-28.

11. Eijsink, V.G.H., Gaseidnes, S., Borchert, T.V., and van den Burg, B., *Directed Evolution of Enzyme Stability*. Biomolecular Engineering, 2005. **22**(1): 21-30.

12. Abian, O., Grazú, V., Hermoso, J., González, R., García, J.L., Fernández-Lafuente, R., and Guisán, J.M., *Stabilization of Penicillin G Acylase from Escherichia coli: Site-Directed Mutagenesis of the Protein Surface To Increase Multipoint Covalent Attachment*. Applied and Environmental Microbiology, 2004. **70**(2): 1249-1251.

13. Polizzi, K.M., Bommarius, A.S., Broering, J.M., and Chaparro-Riggers, J.F., *Stability of Biocatalysts*. Current Opinion in Chemical Biology, 2007. **11**(2): 220-225.

14. Thomas, T.M. and Scopes, R.K., *The effects of temperature on the kinetics and stability of mesophilic and thermophilic 3-phosphoglycerate kinase*. Biochemical Journal, 1998. **330**: 1087-1095.

15. Daniel, R.M., Danson, M.J., and Eisenthal, R., *The temperature optima of enzymes: a new perspective on an old phenomenon*. Trends in Biochemical Sciences, 2001. **26**(4): 223–225.

16. Shushanyan, M., Sujashvili, R., Tabuashvili, E., Makharadze, M., Getashvili, G., and Khoshtariya, D.E., *Kinetic and thermodynamic manifestations of the thermally-induced molten-globule-like state of α-chymotrypsin*. Journal of Biological Physics and Chemistry, 2006. **6**(2): 51-55.

17. Mark, A.E. and van Gunsteren, W.F., *Simulation of the Thermal Denaturation of Hen Egg White Lysozyme: Trapping the Molten Globule State*. Biochemistry, 1992. **31**(34): 7745-7748.

18. Singh, N., Liu, Z., and Fisher, H.F., *The existence of a hexameric intermediate with molten-globule-like properties in the thermal denaturation of bovine-liver glutamate dehydrogenase.* Biophysical Chemistry, 1996. **63**(1): 27-36.

19. Uversky, V.N. and Ptitsyn, O.B., *"Partly Folded" State, a New Equilibrium State of Protein Molecules: Four-state Guanidinium Chloride-Induced Unfolding of β-lactamase at Low Temperature*. Biochemistry, 1994. **33**(10): 2782-2791.

20. Vamvaca, K., Vogeli, B., Kast, P., Pervushin, K, and Hilvert, D., *An enzymatic molten globule: efficient coupling of folding and catalysis*. Proceedings of the National Academy of Sciences of the United States of America, 2004. **101**(35): 12860-12864.

21. Freire, E., Osdol, W.W., Mayorga, O.L., and Sanchez-Ruiz, J.M., *Calorimetrically determined dynamics of complex unfolding transitions in proteins*. Annual Review of Biophysics and Biophysical Chemistry, 1990. **19**: 159-188.

22. Palzkill, T., and Botstein, D., *Identification of Amino Acid Substitutions That Alter the Substrate Specificity of TEM-1 β-Lactamase*. Journal of Bacteriology, 1992. **174**(16): 5237-5243.

23. Ambler, R.P., *The Structure of β-Lactamases.* Philosophical Transactions of the Royal Society of London Series B, 1980. **289**(1036): 321-331.

24. Damblon, C., Raquet, X., Lian, L., Lamotte-Brasseur, J., Fonze, E., Charlier, P., Roberts, G.C.K., and Frere, J.M., *The catalytic mechanism of β-lactamases: NMR titration of an active-site lysine residue of the TEM-1 enzyme*. Proceedings of the National Academy of Sciences of the United States of America, 1996. **93**(5): 1747-1752.

25. Stec, B., Holtz, K.M., Wojciechowski, C.L., and Kantrowitz, E.R., *Structure of the wild-type TEM-1 β-lactamase at 1.55 Å and the mutant enzyme Ser70Ala at 2.1 Å suggest the mode of noncovalent catalysis for the mutant enzyme*. Acta Crystallographica, Section D: Biological Crystallography, 2005. **61**(8): 1072-1079.

26. Jelsch, C., Lenfan, F., Masson, J.M., and Samarna, J.P., *Beta-Lactamase TEM-1 of E. coli: Crystal structure determination at 2.5Å resolution*. Federation of European Biochemical Societies Journal, 1992. **299**(2): 135-142.

27. Wang, X., Minasov, G., and Shoichet, B.K., *Noncovalent Interaction Energies in Covalent Complexes: TEM-1 β-Lactamase and β-Lactams*. Proteins: Structure, Function, and Genetics, 2002. **47**(1): 86-96.

28. Hecky, J. and Muller, K.M., *Structural Perturbation and Compensation by Directed Evolution at Physiological Temperature Leads to Thermostabilization of β-Lactamase*. Biochemistry, 2005. **44**(38): 12640-12654.

29. Shuler, M.L. and Kargi, F., *Bioprocess Engineering: Basic Concepts, Second Edition*. Published by Prentice Hall, 2002. pp. 297-299.

30. Kossen, N.W.F. in *Biotechnology and Bioprocess Engineering* (Ed.: Ghose, T.K.). Published by United India Press Link House, 1985. pp. 365-380.

31. Fogler, H.S., *Elements of Chemical Reaction Engineering, Third Edition*. Published by Prentice Hall, 1999. pp. 816-826.

32. Thomson, J.A., Barnett, B.J., Grimsley, G.R., and Pace, C.N., *Conformational Stability and Activity of Rnase T1 with Zero, One, and 2 Intact Disulfide Bonds.* FASEB Journal, 1988. **2**(5): A1338-a1338.

33. Gibbs, P.R., Uehara, C.S., Neunert, U., and Bommarius, A.S., *Accelerated Biocatalyst Stability Testing for Process Optimization.* Biotechnology Progress, 2005. **21**(3): 762–774.

34. Robson, B., and Pain, R.H., *The Mechanism of Folding of Globular Proteins*. Biochemical Journal, 1976. **155**: 331-344.

35. Vanhove, M., Guillaume, G., Ledent, P., Richards, J.H., Pain, R.H., and Frere, J.M., *Kinetic and thermodynamic consequences of the removal of the Cys-77–Cys-123 disulphide bond for the folding of TEM-1 β-lactamase.* Biochemical Journal, 1997. **321**: 413-417.

36. Pace, C.N. and Shirley, B.A., *Protein Structure: A Practical Approach*, ed. T.E. Creighton. 1989, Oxford: IRL Press.

CHAPTER 3

DEACTIVATION OF TEM-1 β-LACTAMASE INVESTIGATED BY ISOTHERMAL BATCH AND NON-ISOTHERMAL CONTINUOUS ENZYME MEMBRANE REACTOR METHODS

3.1 Introduction

The thermal deactivation of TEM-1 β-lactamase was examined using two experimental techniques: a series of isothermal batch assays and a single, continuous, non-isothermal assay in an EMR. The isothermal batch mode technique was coupled with the three-state Equilibrium Model of enzyme deactivation, while the results of the EMR experiment were fitted to the four-state "molten globule" model. The two methods both led to the conclusions that the thermal deactivation of TEM-1 β-lactamase does not follow the Lumry-Eyring model and that the T_{eq} of the enzyme (the point at which active and inactive states are present in equal amounts due to thermodynamic equilibrium) is at least 10°C from the T_m (melting temperature), contrary to the idea that the true temperature optimum of a biocatalyst is necessarily close to the melting temperature.[6,27]

3.1.1 The Equilibrium Model and Isothermal Applications

The operational stability of a biocatalyst is an important characteristic in determining the suitability of that catalyst in a given process. It is well-understood that catalytic activity tends to increase with temperature, but that in the case of enzymes, elevated temperature also leads to thermal deactivation due to a loss of integrity of the active site.[1,2] When kept at elevated temperatures for extended time periods, enzymes will

undergo denaturation to a permanently inactive state. Some enzymes are capable of recovering catalytic activity after relatively short incubations at elevated temperatures which induce a loss of activity.[3,4] The Equilibrium Model (Figure 3.1) captures this phenomenon by including a reversible transition between active and inactive states, and has been shown to be valid for all of the enzymes (at least thirty at present) on which it has been tested.[5–8]

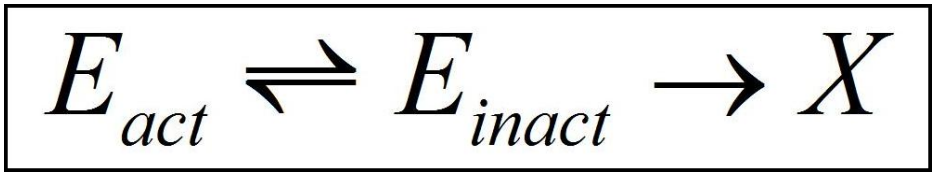

Figure 3.1 Equilibrium Model.

By treating the reversible transition between E_{act} and E_{inact} as a van't Hoff-type equilibrium, and the transition from E_{inact} to X as a time-dependent, first-order decay with Arrhenius-type rate constant, one can derive an expression for the observed reaction rate as a function of temperature and elapsed time.[5,6] Transition state theory is utilized to define the three quantities involved in the deactivation model, according to Equations 3-1 to 3-3. These are k_{cat} (turnover number of enzyme), K_{eq} (equilibrium constant between E_{act} and E_{inact}), and k_{inact} (first-order rate constant for decay from E_{inact} to X). The description of the E_{inact} to X step in the Equilibrium Model is not intended to preclude the presence of multiple, inactive intermediate unfolding states, though it makes no distinction between such states.[8]

$$k_{cat} = \frac{k_B T}{h} \exp\left(-\frac{\Delta G_{cat}}{RT} \right) \qquad [3\text{-}1]$$

$$K_{eq} = \exp\left[\frac{\Delta H_{eq}}{R}\left(\frac{1}{T_{eq}} - \frac{1}{T}\right)\right] \qquad [3\text{-}2]$$

$$k_{inact} = \frac{k_B T}{h}\exp\left(-\frac{\Delta G_{inact}}{RT}\right) \qquad [3\text{-}3]$$

Under isothermal conditions, the values of k_{cat}, K_{eq}, and k_{inact} remain fixed, and depend only on the activation and deactivation parameters of the enzyme at that temperature: ΔG_{cat} (activation energy for enzyme catalyzed reaction), ΔG_{inact} (activation energy for the E_{inact} to X transition), ΔH_{eq} (enthalpy change for the E_{act} to E_{inact} transition), and T_{eq} (temperature at which $[E_{act}] = [E_{inact}]$). When isothermal conditions exist, the expression for the reaction rate V_{max}, as a function of temperature and time, is given by Equation 3-4, where E_0 is the initial enzyme concentration.

$$V_{\max} = \left(\frac{k_{cat} E_0}{1 + K_{eq}}\right)\exp\left[-\frac{k_{inact}\, K_{eq}}{1 + K_{eq}} t\right] \qquad [3\text{-}4]$$

By substituting the results of Equations 3-1 to 3-3 into Equation 3-4, the values of ΔG_{cat}, ΔG_{inact}, ΔH_{eq}, and T_{eq} may be estimated by fitting experimental data of reaction rate vs. temperature vs. time to the model.[9] The established method for estimating these parameters is to perform an array of activity progress curves (including isothermal deactivation), while holding E_0 constant. After several temperatures have been examined, all progress curves are fitted to a three-dimensional surface plot using Powell's algorithm to determine the global minimum of the sum of squares deviation between the experimental curves and the model.[9]

3.1.2 The "Molten Globule" Model and Temperature Ramps

Recently, a method was developed for determining the optimum operating temperature for a biocatalyst using a single, continuous assay rather than an array of isothermal experiments.[10,11] This method utilizes an EMR for soluble enzyme, or a packed-bed reactor for immobilized enzyme, to subject a single sample of enzyme to a continuous, positive, most often linear temperature gradient. Since time and temperature are functionally related in such a linear ramp scheme, the reaction rate may be expressed as a function of a single variable (either time or temperature), plus all of the intrinsic activation and deactivation parameters listed in Equations 3-1 to 3-3.

As certain enzymes are known to lose catalytic activity before the onset of complete unfolding (i.e. the global loss of secondary structure often associated with the T_m of the enzyme),[1] the model used with the continuous temperature ramp experiment assumes that the biocatalyst follows a four-state deactivation model. This four-state model is similar to the Equilibrium Model but allows for two separate inactive states. The native state, *N*, is in equilibrium with a "molten globule" state, *M*, which has undergone slight conformational changes that render it inactive. For some enzymes including chorismate mutase, the molten globule state does undergo changes in tertiary structure but remains catalytically active,[28] but in our model *M* was considered inactive. Herein, states *N* and *M* are taken to be functionally equivalent to E_{act} and E_{inact}, respectively, in the Equilibrium Model. The four-state model includes a second equilibrium between *M* and an unfolded state, *U*, which has unfolded in the sense that it has experienced a widespread loss of secondary structure. This "molten globule" unfolding model is shown in Figure 3.2.

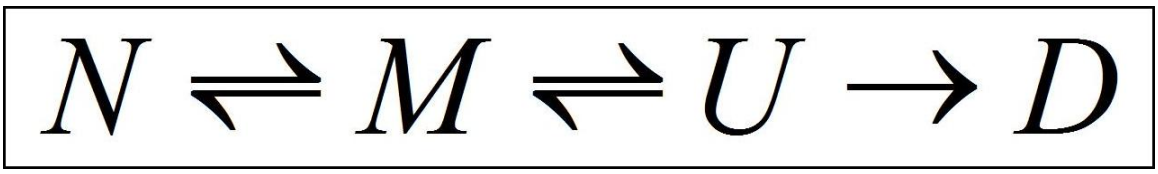

Figure 3.2 "Molten globule" model.

The "molten globule" unfolding model assumes that the enzyme must first enter the unfolded state *U* before it may become permanently denatured and that there are no pathways for denaturation directly from the native or molten globule states. It uses the same parameter as the Equilibrium Model, K_{eq}, to describe the van't Hoff equilibrium between states *N* and *M*. The first-order denaturation constant for state *U*, k_{inact}, is also the same for both models. The molten globule model, however, contains the additional parameter, K_{mg} = [*U*] / [*M*], shown in Equation 3-5, where T_{mg} is the temperature at which [*M*] = [*U*].

$$K_{mg} = \exp\left[\frac{\Delta H_{mg}}{R}\left(\frac{1}{T_{mg}} - \frac{1}{T}\right)\right] \qquad [3\text{-}5]$$

Hence, the four-state model assumes a heterogeneous population of inactive enzyme and seeks to capture both the T_{eq} and the traditional T_m of the enzyme. Both of these values, which do not necessarily coincide with each other, are important when designing and characterizing a stable biocatalyst.[8] When biocatalyst deactivation data is collected in a system which is operated as a continuous stirred-tank reactor (CSTR), the degree of substrate conversion, *X*, is given as a function of temperature, according to Equation 3-6.

$$X = \left(\frac{V}{[S]_0 \nu} \right) k_{cat} [N] \qquad [3\text{-}6]$$

Equation 3-6 contains the system parameters V (reactor volume), $[S]_0$ (substrate feed concentration), and ν (feed volumetric flow rate). Both k_{cat} and $[N]$ vary over the course of the experimental run as temperature is ramped up, and are readily expressed as functions of either time or temperature in the case of a linear heating ramp (the relationship $T = T_0 + mt$ applies, where m is the rate of increase of the reactor temperature). The value of k_{cat} is given by Equation 3-1, and the value of $[N]$ is derived by combining the definitions of K_{eq} and K_{mg}, the mass balance on species N, M, U, and D, and the first-order denaturation rate law which states $d[D]/dt = k_{inact}[U]$.

$$[D] = E_0 - [N] - [M] - [U] \qquad [3\text{-}7]$$

$$\frac{d[D]}{dt} = \frac{d}{dt}(E_0 - [N] - K_{eq}[N] - K_{mg}K_{eq}[N]) \qquad [3\text{-}8]$$

$$k_{inact}K_{mg}K_{eq}[N] = \frac{d}{dt}(E_0 - [N] - K_{eq}[N] - K_{mg}K_{eq}[N]) \qquad [3\text{-}9]$$

Upon rearrangement, and application of the chain rule, Equation 3-9 is transformed into a first-order differential equation for which $K_1 = d(K_{eq})/dt$ and $K_2 = d(K_{mg})/dt$. The rate of disappearance of native enzyme at any time (or temperature) according to the molten globule model is given by Equation 3-10.

$$\frac{d[N]}{dt} = \left(\frac{-k_{inact} K_{mg} K_{eq} - K_2 K_{eq} - K_1 K_{mg} - K_1}{1 + K_{eq} + K_{mg} K_{eq}} \right) [N] \qquad [3\text{-}10]$$

3.1.3 Functional Comparison of Methods/Models

Unlike the three-state, isothermal Equilibrium Model in which all of the equilibrium constants and the deactivation rate constant are constant through the course of an experimental run, this four-state, non-isothermal model equation is not readily integrated analytically. However, provided that the continuous temperature ramp experiment is started at any temperature well below the T_m of the enzyme, such that $K_{mg} << K_{eq}$, Equation 3-10 may be solved numerically by assuming an initial value of $[N]_0 = E_0 / (1+K_{eq})$. Essentially, the continuous ramp method uses variable K_{eq}, k_{cat}, and k_{inact}, whereas the Equilibrium Model (in isothermal batch-mode) allows these all to be held constant. Both methods, however, assume the intrinsic activation and deactivation parameters (ΔG_{cat}, ΔG_{inact}, ΔH_{eq}, T_{eq}) remain nearly constant over the entire temperature range of interest.

In this work, we have studied the thermal deactivation of TEM-1 β-lactamase from *Escherichia coli*, using both the isothermal batch techniques and the continuous EMR temperature ramp, on the same batch of enzyme, to assess the relative strengths of the two methods. Previously, a Class C metallo-β-lactamase from *Bacillus cereus* had been studied using the batch-mode method with the Equilibrium Model, but a Class A β-lactamase such as TEM-1 had not been studied using this method prior to our investigation.[6,12,13]

3.2 Experimental Section

3.2.1 Materials

The TEM-1 β-lactamase (E.C. 3.5.2.6) was over-expressed in *Escherichia coli* and purified from the expression medium via ammonium sulfate precipitation and ion exchange chromatography as in Section 2.3.3. Penicillin G potassium salt was purchased from USB Corp. (Cleveland, OH). Coomassie Protein Assay Reagent was obtained from Thermo Scientific (Rockford, IL). All other chemicals used were of analytical grade.

3.2.2 Batch-mode Experimental Setup

Enzyme activity was measured according to the spectrophotometric penicillin G assay described in Subsection 2.3.4.2., using a Thermospectronic Helios γ-spectrophotometer equipped with a Thermospectronic single-cell Peltier-effect cuvette holder. This system was networked to a computer installed with Vision32 (Version 1.25, Unicam) software for recording absorbance vs. time data. A quartz cuvette with a 0.5 cm path length was used during the course of all experiments, due to the favorable optical and heat transfer properties. The cuvette was kept isothermal during the course of each experimental run and a Cole-Parmer Digi-Sense thermocouple thermometer was used to ensure there was no temperature gradient larger than 0.1°C within the cuvette, or from the beginning to the end of the run. Runs were discarded and repeated if a temperature gradient was detected. The thermometer and the temperature control bath were calibrated using a Cole-Parmer NIST-traceable glass thermometer.

For each run, 1.0 mL of substrate solution was added to the cuvette, along with a 2 mm diameter Teflon-coated stir wire, and the system was allowed to thermally equilibrate for a minimum of 5 min. A stock solution of enzyme, with concentration

determined by Bradford assay (measurement of A_{280} in the presence of Coomassie Protein Assay Reagent), was used to prepare a sample with a final concentration of 32 μg/mL. After thermal equilibration, 5 μL of the enzyme solution (for a total enzyme concentration of 5.5 nM) was injected directly into the cuvette using a positive displacement pipettor and the contents of the cuvette were agitated rapidly for 3 seconds using the preheated stir wire. After stirring was completed, the software began recording absorbance data.

The combination of substrate concentration, cuvette path length, and enzyme loading was chosen such that the starting absorbance never exceeded 1.5 AU (to preclude instrument saturation), and the substrate conversion never exceeded approximately 40% at any of the temperatures examined. Hence, the substrate concentration was never lower than about 2.6 mM; a value over 100 times the published K_M value of the enzyme for penicillin G at 25°C.[14] Reactions were allowed to proceed for 120 s, with data points acquired at two-second intervals.

Triplicate assays were performed at each temperature, and the absorbance vs. time data were converted to reaction rate vs. time data. The average of the three rates at each time point was used to construct a single progress curve of reaction rate vs. elapsed assay time for each given temperature. The progress curves were smoothed using a Loess transformation (SigmaPlot® 2001 for Windows) to eliminate noise from the data, and the smoothed curves for all temperatures were initially fitted to the Equilibrium Model using MATLAB®, with initial parameter estimates of ΔG_{cat} = 85 kJ/mol, ΔG_{inact} = 100 kJ/mol, ΔH_{eq} = 120 kJ/mol, T_{eq} = 320 K. The resulting fitting parameters resulting from the first

run were used as improved initial estimates for a second run, which then provided the final parameter values.[9]

3.2.3 Continuous-mode EMR Experimental Setup

Substrate conversion vs. time data were collected in an EMR which was configured to operate as a CSTR. A single sample of enzyme was charged to a reactor with a working volume of 10.0 mL and a solution of 200 mM sodium phosphate buffer and 20 mM penicillin G (pH 7.0) was continuously fed to the reactor at a rate of 1.25 mL/min. The buffer system was selected and tested to ensure that the pH remained at 6.8–7.0 over the entire experimental temperature range and all levels of substrate conversion. The penicillin G feed solution was kept refrigerated at 4°C during experiments to preclude thermal degradation. To counteract the effects of β-lactamase absorption to the membrane surface, a loading of 1.0 mg/mL bovine serum albumin (BSA), which exhibited no activity toward the substrate, was charged to the reactor at least one hour prior to each injection of β-lactamase. Control runs were performed at 4°C, in the absence of thermal enzyme deactivation, to rule out the effects of membrane absorption and shear stress damage to the enzyme due to stirring. Zero activity loss was detected after 36 h of reactor operation during the control runs.

After a one-hour equilibration period at the initial temperature of 295 K, the reactor temperature was progressively increased to 330 K using a linear temperature ramp of 2 K/h. The substrate conversion was monitored by measuring the optical rotation of the reactor effluent stream via an in-line polarimeter with a sample cell which was kept at 25°C by external water bath. At 25°C, the specific optical rotation of the substrate mixture was $\alpha_{589} = 1078\ M^{-1}$ while that of the product was $\alpha_{589} = 578\ M^{-1}$. To account for

background thermal degradation of the substrate, a calibration curve was constructed by first running pure unreacted feed and then completely hydrolyzed product through the entire temperature ramp (see Subsection 2.3.4.3 for full details).

The conversion vs. time data were smoothed with the MATLAB® Curve Fitting Toolbox™, using a Robust Loess method with span = 85. The smoothed experimental data were fitted according to Equations 3-6 and 3-10, using an iterative solving procedure to minimize the sum of squared residuals by adjusting the fitting parameters (see Appendix B). Two different numerical techniques were used to solve the initial value problem (IVP) of Equation 3-10: an implicit Euler method with a time interval of Δt = 120 s and an area-under-the-curve approximation according to the trapezoidal rule, with a time interval of Δt = 120 s. In addition, a model was generated which omitted the folding state, U, and assumed only a three-state model equivalent to the Equilibrium Model. An attempt was then made to fit the continuous EMR data to this three-state model for purposes of comparison, using the area-under-the-curve approximation per the trapezoidal rule for the numerical integration.

3.3 Results and Discussion

3.3.1 Batch-mode Results

A total of ten progress curves for the enzyme were measured, each in triplicate, over the temperature range from 292 K to 332 K. The temperature spacing between progress curves was varied through the course of the experiments, and two of the progress curves were measured at high temperatures, such that the initial reaction rate had fallen below its peak value (i.e. the temperature was above T_{opt}). The experimental data

for rate vs. temperature vs. time, overlaid with the rate predicted by the MATLAB® routine according to Equation 3-4, is shown in Figure 3.3.

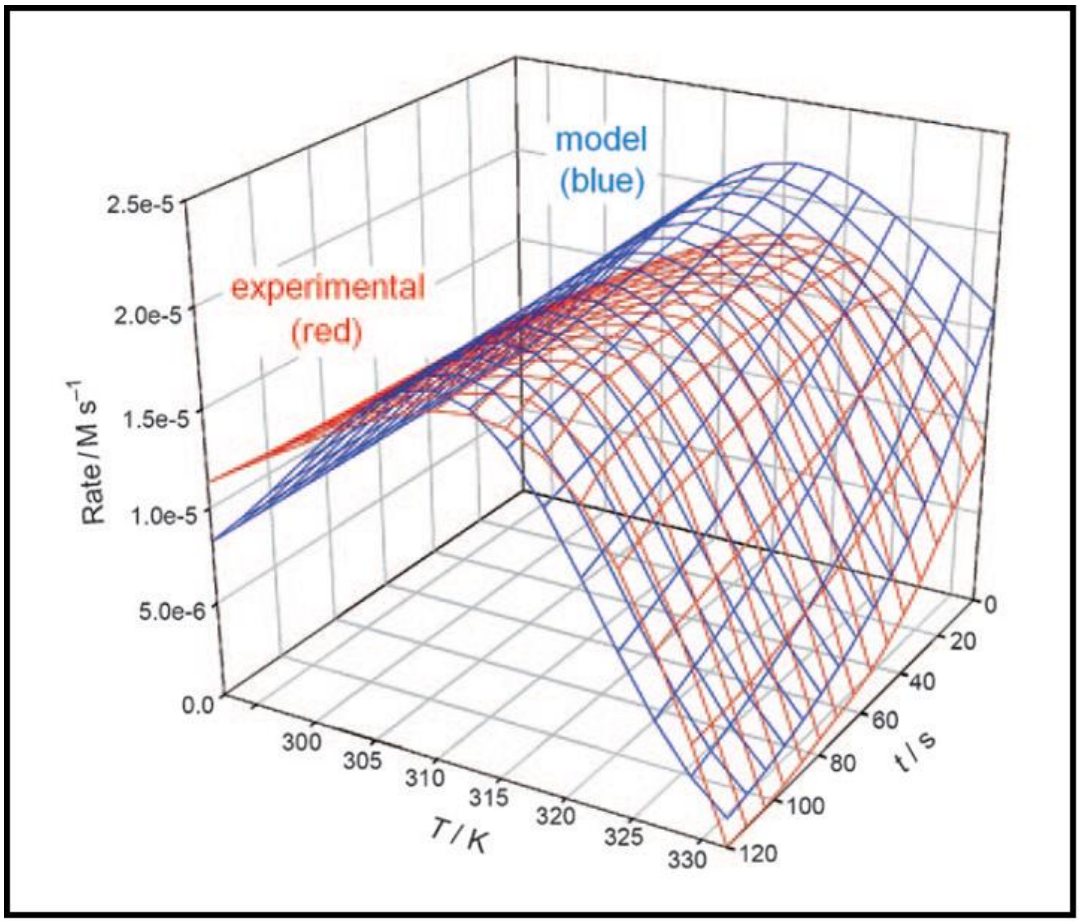

Figure 3.3 Isothermal batch-mode results. Experimental data shown in red, fit to the Equilibrium Model shown in blue (the model is the higher surface at the "peak")

3.3.2 Continuous-mode EMR Results

Figure 3.4 depicts the experimental data from the continuous EMR temperature ramp experiment, overlaid with three different model predictions: the four-state molten globule model using the implicit Euler technique, the four-state molten globule model using the trapezoidal rule, and the three-state Equilibrium Model. The values of the

deactivation parameters which were found by the various experimental methods and model fitting procedures are shown in Table 3.1.

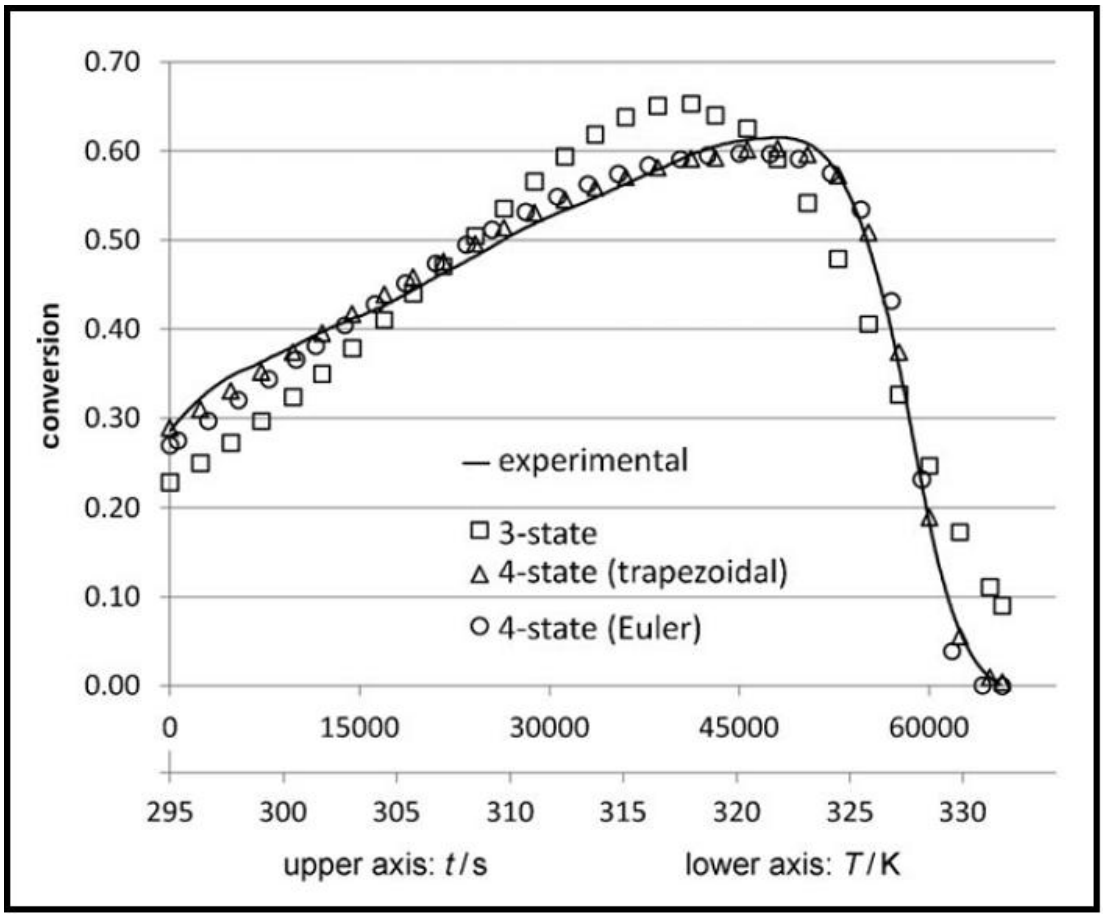

Figure 3.4 Continuous temperature ramp results.

3.3.3 Comparison of Models to Experimental Data

Figures 3.3 and 3.4 show the experimental data for the batch mode and continuous methods, respectively, overlaid with the predictions of the models. One conspicuous feature of the experimental data for both the isothermal batch and temperature ramp methods is that the early (low-temperature) segment of the curve shows a near-linear increase of activity with temperature. In the absence of any deactivation

effects in this regime, one would expect the curve to be concave upward, more closely resembling an Arrhenius-type activation profile. The near-linear increase in the isothermal batch-mode data suggests the onset of activity loss at a temperature well below the traditional T_m of TEM-1 β-lactamase, which is 51.5°C as evidenced by interpretation of the circular dichroism spectrum.[15] It is clear that a different effect must be responsible for the activity loss in the vicinity of 310–315 K, more than 10°C below the T_m, contrary to the widely held belief that the optimum operating temperature of a biocatalyst is very close (within a degree or two) to its melting temperature, but is expected for an enzyme following the Equilibrium Model.[10,16] This may only hold true for those enzymes for which global secondary structure and active site integrity are compromised simultaneously.

Table 3.1 Estimation of deactivation parameters. Isothermal batch-mode tests and continuous temperature ramp EMR methods (standard deviations for batch isothermal data are shown in parentheses).

Method	ΔG_{cat} (kJ/mol)	ΔH_{eq} (kJ/mol)	T_{eq} (K)	ΔH_{eq} (kJ/mol)	T_{eq} (K)	ΔG_{inact} (kJ/mol)	$\Sigma(\text{residual})^2$
batch isothermal	53.6 (0.04)	98.5 (2.0)	313.8 (0.3)	-	-	92.1 (0.2)	-
EMR (four-state, Euler)	54.0	64.6	317.9	716.5	328.6	101.2	0.1835
EMR (four-state, trapezoidal)	54.2	74.9	309.2	699.7	324.7	100.6	0.0497
EMR (three-state, trapezoidal)	54.8	69.4	330.5	-	-	101.0	1.7198

The three-state deactivation model resulted in a relatively poor fit to the continuous non-isothermal data from the EMR. Similar to the fit of the Equilibrium Model to the batch results in Figure 3.3, the three-state deactivation model, numerically integrated by the trapezoidal rule, tends to underestimate the enzyme activity on the low-temperature end of the EMR experiment, anticipating an Arrhenius-type increase as temperature rises. It can be clearly seen that the predicted slope of the rate vs.

temperature trend, in the low-temperature regime, is significantly greater than that of the experimental data, for both the three-state batch and three-state temperature ramp models.

Notably, however, the three-state isothermal Equilibrium Model (MATLAB® routine) resulted in a relatively good fit to the batch data in the high temperature regime, particularly near the T_{eq} of 314 K, whereas the three-state EMR model was unable to converge upon a good fit in this regime. One explanation for this inequality could be the large difference in time scales between the two experimental methods. At temperatures a few degrees below the T_{eq}, denaturation during the course of the experimental run may be nearly invisible in the two-minute isothermal batch assay. The three-state EMR model, however, is forced to include the cumulative effects of denaturation over a much longer time, as the time between each data point in the EMR model is 120 s, the same length as the entire progress curve of the batch model.

Thus, at a moderate temperature, which is apparently "nondenaturing" as seen in the shorter batch assay, a significant amount of time has passed in the continuous EMR run and there is already much less active enzyme present than if the enzyme was exposed to that temperature for the first time. Indeed, it has been previously shown in the literature that insufficient monitoring time, particularly at higher temperatures, can disguise the equilibrium character of inactivation and thus make it difficult to fit data to a model which would remain consistent in longer assays.[17] Effects such as uncooperative unfolding and grace-period inactivation can influence the accuracy of such short-term assays. The effects of varying the temperature ramp rate in the continuous EMR are explored in further detail in Chapter 5.

3.3.4 Physical Significance of Parameters

There is ample evidence in the literature that several β-lactamases follow a four-state unfolding mechanism.[18–20] It has been previously established by use of guanidinium chloride denaturation experiments that TEM-1 β-lactamase does not follow a simple "one-step, two-state" folding mechanism, but rather exhibits a thermodynamically stable intermediate state in equilibrium with the native and unfolded states, likely influenced by the cis/trans isomerization of Xaa-Pro peptide bonds.[21] This intermediate state, described in the literature, is modeled here to correspond to the molten globule state of the four-state model.

The batch-mode isothermal Equilibrium Model and the non-isothermal four-state temperature ramp models, remarkably, were in good agreement with respect to the location of the T_{eq}, though the batch-mode Equilibrium Model predicted a higher ΔH_{eq}, which may be because the three-state model is converging on an intermediate value somewhere between the enthalpy change necessary to enact a conformational change at the active site (ΔH_{eq} of the four-state model), and the enthalpy change associated with the onset of unfolding (ΔH_{mg} of the four-state model). The four-state model makes a distinction between these two transitions, in which the molten globule state *M* exhibits no activity but also does not readily become permanently denatured, whereas the unfolded state is much more readily denatured, an effect which corresponds to the sudden loss of activity in the vicinity of T_{mg}. In addition, the nature of the Equilibrium Model equation is such that ΔH_{eq} is subject to relatively high errors.[6,9] Discrepancies between the two models may be due to the fact that the Equilibrium Model treats the E_{inact} to *X* transition as a single event, although not necessarily via a single product.[7] Alternatively, it may be

due to the fact that, for this enzyme, data for the Equilibrium Model has only been collected for two minutes. The value of T_{mg} predicted by the temperature ramp four-state trapezoidal model (the better fit of the two four-state models) is 51.7°C, which coincides almost exactly with the documented T_m of the enzyme, as measured by circular dichroism.[15]

The values for ΔG_{inact} predicted by the four-state continuous model were somewhat higher than those from the three-state batch-mode Equilibrium Model. Again, this may be attributable to the fact that there is a very large timescale difference between the two experiments, and the prediction of the first-order denaturation rate constant k_{inact} may appear to be quite different during a two-minute assay than over the course of several hours.

The ΔG_{cat} value of 54.2 kJ/mol predicted by the continuous four-state trapezoidal model gives a turnover number of 1530 s^{-1} at 25°C, which is in excellent agreement with the literature value of 1500 s^{-1} for TEM-1 using penicillin G as a substrate.[22] The predicted ΔG_{cat} was slightly lower in the three-state batch-mode Equilibrium Model, at 53.6 kJ/mol, corresponding to a turnover number of 2550 s^{-1} at 25°C. The discrepancy between these two values could be a consequence of experimental error associated with the Bradford assay in determining the initial enzyme concentration, or it may be due to determinations of k_{cat} having been made under conditions for which not all of the enzyme is active.[7,23] However, the difference is not far from the sum of the fitting and experimental errors expected for the determination of Equilibrium Model parameters.[9]

The four-state continuous temperature ramp models predict the ΔH_{mg} to be nearly an order of magnitude higher than the ΔH_{eq} value, which is in agreement with the notion

that the conformational shift needed to render the enzyme inactive is slight compared to the complete unfolding of the enzyme.[7,8,24,25] The value of 700 kJ/mol for the enthalpy change upon unfolding is in the typical range for globular proteins such as β-lactamase I from *Bacillus cereus*, which exhibits a denaturation enthalpy of 646 kJ/mol, although this is low compared with subtilisin.[26]

The two numerical integration methods used with the four-state model (implicit Euler method and trapezoidal rule) predicted nearly the same values for ΔG_{cat}, ΔH_{mg}, and ΔG_{inact}. The two methods produced slightly different predictions for the T_{mg}, which may be due to the different behavior of the two integration techniques in the vicinity of T_{mg}. The trapezoidal rule method, which resulted in a better overall fit, was particularly more effective than the implicit Euler method at tracking the experimental data in this regime where the rate of change of conversion with respect to time is high. The significant difference between the two models was in their predictions of ΔH_{eq} and T_{eq}. The implicit Euler method showed a higher T_{eq} with a lower energy barrier, while the trapezoidal method showed the converse arrangement. Nevertheless, both methods confirmed that ΔH_{eq} was about an order of magnitude less than the ΔH_{mg} indicated by both the four-state continuous experiment and CD data from literature and that the T_{eq} was at least 10°C lower than T_{mg} (i.e. melting temperature T_m).

3.4 Conclusions

Though the three-state Equilibrium Model (Figure 3.1) did not result in a good fit to the data obtained by the continuous temperature ramp method, it resulted in a relatively good fit to the isothermally obtained batch data, although the predicted value of

ΔG_{cat} was slightly low and the abbreviated increase of actual reaction rate with temperature was not fully captured by the model. The four-state deactivation model (Figure 3.2), especially when the steep changes around T_{mg} were tracked by a routine employing the trapezoidal rule rather than Euler's method, resulted in an excellent fit to the data collected by the continuous temperature ramp EMR experiment, and furthermore showed good agreement with the batch-mode Equilibrium Model regarding the location of T_{eq}, the temperature of transition between native, active enzyme and conformationally compromised, inactive enzyme.

Whereas the four-state model contains a higher number of fitting parameters and should admittedly result in an improved fit over the three-state model, there is, as discussed earlier, copious evidence in the literature which indicates TEM-1 β-lactamase unfolds via a four-state mechanism. Both the three-state Equilibrium Model and four-state continuous model were effective at pinpointing the transition between active and inactive enzyme. The finding of two distinct transitions in the temperature ramp EMR model corroborates the previously established notion that T_{eq} is separate from T_{opt}, with the latter depending on a mix of T_{eq}, ΔG_{cat}, and ΔH_{eq}.[5–7] Both are important to protein engineers who wish to characterize and design biocatalysts. It is clear that the difference in timescale of these two experimental modes may affect the parameters predicted by model fitting. Denaturing effects which may be ignored during an assay lasting only a few minutes will have a greater effect on models which seek to capture the cumulative deactivation over several hours. A low degree of cooperativity in the process of transitioning between native and denatured states is likely one source of discrepancy between the two experimental methods.

The discontinuous Equilibrium Model batch method has a string of advantages. The collection of an array of isothermal progress curves, while labor-intensive compared to the continuous temperature ramp experiment, can be fitted to a model which is mathematically straightforward in that all temperature-dependent equilibrium constants remain unchanged during progress curves. The batch method also uses smaller quantities of substrates, buffers, and other reagents and can be performed with commonplace instrumentation and equipment, so there is no need to configure a CSTR. In the current study with TEM-1 β-lactamase, the Equilibrium Model was equally as capable as the more complex four-state continuous model in identifying the T_{eq} of the enzyme. So far, all enzymes for which Equilibrium Model data has been collected obey the model.[7,8]

The temperature ramp method, although it is faster and requires minimal direct monitoring, and furthermore utilizes a single injection of enzyme (minimizing systematic error), requires a model which relies on numerical integration techniques due to the complicated behavior of native enzyme population when temperature increases with time. However, the ability of the continuous EMR system, in conjunction with the four-state deactivation model, appears to be a powerful tool for examining multiple thermodynamic transitions (*N* to *M* as well as *M* to *U*), both of which are of great importance in biocatalyst design, in a single experiment. This technique can likely be extended to other biocatalysts which do not deactivate according to a simple two-state cooperative mechanism.

3.5 Publication Information

The work presented in Chapter 3 of this dissertation was published in the inaugural issue of *ChemCatChem* (Issue 1, pages 131-137) with my thesis advisor, Andreas S. Bommarius, and my collaborator at University of Waikato in New Zealand, Roy M. Daniel, as co-authors. The date of initial on-line publication was July 14, 2009.

3.6 References

1. Manetto, G.D., La Rosa, C., Grasso, D.M., and Milardi, D., *Evaluation of thermodynamic properties of irreversible protein thermal unfolding measured by DSC*. Journal of Thermal Analysis and Calorimetry, 2005. **80**(2): 263–270.

2. Aymard, C. and Belarbi, A., *Kinetics of thermal deactivation of enzymes: a simple three parameters phenomenological model can describe the decay of enzyme activity, irrespectively of the mechanism.* Enzyme and Microbial Technology, 2000. **27**(8): 612–618.

3. Vieille, C. and Zeikus, G.J., *Hyperthermophilic Enzymes: Sources, Uses, and Molecular Mechanisms for Thermostability*. Microbiology and Molecular Biology Reviews, 2001. **65**(1): 1–43.

4. Machado, M.F. and Saraiva, J.M., *Thermal stability and activity regain of horseradish peroxidase in aqueous mixtures of imidazolium-based ionic liquids*. Biotechnology Letters, 2005. **27**(16): 1233–1239.

5. Daniel, R.M., Danson, M.J., and Eisenthal, R., *The temperature optima of enzymes: a new perspective on an old phenomenon.* Trends in Biochemical Sciences, 2001. **26**(4): 223–225.

6. Peterson, M.E., Eisenthal, R., Danson, M.J., Spence, A., and Daniel, R.M., *A New Intrinsic Thermal Parameter for Enzymes Reveals True Temperature Optima*. Journal of Biological Chemistry, 2004. **279**(20): 20717–20722.

7. Daniel, R.M., Danson, M.J., Hough, D.W., Lee, C.K, Peterson, M.E., and Cowan, D. A., "Enzyme stability and activity at high temperatures" in *Protein Adaptation in Thermophiles* (Eds.: T. Thomas, K. S. Sidiqui). Published by Nova Science, 2009. pp. 1-34.

8. Daniel, R.M., Danson, M.J., Eisenthal, R., Lee, C.K., and Peterson, M.E., *New parameters controlling the effect of temperature on enzyme activity.* Biochemical Society Transactions, 2007. **35**(6): 1543–1546.

9. Peterson, M. E., Daniel, R.M., Danson, M. J., and Eisenthal, R., *The dependence of enzyme activity on temperature: determination and validation of parameters*. Biochemical Journal, 2007. **402**(2): 331–337.

10. Gibbs, P.R., Uehara, C.S., Neunert, U., and Bommarius, A.S., *Accelerated Biocatalyst Stability Testing for Process Optimization.* Biotechnology Progress, 2005. **21**(3): 762–774.

11. Rogers, T.A. unpublished results, see Chapter 5 of this dissertation.

12. Peterson, M.E., "Evidence for a third thermal parameter of enzymes". PhD thesis, University of Waikato, 2005.

13. Peterson, M.E., Eisenthal, R., Danson, M.J., Spence, A., and Daniel, R.M., *A New Intrinsic Thermal Parameter for Enzymes Reveals True Temperature Optima*. Journal of Biological Chemistry, 2004. **279**(20): 20717–20722.

14. Lejeune, A., Pain, R.H., Charlier, P., Frere, J., and Matagne, A., *TEM-1 β-Lactamase Folds in a Nonhierarchical Manner with Transient Non-Native Interactions Involving the C-Terminal Region*. Biochemistry, 2008. **47**(4): 1186-1193.

15. Wang, X., Minasov, G., and Shoichet, B.K., *Non-covalent interaction energies in covalent complexes: TEM-1 ß-lactamase and ß-lactams*. Proteins: Structure, Function, and Genetics, 2002. **47**(1): 86–96.

16. Eisenthal, R., Peterson, M.E., Daniel, R. M., and Danson, M.J., *The thermal behaviour of enzyme activity: implications for biotechnology*. Trends in Biotechnology, 2006. **24**(7): 289–292.

17. Polakovic, M. and Vrabel, P., *Analysis of the Mechanism and Kinetics of Thermal Inactivation of Enzymes: Critical Assessment of Isothermal Inactivation Experiments*. Process Biochemistry, 1996. **31**(8): 787–800.

18. Uversky, V.N. and Ptitsyn, O.B., *"Partly Folded" State, a New Equilibrium State of Protein Molecules: Four-State Guanidinium Chloride-Induced Unfolding of β-Lactamase at Low Temperature.* Biochemistry, 1994. **33**(10): 2782–2791.

19. Vijayakumar, S., Vishveshwara, S., Ravishanker, G., and Beveridge, D.L., *Differential Stability of β-Sheets and α-Helices in β-Lactamase: A High Temperature Molecular Dynamics Study of Unfolding Intermediates*. Biophysical Journal, 1993. **65**(6): 2304–2312.

20. Bone, S., *Dielectric studies of native, unfolded and intermediate forms of β-Lactamase.* Physics in Medicine and Biology, 1994. **39**(11): 1801–1809.

21. Vanhove, M., Raquet, X., and Frere, J., *Investigation of the folding pathway of the TEM-1 β-lactamase*. Proteins: Structure, Function, and Genetics, 1995. **22**(2): 110–118.

22. Mathonet, P., Deherve, J., Soumillion, P., and Fastrez, J., *Active TEM-1 β-lactamase mutants with random peptides inserted in three contiguous surface loops.* Protein Science, 2006. **15**(10): 2323–2334.

23. Lee, C.K., Daniel, R.M., Shepherd, C., Saul, D., Cary, S.C., Danson, M.J., Eisenthal, R., and Peterson, M.E., *Eurythermalism and the temperature dependence of enzyme activity*. Journal of the Federation of American Societies for Experimental Biology, 2007. **21**(8): 1934–1941.

24. Lee, C.K., "Eurythermalism of a deep-sea symbiosis system from an enzymological aspect". PhD thesis, University of Waikato, 2007.

25. Daniel, R.M., Danson, M.J., Eisenthal, R., Lee, C.K., and Peterson, M.E., *The effect of temperature on enzyme activity: new insights and their implications.* Extremophiles, 2008. **12**(1): 51–59.

26. Arriaga, P., Menendez, M., Villacorta, J.M., and Laynez, J., *Differential scanning calorimetric study of the thermal unfolding of β-lactamase I from Bacillus cereus*. Biochemistry, 1992. **31**(28): 6603–6607.

27. Broering, J.M. and Bommarius, A.S., *Evaluation of Hofmeister Effects on the Kinetic Stability of Proteins*. Journal of Physical Chemistry B, 2005. **109**(43): 20612-20619.

28. Vamvaca, K., Vogeli, B., Kast, P., Pervushin, K, and Hilvert, D., *An enzymatic molten globule: efficient coupling of folding and catalysis*. Proceedings of the National Academy of Sciences of the United States of America, 2004. **101**(35): 12860-12864.

CHAPTER 4

UTILIZING SIMPLE BIOCHEMICAL MEASUREMENTS TO PREDICT LIFETIME OUTPUT OF BIOCATALYSTS IN CONTINUOUS ISOTHERMAL PROCESSES

4.1 Introduction

The expected product yield of a biocatalyst during its useful lifetime is an important consideration when designing a continuous biocatalytic process. One important indicator of lifetime biocatalyst productivity is the dimensionless total turnover number (*TTN*). The *TTN* represents the total number of catalytic events performed by a single enzyme molecule during its lifetime (i.e. before it is permanently deactivated) or, alternatively, the number of moles of product which will be yielded by one mole of biocatalyst under the specified process conditions. Here, a method is proposed for estimating the *TTN* of a given biocatalyst from readily measured biochemical quantities, namely the specific activity and the deactivation half-life, measured under identical conditions. We demonstrate that this method may be applied to any enzyme whose thermal deactivation follows first-order kinetics, regardless of the number of unfolding intermediates, and that the *TTN* method circumvents the potential problems associated with measuring specific catalyst output when a portion of the enzyme is already unfolded. The *TTN* estimation was applied to several representative biocatalysts to demonstrate its applicability in identifying the most cost-effective catalyst from a pool of engineered mutants with similar activity and thermal stability.

4.1.1 Stability Considerations for Industrial Biocatalysts

Biocatalysts are often superior to conventional catalysts in terms of high specificity, enantioselectivity, and catalytic efficiency.[1-3] In addition, enzyme catalysts possess many environmentally attractive attributes such as their biodegradability and propensity to operate at moderate temperature and pH in aqueous systems.[4-6] As such, biocatalysts are of great interest, particularly in the pharmaceutical and specialty chemicals industries where enzymes can often provide the needed level of product purity in relatively few process steps. Despite all of these advantages, the use of biocatalysts remains somewhat limited on the industrial scale.[7-8] In large part, this is due to the fact that enzymes, derived from biological sources, have evolved to function most efficiently in conditions resembling those found in biological systems. When taken out of their highly-evolved biological niche and placed under the conditions of a foreign commercial chemical process, many enzymes suffer in terms of long-term stability. There are, of course, exceptions to this rule and researchers are increasingly able to impart stability to biocatalysts by learning from the amino acid sequences of enzymes which tolerate harsh conditions, or by adding compounds to the reaction mixture.[9-11] Enzymes can be tailored to resist organic solvents as well as salts,[12] but thermal stability is an especially important trait since elevated temperature leads to more favorable reaction kinetics in a wide variety of processes.[13]

The choice of operating temperature in an enzyme-catalyzed process involves the consideration of two competing processes: the rise in catalytic activity with increased temperature according to the well-known Arrhenius rate law, and the loss of structural integrity at the enzyme's active site due to thermally induced conformational changes

and/or protein unfolding.[14,15] Operating a process at a temperature very near the melting temperature (T_m) of an enzyme generally results in maximal turnover number but also in rapid deactivation. Since the cost of the biocatalyst itself is often significant, along with the potential down-time required to frequently replace spent catalyst, this may be an unfavorable operating regime. On the other hand, operating at temperatures far below T_m may prolong the catalyst lifetime and reduce energy costs but could result in unreasonably low space-time yields. As demonstrated in the literature, the true optimum temperature for an enzyme may be well below that at which denaturation becomes apparent through short-term experiments.[16,17]

4.1.2 Total Turnover Number as a Productivity Indicator

In many cases, the range of acceptable operating temperature may be dictated by process constraints and the biocatalyst must be engineered to operate within that range. The protein engineer may be confronted with a large library containing several variants with similar activity and stability at the desired temperature, and must decide which variant will be most cost-effective over its process lifetime. While traditional indicators of biocatalyst performance based on intrinsic enzyme properties such as the V_{max}/K_M ratio are often utilized, these overlook the features of the specific process. Therefore, an indicator such as the catalytic effectiveness, which incorporates the enzyme behavior over the entire course of the reaction, is likely more applicable.[18] However, the *TTN* is an even more meaningful indicator of the suitability of a biocatalyst in a given process, as it directly scales the product yield to the catalyst input which renders it especially useful in cost estimation.

In a continuous process using soluble, polymer-bound transfer hydrogenation catalysts (‘‘chemzymes’’), the *TTN* has been estimated to be the quotient of the catalyst turnover number and the rate constant of spent catalyst replacement.[19] The notion of scaling activity to catalyst loss, i.e. deactivation rate, to estimate *TTN* has been developed for enzymatic systems by incorporating protein stability models such as the Lumry–Eyring model.[3] However, enzymes can lose catalytic activity before they undergo a global loss of secondary structure, i.e. unfolding, and as such the deactivation process may involve multiple stable intermediate states.[20] Thus, the question of catalyst activity loss is relatively complicated in the case of enzymes and can depend on several thermodynamic equilibrium processes.

Here, it is demonstrated that the *TTN* of a biocatalyst in a continuous, isothermal process can be estimated by performing two simple biochemical measurements. These measurements, the observed catalytic constant ($k_{cat,obs}$) and the observed deactivation rate constant ($k_{D,obs}$), take into account the operating conditions of the actual process and do not require a detailed knowledge of the enzyme’s deactivation mechanism. Assuming only that thermal deactivation of all active and intermediate forms of the enzyme proceeds via first-order kinetics, it is shown that regardless of the number of steps in the unfolding process, the *TTN* is simply the quotient $k_{cat,obs}/k_{D,obs}$ when both values are measured at the chosen process temperature. These data are readily measured with common laboratory instrumentation and eliminate the potential problem of errant activity readings which ignore the fact that all of the enzyme in the initial sample may not be in its native (active) state.

4.2 Methods

4.2.1 Observed Enzyme Activity in an Isothermal Process

An enzyme will only exhibit catalytic activity when its native conformation is preserved. The maximum catalytic output is achieved when the enzyme is continuously kept saturated with substrate during its lifetime, i.e. when operating conditions are such that substrate concentration >> K_M of enzyme at all times. Under saturated conditions, the instantaneous reaction rate $V_{\max}$ is given by Equation 4-1, where [N] is the concentration of native (active) enzyme present.

$$V_{\max} = k_{cat}[N] \qquad [4\text{-}1]$$

The specific turnover number of the enzyme, k_{cat}, is a function of temperature which can be defined according to thermodynamic transition state theory, as seen in Equation 4-2, where k_B = Boltzmann constant, h = Planck's constant, and R = gas constant. In an isothermal process, the value of k_{cat} remains constant and depends only on the intrinsic activation parameter ΔG_{cat}, the change in Gibbs free energy associated with activation of the enzyme-catalyzed reaction. Thus, for a given enzyme in an isothermal process, the observed $V_{\max}$ depends only on one quantity which is variable with respect to time: the concentration of enzyme [N] which is still in its native state. Furthermore, the expression for the observed reaction rate may be written with time as the only variable, as shown in Equation 4-3, where k_{cat} is taken to remain constant for the duration of the isothermal process. Therefore, to calculate product yield over the course of the process, it is necessary to obtain an expression for [N](t).

$$k_{cat} = \frac{k_B T}{h} \exp\left(-\frac{\Delta G_{cat}}{RT} \right) \quad [4\text{-}2]$$

$$V_{\max}(t) = k_{cat}[N](t) \quad [4\text{-}3]$$

4.2.2 Generalizable Model for Long-term Enzyme Deactivation

Upon exposure to a denaturing condition such as a chemical denaturant or heat, an enzyme loses its native conformation and is rendered inactive, at least temporarily. Removal from the denaturing condition can result in the partial recovery of catalytic activity, but if the inactivated enzyme is held under the denaturing condition for a sufficiently long time it will become permanently and irreversibly denatured.[21] The well-known Lumry-Eyring model of protein stability, shown in Figure 4.1, treats enzyme denaturation as a two-step process: first, equilibrium between the native and unfolded conformations of the enzyme, designated *N* and *U*, respectively (the equilibrium constant $K = [U]/[N]$), and second, a first-order permanent denaturation (with rate constant k_D) of the unfolded enzyme to a final state *D*.[22] More recent deactivation models, such as the Equilibrium Model recognize that, in general, any conformational change which compromises the integrity of the active site of the enzyme will cause catalytic activity to cease, whether or not this conformational change corresponds to the unfolding of the enzyme, i.e. loss of secondary structure.[15,17] In such a case, an equilibrium is assumed between the native and inactive (though not necessarily unfolded) states. Figure 4.2 shows the Equilibrium Model, in which E_{act} represents enzyme in its native

conformation, E_{inact} represents reversibly inactivated enzyme, and X is permanently denatured enzyme.

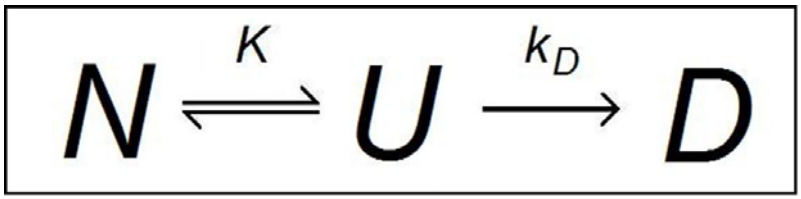

Figure 4.1. Lumry-Eyring model.

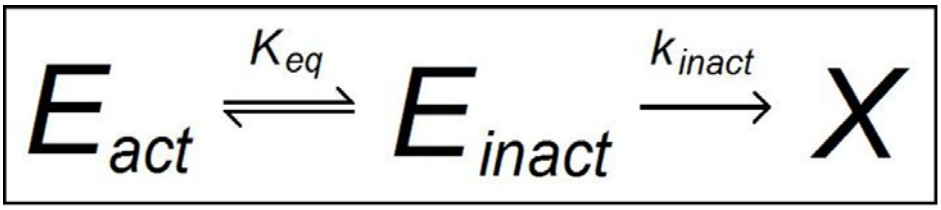

Figure 4.2. Equilibrium Model with associated constants. (Daniel et al., 2001)[23]

Both the Equilibrium Model, which in practice is often applied to short-term enzyme deactivation data with assays on the order of several minutes[15,23] and the Lumry-Eyring model assume that an enzyme must reach the unfolded or inactive state before it may become permanently denatured. When modeling enzyme deactivation over relatively long time periods, it may be necessary to consider other denaturing events which are not preceded by equilibrium unfolding, otherwise the models may result in artificially high total turnover predictions by ignoring effects which are best observed during assays longer than a few minutes. Gibbs et al. (2005) have previously suggested an "Extended Lumry-Eyring" model which includes a direct path for first-order denaturation from the native state, as seen in Figure 4.3.

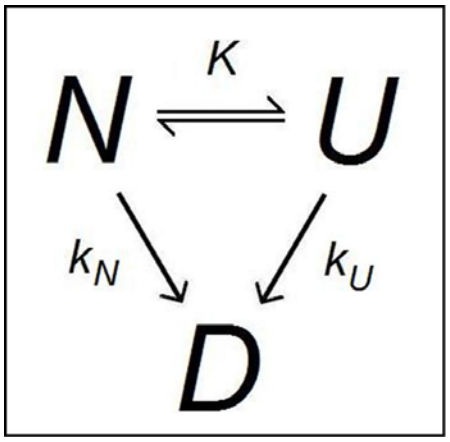

Figure 4.3. Extended Lumry-Eyring model. (Gibbs et al., 2005)[3]

Another feature common to the models in Figures 4.1-4.3 is that they model only one intermediate state between the native and permanently denatured states. Even though none of these models explicitly preclude the existence of additional unfolding intermediates, none are able to make a distinction between stable intermediates which have attained different degrees of unfolding. The existence of multiple unfolding equilibria would result in a deactivation model such as the one shown in Figure 4.4, in which only the *n*th intermediate state, here represented as I_n, undergoes irreversible denaturation.[24]

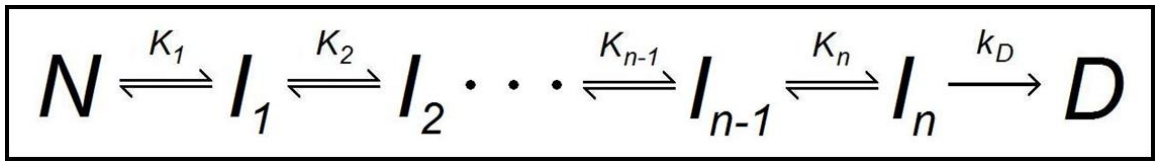

Figure 4.4. Multiple-intermediate model. (Freire et al., 1990)[24]

By combining the elements of the schemes in Figure 4.3 and 4.4, a generalizable theoretical model is proposed here which not only allows for multiple stable unfolding intermediates but also recognizes that each of these intermediates may proceed directly to a permanently denatured state, as shown in Figure 4.5. For clarification, the use of a single state *D* in Figure 4.5 is not an attempt to assert that all permanently denatured conformations which may be attained are identical, merely that they are all irreversible and nondescript, i.e. no longer considered to be species which participate in equilibria.

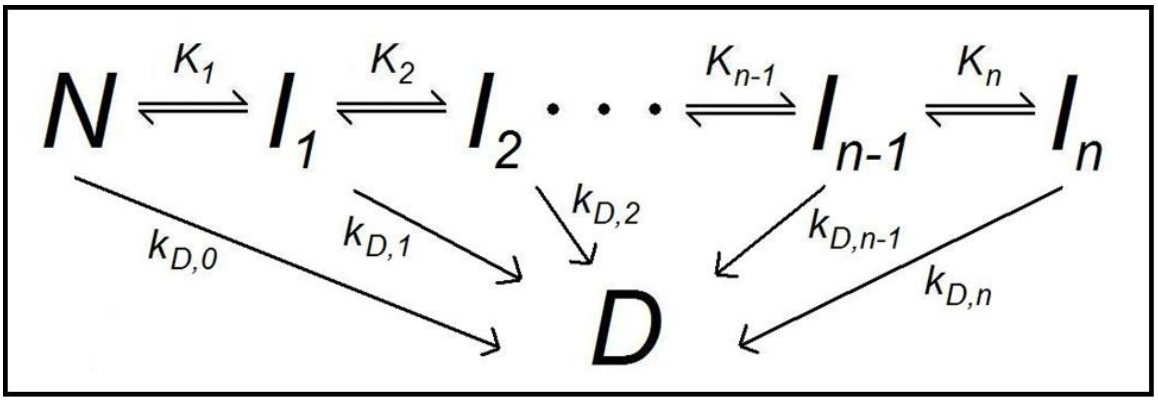

Figure 4.5. Multiple intermediate model with direct denaturation pathways

4.2.3 Progress of Enzyme Deactivation During an Isothermal Process

By adopting the general deactivation model in Figure 4.5, an expression can be derived for the amount of native enzyme remaining at any time during an isothermal process, i.e. the $[N](t)$ term needed to complete Equation 4-3. The complete derivation of this term from the mass balance on all enzyme species and the thermodynamic definitions of the equilibrium constants and rate constants is shown in Appendix A. The result in terms of the model in Figure 4.5 is shown in Equation 4-4.

$$[N](t) = \left(\frac{[E]_0}{1 + \sum_{j=1}^{n} \prod_{i=1}^{j} K_i} \right) e^{-\left(\frac{k_{D,0} + \sum_{j=1}^{n} k_{D,j} \prod_{i=1}^{j} K_i}{1 + \sum_{j=1}^{n} \prod_{i=1}^{j} K_i} \right) t} \qquad [4\text{-}4]$$

In an isothermal deactivation experiment, the "observed" or apparent deactivation rate constant ($k_{D,obs}$) resulting from the combination of all deactivation pathways will be equivalent to the exponential term of Equation 4-4, which may then be written more concisely as Equation 4-5. Substitution of this result into Equation 4-3 gives the desired expression for $V_{\max}$ as a function of time, as shown in Equation 4-6.

$$[N](t) = \left(\frac{[E]_0}{1 + \sum_{j=1}^{n} \prod_{i=1}^{j} K_i} \right) e^{-k_{D,obs} t} \qquad [4\text{-}5]$$

$$V_{\max}(t) = \left(\frac{k_{cat}[E]_0}{1 + \sum_{j=1}^{n} \prod_{i=1}^{j} K_i} \right) e^{-k_{D,obs} t} \qquad [4\text{-}6]$$

The entire pre-exponential of Equation 4-6, except for $[E]_0$, is equivalent to the "observed" or apparent k_{cat} in an isothermal experiment. Assuming that all

thermodynamic equilibria between the native state and the *n* intermediate states are established very rapidly, the k_{cat} observed by instrumentation will be necessarily lower than the intrinsic k_{cat} since some of the enzyme sample has already been rendered inactive and the activity calculation must be corrected by this factor. Hence, the final expression for instantaneous reaction rate as a function of time is given in Equation 4-7.

$$V_{\max}(t) = k_{cat,obs}[E]_0 e^{-k_{D,obs}t} \quad [4\text{-}7]$$

4.3 Results and Discussion

4.3.1 Total Turnover Number Expression from Stability Model

The process yield during the lifetime of a biocatalyst is equivalent to the integral of the instantaneous rate ($V_{\max}$) with respect to time, from zero to infinity (Equation 4-8). The expression for yield is obtained directly from the result of Equation 4-8, in which the non-varying terms k_{cat} and $[E]_0$ may be taken outside the integral (Equation 4-9). The integrated solution for overall yield is shown in Equation 4-10. The solution is then transformed to the dimensionless *TTN* after dividing by the concentration of biocatalyst initially present (specific yield per mole of catalyst). The final expression for *TTN* is shown in Equation 4-11.

$$yield = \int_0^\infty V_{\max}(t)dt \quad [4\text{-}8]$$

$$yield = k_{cat,obs}[E]_0 \int_0^\infty e^{-k_{D,obs}t}dt \quad [4\text{-}9]$$

$$yield = k_{cat,obs}[E]_0\left(\frac{1}{k_{D,obs}}\right) \qquad [4\text{-}10]$$

$$TTN = \frac{k_{cat,obs}}{k_{D,obs}} \qquad [4\text{-}11]$$

4.3.2 Estimation of *TTN* from Activity and Deactivation Data

To obtain an idea about the order of magnitude of *TTN* for stable biocatalysts, the result of Equation 4-11 was applied to an assortment of different biocatalysts which exhibit first-order deactivation behavior, and for which both activity and deactivation data were available at the same temperature and buffer/substrate system. The first requirement for the application of this method is a first-order deactivation rate constant at the desired process temperature. Frequently, published first-order deactivation data are expressed in terms of a half-life, from which the rate constant can easily be extracted. The second requirement is the apparent turnover number ($k_{cat,obs}$) measured at the same temperature as the deactivation data. In cases where the apparent value of k_{cat} is not given explicitly in the literature, it can be calculated from the more prevalent specific activity data (U/mg) provided that the molecular weight of the enzyme per active site, or alternatively the overall molecular weight and number of active sites per enzyme molecule, is known. Equations 4-12 and 4-13 give the conversion formulas to derive $k_{cat,obs}$ from specific activity (U/mg) and $k_{D,obs}$ from half-life (converted to seconds).

$$k_{cat,obs}\,(s^{-1}) = \frac{specific\ activity\ (U/mg) \times enzyme\ molecular\ mass\ (g/mol)}{60000} \qquad [4\text{-}12]$$

$$k_{D,obs}\ (s^{-1}) = \frac{\ln 2}{half\ life\ (s)} \qquad [4\text{-}13]$$

Half-life and specific activity are indeed two of the most important parameters which characterize the thermal stability of an enzyme, and are thus available for a wide variety of biocatalysts; however, it is important to stress that the data must be obtained under the same conditions of temperature, pH value, and buffer content. Table 4.1 shows estimates of *TTN* for several biocatalysts which have been calculated according to Equation 4-11.

The *TTN*, which itself is a dimensionless quantity, in each case corresponds to the expected yield in moles of product per mole of catalyst over the enzyme's lifetime. Not surprisingly, the β-glucosidase and the glucose dehydrogenase from *Sulfolobus solfataricus*, which are industrial-grade catalysts derived from thermophilic organisms for their high thermal stability, exhibit relatively high *TTN* (on the order of 1-10 million). The data for subtilisin S41 illustrate how the engineered improvements to activity and stability translate into overall productivity; between the wild-type S41 and the improved variant 3-2G7 the specific activity was improved by a factor of 2.1 and the half-life increased by a factor of 59. Per the *TTN* estimation, the improved biocatalyst can be expected to yield approximately 127 times more product than the S41 over its lifetime.

The utility of Equation 4-11 in selecting the best candidate catalyst for a given process from a pool of similar mutants can be seen in the data for cephalosporin acylase. Compared to the CA130 wild-type, the R121βA mutant has nearly the same specific activity but a longer half-life, and as expected exhibits a higher *TTN*. The D286βA mutant, compared to wild-type, shows a very slight (3%) increase in activity but a 21%

Table 4.1. *TTN* estimates for several representative biocatalysts.

Enzyme (organism)	Substrate	Temp. (°C)	$k_{cat,obs}$ (s^{-1})	half-life (hr)	$k_{d,obs}$ (s^{-1})	*TTN*	Refs.
enoate reductase (*Yersinia bercovieri*)	2-cyclo-hexenone	45	4.5	1.95	9.87×10^{-5}	4.56×10^{4}	25
β-glucosidase (*Pyrococcus furiosus*)	GlcpβNp[1]	100	10.8	85	2.26×10^{-6}	4.77×10^{6}	28
glucose dehydrogenase (*Sulfolobus solfataricus*)	D-glucose	70	74.9	45	4.28×10^{-6}	1.75×10^{7}	26,27
subtilisin S41 (Antarctic *Bacillus* TA41)	s-AAPF-*p*Na[2]	60	264	0.16	1.24×10^{-3}	2.13×10^{5}	29
subtilisin 3-2G7 (Antarctic *Bacillus* TA41)		60	553	9.43	2.04×10^{-5}	2.71×10^{7}	
cephalosporin acylase CA130 wild-type (*Pseudomonas* sp.)	GL-7-ACA[3]	37	12.3	68.1	2.83×10^{-6}	4.34×10^{6}	30
cephalosporin acylase CA130-R121βA mutant (*Pseudomonas* sp.)		37	12.2	88.3	2.18×10^{-6}	5.59×10^{6}	
cephalosporin acylase CA130-K198βA mutant (*Pseudomonas* sp.)		37	11.7	107.5	1.79×10^{-6}	6.54×10^{6}	
cephalosporin acylase CA130-D286βA mutant (*Pseudomonas* sp.)		37	12.7	53.9	3.57×10^{-6}	3.56×10^{6}	
glucose dehydrogenase strain 168 wild-type (*Bacillus subtilis*)	D-glucose	25	40.6	0.37	5.25×10^{-4}	7.73×10^{4}	12
glucose dehydrogenase A246V mutant (*Bacillus subtilis*)		25	51.8	0.31	6.08×10^{-4}	8.52×10^{4}	
glucose dehydrogenase P105S mutant (*Bacillus subtilis*)		25	6.1	0.52	3.73×10^{-4}	1.64×10^{4}	
glucose dehydrogenase V227A mutant (*Bacillus subtilis*)		25	33.1	0.67	2.89×10^{-4}	1.15×10^{5}	

[1]: p-nitrophenyl-b-D-glucopyranoside
[2]: succinyl-LAla-LAla-LPro-LPhe-*p*-nitroanilide
[3]: glutaryl 7-aminocephalosporanic acid

shorter half-life, and accordingly can be expected to have an 18% lower *TTN*. The K198βA mutant, though it has 5% lower activity than the wild-type, has a 58% longer half-life. This translates into a 50% higher *TTN* and thus makes it the most productive variant for the given substrate at a process temperature of 37°C.A similar pattern is seen in the data for the glucose dehydrogenase strain 168, from *Bacillus subtilis*, and its mutants. The A246V mutant illustrates that in some cases one property (activity) may be increased at the expense of another (half-life) and result in an improved *TTN*, while the P105S mutant shows that this will not always be the case. The V227A mutant, though 19% less active than the wild-type, has an 80% longer half-life; the combination translates into a *TTN* which is 49% higher than that of the wild-type.

4.3.3 Strengths and Limitations of the *TTN* Method

The *TTN* captures the amount of product synthesized per amount of enzyme expended. As such, and with the assumption that prices for both product and biocatalyst are known, the contribution of the biocatalyst to the overall variable costs of production can easily be determined. At that point already, such a determination results in one of three situations: i) the cost contribution of the biocatalyst is negligible (no further work required), ii) the cost contribution of the biocatalyst is overwhelming, maybe more than the price of the product (different biocatalyst or process is required), or iii) the cost contribution is neither negligible nor overwhelming, i.e. acceptable but can often be improved. The method allows straightforward comparison between different biocatalysts. As such, *TTN* is one of the most important criteria for process development.

The *TTN* estimation should not be employed as the sole criterion for process suitability because biocatalysts can exhibit very large *TTN* at temperatures well below

their optimum operating range. One study concluded that *TTN* of a given enzyme continues to increase as temperature is decreased due to the extended lifetime of the enzyme - however these yields could not be achieved in a practical sense, i.e. without unreasonably long residence times.[3] Therefore, the *TTN* should also not be used as a tool for deciding the best operating temperature for the enzyme, as this will invariably be the lowest available temperature. Rather, the *TTN* method is highly applicable when an approximate design temperature is already known and several catalysts must be compared to decide which one is the best performer at that temperature.

Another limitation of the *TTN* method is the assumption that all deactivation pathways obey first-order kinetics. In real processes, many effects such as protein aggregation may lead to loss of catalytic activity, and these may not always follow first-order rate laws. The inclusion of $k_{cat,obs}$ as a parameter also introduces some potential for inaccuracy. At higher operating temperatures where denaturation is relatively rapid, it may become increasingly difficult to capture the true initial enzyme activity in a conventional assay. A trade-off may occur in which the assay must be short enough in duration to exclude the time-dependent effects of denaturation but long enough to capture enough data points for a good fit and an acceptable signal-to-noise ratio from the instrumentation. It should also be noted that the isothermal experiments to determine $k_{d,obs}$ in cases where no literature exists, though very simple in design, may still need to span days or weeks especially in the case of industrially useful enzymes. An accelerated non-isothermal method for determining the *TTN* may be preferable in such cases.[3]

The primary advantage of the *TTN* method is that it uses two quantities which are easily observed with common laboratory instrumentation, if not already available in the

literature. Both the $k_{cat,obs}$ and $k_{D,obs}$ are easily extracted from specific activity and half-life data, respectively, which are widely published for a large number of biocatalysts. Another advantage of this method over some others which track the enzyme behavior through the course of an entire scaled-down reaction is that here the necessary parameters may be measured in discontinuous batch experiments, which involves less experimental labor, smaller quantities of substrate, and potentially lower costs.

4.4 Conclusions

A method has been presented for estimating the total turnover number (*TTN*), a dimensionless number which expresses the total moles of product yield per mole of biocatalyst during its operational lifetime. The *TTN* for a biocatalyst at a given temperature of interest can be calculated as the quotient of the $k_{cat,obs}$ (apparent turnover number) and the $k_{D,obs}$ (first-order deactivation rate constant), both measured at the same temperature. Many biocatalysts have been characterized in terms of specific activity and half-life, from which $k_{cat,obs}$ and $k_{D,obs}$ are easily derived. This heuristic *TTN* estimation method assumes minimal prior knowledge of the enzyme's deactivation pathway; it holds true for enzymes with any number of intermediate unfolding states provided that all inactive intermediates become permanently denatured via first-order kinetics. This method has been shown to be effective in distinguishing the most suitable catalyst from a group of candidates with similar characteristics, though it should not be used as a method for determining an enzyme's optimum operating temperature. The *TTN* method may be extended to any biocatalyst which fits an apparent first-order denaturation profile and has an established activity assay method at the desired process temperature. This method

allows the enzyme engineer to quickly, and with minimal experimental data, estimate the cost contribution of biocatalyst to the variable process costs and to select the most cost-efficient candidate from a group of engineered catalysts with similar activity and stability.

4.5 Publication Information

The work presented in Chapter 4 of this dissertation was published in *Chemical Engineering Science* (Volume 65, Issue 6, pages 2118-2124) with my thesis advisor, Andreas S. Bommarius as co-author. The date of initial on-line publication was December 29, 2009.

4.6 References

1. Illanes, A., *Stability of Biocatalysts*. Electronic Journal of Biotechnology, 1999. **2**(1): 1-9.

2. Tao, J., Zhao, L., and Ran, N., *Recent Advances in Developing Chemoenzymatic Processes for Active Pharmaceutical Ingredients*. Organic Process Research & Development, 2007. **11**(2): 259-267.

3. Gibbs, P.R., Uehara, C.S., Neunert, U., and Bommarius, A.S., *Accelerated Biocatalyst Stability Testing for Process Optimization*. Biotechnology Progress, 2005. **21**(3): 762-774.

4. Robles-Medina, A., Gonzalez-Moreno, P.A., Esteban-Cerdan, L., and Molina-Grima, E., *Biocatalysis: Towards even greener biodiesel production*. Biotechnology Advances, 2009. **27**(4): 398-408.

5. Ran, N., Zhao, L., Chen, Z., and Tao, J., *Recent applications of biocatalysis in developing green chemistry for chemical synthesis at the industrial scale*. Green Chemistry, 2008. **10**(4): 361-372.

6. Tramper, J., *Chemical versus Biochemical Conversion: When and How to Use Biocatalysts*. Biotechnology and Bioengineering, 1996. **52**(2): 290-295.

7. Bommarius, A.S. and Polizzi, K.M., *Novel biocatalysts: Recent developments*. Chemical Engineering Science, 2006. **61**(3): 1004-1016.

8. Makart, S., Bechtold, M., and Panke, S., *Towards preparative asymmetric synthesis of β-hydroxy-α-amino acids: l-allo-Threonine formation from glycine and acetaldehyde using recombinant GlyA*. Journal of Biotechnology, 2007. **130**(4): 402-410.

9. Kazlauskas, R. and Lutz, S., *Engineering Enzymes by "Intelligent" Design*. Current Opinion in Chemical Biology, 2009. **13**(1): 1-2.

10. Vieille, C. and Zeikus, G.J., *Hyperthermophilic Enzymes: Sources, Uses, and Molecular Mechanisms for Thermostability*. Microbiology and Molecular Biology Reviews, 2001. **65**(1): 1-43.

11. Azevedo, A.M., Fonseca, L.P., and Prazeres, D.M.F., *Stability and stabilization of penicillin acylase*. Journal of Chemical Technology and Biotechnology, 1999. **74**(11): 1110-1116.

12. Vazquez-Figueroa, E., Chaparro-Riggers, J., and Bommarius, A.S., *Development of a Thermostable Glucose Dehydrogenase by a Structure-Guided Consensus Concept*. ChemBioChem, 2007. **8**(18): 2295-2301.

13. Zale, S.E. and Klibanov, A.M., *On the Role of Reversible Denaturation (Unfolding) in the Irreversible Thermal Inactivation of Enzymes*. Biotechnology and Bioengineering, 1983. **25**(9): 2221-2230.

14. Yoshioka, S., Izutsu, K., Aso, Y., and Takeda, Y., *Inactivation kinetics of enzyme pharmaceuticals in aqueous solution*. Pharmaceutical Research, 1991. **8**(4): 480-484.

15. Peterson, M.E., Daniel, R.M., Danson, M.J., and Eisenthal, R., *The dependence of enzyme activity on temperature: determination and validation of parameters*. Biochemical Journal, 2007. **402**(2): 331-337.

16. Polakovic, M. and Vrabel, P., *Analysis of the Mechanism and Kinetics of Thermal Inactivation of Enzymes: Critical Assessment of Isothermal Inactivation Experiments*. Process Biochemistry, 1996. **31**(8): 787-800.

17. Rogers, T.A., Daniel, R.M., and Bommarius, A.S., *Deactivation of TEM-1 β-Lactamase Investigated by Isothermal Batch and Non-Isothermal Continuous Enzyme Membrane Reactor Methods*. ChemCatChem, 2009. **1**(1): 131-137.

18. Fox, R.J. and Clay, M.D., *Catalytic effectiveness, a measure of enzyme proficiency for industrial applications*. Trends in Biotechnology, 2009. **27**(3), 137-140.

19. Laue, S., Greiner, L., Woltinger, J., and Liese, A., *Continuous Application of Chemzymes in a Membrane Reactor: Asymmetric Transfer Hydrogenation of Acetophenone*. Advanced Synthesis and Catalysis, 2001. **343**(6-7): 711-720.

20. Vanhove, M., Raquet, X., and Frere, J.M., *Investigation of the folding pathway of the TEM-1 β-lactamase*. Proteins: Structure Function and Genetics, 1995. **22**(2): 110-118.

21. Machado, M.F. and Saraiva, J.M., *Thermal stability and activity regain of horseradish peroxidase in aqueous mixtures of imadazolium-based ionic liquids*. Biotechnology Letters, 2005. **27**(16): 1233-1239.

22. Lumry, R. and Eyring, H., *Conformation changes of proteins*. Journal of Physical Chemistry, 1954. **58**(2): 110-120.

23. Daniel, R.M., Danson, M.J., and Eisenthal, R., *The temperature optima of enzymes; a new perspective on an old phenomenon*. Trends in Biochemical Sciences, 2001. **26**: 223-225.

24. Freire, E., Osdol, W.W., Mayorga, O.L., and Sanchez-Ruiz, J.M., *Calorimetrically Determined Dynamics of Complex Unfolding Transitions in Proteins*. Annual Review of Biophysics and Biophysical Chemistry, 1990. **19**: 159-188.

25. Chaparro-Riggers, J.F., Rogers, T.A., Vazquez-Figueroa, E., Polizzi, K.M., and Bommarius, A.S., *Comparison of Three Enoate Reductases and their Potential Use for Biotransformations*. Advanced Synthesis and Catalysis, 2007. **349**(8-9): 1521-1531.

26. Lamble, H.J., Heyer, N.I., Bull, S.D., Hough, D.W., and Danson, M.J., *Metabolic Pathway Promiscuity in the Archaeon Sulfolobus solfataricus Revealed by Studies on Glucose Dehydrogenase and 2-keto-3-deoxygluconate Aldolase*. Journal of Biological Chemistry, 2003. **278**(36): 34066-34072.

27. Giardina, P., De Biasi, M., De Rosa, M., Gambacorta, A., and Buonocore, V., *Glucose dehydrogenase from the thermoacidophilic archaebacterium Sulfolobus solfataricus*. The Biochemical Journal, 1986. **239**(3): 517-522.

28. Kengen, S.W.M., Luesink, E.J., Stams, A.J.M., and Zehnder, A.J.B., *Purification and characterization of an extremely thermostable β-glucosidase from the hyperthermophilic archaeon Pyrococcus furiosus*. European Journal of Biochemistry, 1993. **213**(1): 305-312.

29. Miyazaki, K., Wintrode, P.L., Grayling, R.A., Rubingh, D.N., and Arnold, F.H., *Directed Evolution Study of Temperature Adaptation in a Psychrophilic Enzyme*. Journal of Molecular Biology, 2000. **297**(4): 1015-1026.

30. Zhang, W., Liu, Y., Zheng, H., Yang, S., and Jiang, W., *Improving the Activity and Stability of GL-7-ACA Acylase CA130 by Site-Directed Mutagenesis*. Applied and Environmental Microbiology, 2005. **71**(9): 5290-5296.

CHAPTER 5

VALIDATION OF HEURISTIC AND ACCELERATED MODELING APPROACHES FOR ESTIMATING BIOCATALYST TOTAL TURNOVER NUMBER

5.1 Introduction

Much research effort continues to be devoted to improving the stability of enzymes which have the potential to be used as biocatalysts in processes where high degrees of specificity and enantioselectivity are imperative. By isolating or identifying enzymes with activity toward a desired substrate, and then incorporating structurally stabilizing mutations (either by random screening, analogy to known elements in similar thermophilic proteins, or a balance of the two), biocatalysts may be engineered to be specialized toward a given reaction.

Identifying potentially useful protein sequences is only part of the task; often, the search does not begin with one or two candidates, but rather dozens or even hundreds. In the context of industrially viable biocatalysts, these candidates should have the ability to remain stable for weeks or months under the intended process conditions. To independently measure the lifetime yield of a large number of potentially interesting enzymes becomes expensive in terms of substrate consumption, energy usage, and experimental time. The work presented herein compares two proposed alternatives to direct measurement of a biocatalyst's lifetime yield, using TEM-1 β-lactamase as a test

case. The total turnover number (*TTN*) is used in both cases as the preferred indicator of the productivity (which is then easily used to compare lifetime cost-effectiveness) of the enzyme.

The first alternative is a heuristic method which scales the observed activity ($k_{cat,obs}$) to the observed deactivation rate constant ($k_{D,obs}$) at a selected operating temperature.[1] For purposes of consistency, the quantity $k_{cat,obs}$ should not be confused with the true k_{cat} of the enzyme.[2] Rather, it is the observed turnover frequency, with units of inverse time, of the enzyme-catalyzed reaction at the specified temperature. Importantly, $k_{cat,obs}$ takes into account the possibility that some of the enzyme has assumed a reversibly inactivated form (in rapid equilibrium with the active form at the time of measurement.[3] Experiments which seek to measure the true k_{cat} but fail to apply this inactivation "correction factor" are potentially erroneous. Conveniently, the value of $k_{cat,obs}$ can be calculated from a specific activity measurement (U/mg) if the molecular weight of the enzyme is known (Equation 4-12). The value of $k_{D,obs}$ is simply the observed rate constant when the enzyme's residual activity vs. time curve is fitted to a first-order exponential decay rate law. The majority of biocatalysts, even if multiple first-order deactivation pathways are present, will exhibit an <u>overall</u> first-order observed deactivation. Exceptions to this rule occur when second order effects such as protein aggregation become dominant.

The second alternative to direct measurement of lifetime yield is to conduct a single non-isothermal experiment in a continuous stirred-tank reactor (CSTR).[4] This approach incorporates the principles of a temperature scanning reactor[5] but applies a number of protein stability models (of varying complexity) to extract the intrinsic activity

and unfolding parameters of the enzyme, and identify the most relevant deactivation scheme. The effects of the temperature scan rate on the mathematically-predicted enzyme parameters are critically examined, and guidelines for ensuring proper reactor configuration are developed. The results are compared to direct measurements of *TTN* at selected temperatures several degrees below the enzyme's maximum operating temperature, which was not done in previous studies due to the extreme thermostability of the tested biocatalyst.[4]

To our knowledge, this is the only study to date which applies the accelerated modeling method to a soluble enzyme in a continuous system. A few examples of accelerated biocatalyst deactivation studies on immobilized enzymes can be found in the literature.[6] Recently, a method was proposed for carrying out a similar analysis with a soluble esterase in 96-well plates through batch-mode experiments, and corroborated through direct measurement over the partial lifetime of the enzyme in fed-batch experiments.[7] It should be noted that a batch-mode well-plate approach would become more difficult to use with highly active enzymes or enzymes with high K_M values relative to the solubility of substrate, as substrate depletion in the wells can affect observed reaction rate.

5.2 Experimental Methods

5.2.1 Batch-mode Experiments

The corresponding values of $k_{cat,obs}$ and $k_{D,obs}$ were determined at several different temperatures through a series of initial activity and isothermal deactivation experiments, respectively, all performed in batch mode. For the initial activity readings, 7.0 mL of the

substrate solution (20 mM penicillin G in 200 mM sodium phosphate buffer, pH 7.0) was placed into a sealed 15-mL centrifuge tube and pre-heated to the desired temperature for a minimum of 10 min. A 50 μL sample containing 300 μg/mL of enzyme was added to the pre-heated tube of substrate solution, which was rapidly mixed by inversion (resulting in a final enzyme concentration of 66 nM). The contents of the tube were immediately transferred to the sample cell of the polarimeter (Autopol II, Rudolph Research Analytical - Hackettstown, NJ), which was equipped with a temperature control jacket (set and preheated to the desired temperature).

The optical rotation of the mixture at 589 nm was recorded for a period of two minutes, over which the reaction kinetics remained pseudo-zero-order due to the substrate concentration (very well above K_M) and the short timescale of the experiment. The methods presented in Subsection 2.3.4.3 were used to convert the optical rotation data into reaction rate data. At 57°C (the highest temperature used in the study) there was already slight non-linearity to the absorbance vs. time data (R^2 = 0.96) but at 60°C the apparent deactivation was very fast and linearity was lost even through the first two minutes. This observation, coupled with the fact that several seconds are required to mix and transfer the contents to the polarimeter - during which significant deactivation can occur at 60°C - none of the data above 57°C were used.

For the isothermal deactivation experiments, the enzyme was incubated in an external water bath at the desired temperature, and 50 μL samples were withdrawn at appropriate time intervals, with a minimum of six time points for each temperature tested. Each withdrawn sample was assayed for activity at the desired temperature using the

methods described in the preceding paragraphs. For all temperatures used in this study, the residual activity vs. time plots obeyed a first-order decay equation, and so the apparent deactivation rate constant was determined at each temperature.

5.2.2 EMR Temperature Ramps

The EMR described in Section 2.4 was programmed with linear heating profiles for each of the experiments at 1 K/h, 2 K/h, 4 K/h, 8 K/h, 12 K/h, and 16 K/h. The feed solution used in all ramp experiments was 20 mM penicillin G in 200 mM sodium phosphate buffer, pH 7.0. For each experiment, 2.6 μg of enzyme was injected into the reactor (for a total enzyme concentration of 8.2 nM) and the reactor was allowed to equilibrate for 1 h at 20°C as substrate solution was fed through the reactor at 1 mL/min. After the equilibration period, the linear heating profile was started and the optical rotation of the effluent stream was recorded at 30 s intervals using the attached polarimeter, along with the temperatures of the water bath and the reactor temperature jacket. The polarimeter sample cell was maintained at 25°C by a dedicated water bath to eliminate any fluctuations in ambient temperature. Due to apparent heat loss through the reactor vessel walls, the temperature in the reactor jacket deviated slightly from that of the programmed temperature bath at the extremes, so the reactor jacket temperature was used in all calculations.

The raw optical conversion data was processed by first manually removing outlier data points which resulted from transient air bubbles in the polarimeter cell channel. Secondly, when necessary for the longer-duration ramps, the data was truncated shortly after the enzyme had decayed to zero residual activity, as some of the models had

difficulty fitting a long "tail" where the instrument noise eclipses the activity reading. Next, the data was smoothed in MATLAB® with the Curve Fitting Toolbox™, using a Robust Loess method with span = 85. Lastly, the optical rotation data was converted to reaction rate data using Equations 2-10 and 2-11.

5.2.3 Direct Isothermal Measurement

Measurements of the total product output over the enzyme lifetime were conducted by operating the EMR isothermally until the apparent reaction rate was too low to be measured. The total yield was measured at five different temperatures: 42°C, 45°C, 48°C, 51°C, and 54°C. The experimental duration and efficiency of substrate use would have been unreasonable at lower temperatures, and the timescales of enzyme deactivation and reactor mixing would have been too similar at higher temperatures (see Section 5.2.4). In each case, a feed flow rate of 1 mL/min was used and 2.6 μg of enzyme were injected into the reactor, for a final catalyst concentration of 8.2 nM. The reactor was preheated for a minimum of 1 h prior to the addition of enzyme, after which the measurement of effluent optical rotation began immediately. Once the conversion had decreased to a value nearly indistinguishable from instrument noise (generally 3-5% residual activity), the reactions were stopped.

Outlier data points due to transient air bubbles in the polarimeter cell were manually removed, and the optical rotation data was converted to reaction rate data according to Equations 2-10 and 2-11. The area under the reaction vs. time curve for the entire experiment was found using the "Area below curves" toolbox command in

SigmaPlot® (Version 8.0), giving the total yield per unit volume of the reactor. This area was then divided by the enzyme concentration in the reactor to give the *TTN*.

5.2.4 Timescale Considerations

In both the temperature ramp and isothermal experiments involving the EMR, proper reactor design principles must be followed to ensure that the reaction rate behavior accurately reflects the phenomena under study - enzyme deactivation - rather than mixing or other transport effects. In essence, the characteristic time for deactivation should always be the longest (rate-limiting) timescale in an experiment. Similarly, in the ramp experiments, the rate of increase in reactor temperature should not be so fast that the contents of the reactor do not have time to equilibrate to the rapidly changing conditions. The relevant timescales for this experiment (which were defined in Section 2.4.3), using the physical parameters of the system as well as activity and deactivation data from the batch experiments, are shown in Table 5.1.

5.2.5 Modeling Analysis

For each ramp rate, five different deactivation models were used to describe the reaction rate with respect to temperature and time. These five models are shown in Figure 5.1. In the case of all five models, the expression for the modeled reaction rate at any point during the course of an experiment is given by Equation 5-1.

$$r(T,t) = k_{cat}(T,t)[N](T,t) \qquad [5\text{-}1]$$

The functional form of k_{cat} is known (Equation 3.1) and thus its value is easily calculated. However, the quantity [*N*] depends on the history within the reactor (i.e. the cumulative

Table 5.1 Relevant timescales for TEM-1 β-lactamase deactivation study in EMR.

Phenomenon	Characteristic Time	Calculated Value
Chemical Reaction	$\frac{1}{k_{cat}}$	48-590 μs
Reactor Mixing	$\frac{4V}{1.5ND^3}$	32 ms
CSTR Flow	$\frac{V}{Q}$	10 min
Heat Transfer	$\frac{V\rho C_p}{UA}$	47 s
Enzyme Deactivation	$\frac{1}{k_{D,obs}}$	20 min – 10 hr
Reactor Dynamics*	$\frac{\text{seconds per residence time}}{\text{seconds per 1K increase}}$	Guideline: Keep above 1.0

loss of protein to the denatured state as the non-isothermal experiment progresses). Since temperature and time are conveniently coupled in a linear relationship, as in Equation 5-2 where m is equal to the experimentally measured slope of the heating profile, $[N]$ can be reduced to a function of time only.

$$T(t) = T_0 + mt \qquad [5\text{-}2]$$

Even with the above simplification, however, an analytical solution for $[N](t)$ is exceedingly unlikely. Indeed, even with the simplest model (model 1), the expression for $[N]$ as a function of elapsed time t_x is given by Equation 5-3.

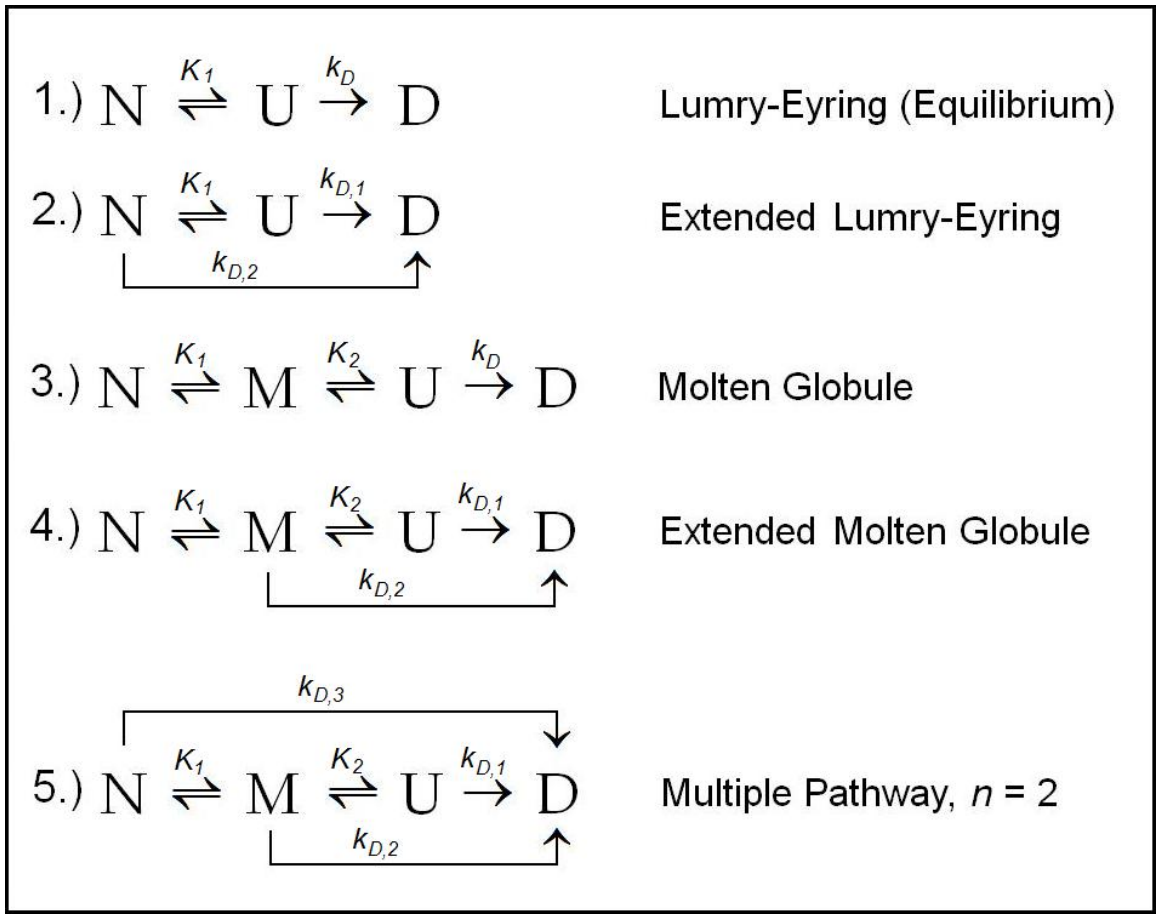

Figure 5.1 Five models of deactivation applied to non-isothermal experiments.

$$[N](t) = \frac{[E]_0 - \int_0^{t_x} k_D(t) K_1(t) [N](t)}{1 + K_1(t)} \qquad [5\text{-}3]$$

Not only are none of the three quantities inside the integral constant with respect to time in these non-isothermal experiments, but the function [*N*](*t*) appears both inside and outside of the integral; its value depends on its own integral in accordance with the notion that its value depends on the reaction history. It is therefore easier to derive a first-order differential equation for [*N*] based on the species balance, which for model 1 takes the form of Equations 5-4 and 5-5.

$$\frac{d[N]}{dt} = \left(\frac{-\frac{dK_1}{dt} - k_D K_1}{1 + K_1} \right) [N] \qquad [5\text{-}4]$$

$$[N]_{t=0} = \frac{[E]_0}{1 + K_1} \qquad [5\text{-}5]$$

In this manner, the value of $[N](t)$ can be numerically evaluated by means of a simple Euler method: using the starting value of $[N]$, approximating $\Delta[N]/\Delta t$ over each sufficiently small 30 s time step via Equation 5-4, and using the result as the model value of $[N]$ at the end point (which is fed as the initial value to the next time step). The modeled reaction rate can then be expressed by Equation 5-1 - but since the experimental data measures the rate and does not directly measure $[N]$, incremental changes in *r(t)* involve application of the chain rule, as in Equation 5-6.

$$\frac{dr}{dt} = k_{cat} \frac{d[N]}{dt} + [N] \frac{dk_{cat}}{dt} \qquad [5\text{-}6]$$

The final expressions for the incremental change in reaction rate with respect to time for each of the five models, as well as the associated initial value $[N]_{t=0}$ used in each numerical approximation, are given in Table 5.2. Note that the derivatives of equilibrium expressions and rate constants appear in each final derivative, but the forms of these derivatives are known and are given by Equations 5-7 and 5-8.

$$\frac{dk_{cat}}{dt} = \frac{k_B m}{h} \left(1 + \frac{\Delta G_{cat}}{RT} \right) \exp\left(-\frac{\Delta G_{cat}}{RT} \right) \qquad [5\text{-}7]$$

$$\frac{dK_i}{dt} = \left(\frac{m\Delta H_i}{RT^2}\right)\exp\left[\frac{\Delta H_i}{R}\left(\frac{1}{T_{m,i}} - \frac{1}{T}\right)\right] \qquad [5\text{-}8]$$

Table 5.2 Expressions for differential change in reaction rate.

Model	$\frac{dr}{dt}$	$[N]_0$
1	$\left[\frac{dk_{cat}}{dt} - k_{cat}\left(\frac{\frac{dK_1}{dt} + k_D K_1}{1 + K_1}\right)\right][N]$	$\frac{[E]_0}{1 + K_1}$
2	$\left[\frac{dk_{cat}}{dt} - k_{cat}\left(\frac{\frac{dK_1}{dt} + k_{D,1}K_1 + k_{D,2}}{1 + K_1}\right)\right][N]$	$\frac{[E]_0}{1 + K_1}$
3	$\left[\frac{dk_{cat}}{dt} - k_{cat}\left(\frac{\frac{dK_1}{dt} + K_1\frac{dK_2}{dt} + K_2\frac{dK_1}{dt} + k_D K_2 K_1}{1 + K_1 + K_2 K_1}\right)\right][N]$	$\frac{[E]_0}{1 + K_1 + K_2 K_1}$
4	$\left[\frac{dk_{cat}}{dt} - k_{cat}\left(\frac{\frac{dK_1}{dt} + K_1\frac{dK_2}{dt} + K_2\frac{dK_1}{dt} + k_{D,1}K_2K_1 + k_{D,2}K_1}{1 + K_1 + K_2 K_1}\right)\right][N]$	$\frac{[E]_0}{1 + K_1 + K_2 K_1}$
5	$\left[\frac{dk_{cat}}{dt} - k_{cat}\left(\frac{\frac{dK_1}{dt} + K_1\frac{dK_2}{dt} + K_2\frac{dK_1}{dt} + k_{D,1}K_2K_1 + k_{D,2}K_1 + k_{D,3}}{1 + K_1 + K_2 K_1}\right)\right][N]$	$\frac{[E]_0}{1 + K_1 + K_2 K_1}$

An Excel routine was written which uses the built in Solver function, based on the Generalized Reduced Gradient (GRG2) nonlinear optimization code,[8] to minimize the sum of residuals squared between the experimental data points and the rate data predicted at each time/temperature point by the respective model. The Excel which was used to create the solver objective function is shown in Appendix B. The following algorithm options were selected: tangent estimates, central derivatives, Newton search. The solver routine was set to terminate when the fitted parameters converged to values which varied less than 0.01 over five consecutive iterations, or when 200 iterations had been attempted, whichever occurred first. Initial guesses for every fitting parameter were supplied to the model, and the best results were achieved when two of the parameters in particular - ΔG_{cat} and the T_m leading to state U - matched well to the experimental data. These two parameters are tied closely to the shape of the reaction profile, as the ΔG_{cat} should give an initial rate which matches the observed rate at the start of the ramp, and the final T_m sets the point at which the sudden drop in rate occurs. Poor initial estimates of these parameters had tremendous effect on the model's degree of fit. Fitting was performed at each of the six scan rates, for each of the five models.

5.3 Results and Discussion

5.3.1 Heuristic *TTN* Estimation

The values of $k_{cat,obs}$ and $k_{d,obs}$ for each of the seven tested temperatures are shown in Table 5.3. The calculated enzyme half-life from $k_{D,obs}$, assuming a first-order deactivation rate law, is also shown for each temperature. Interestingly, the observed initial activity remains relatively constant as the temperature increases from 37°C to 45°C

and clearly does not follow an exponentially increasing Arrhenius-type behavior. This indicates that there is a likely effect of thermodynamic unfolding equilibrium competing with the expected increase in reaction rate. The *TTN* at each temperature was calculated according to the heuristic method of Equation 4-11, and it was observed that there was approximately a three order of magnitude decrease in *TTN* as the temperature increased from 42°C to 54°C. Error bars were not constructed for TTN estimates, as the low temperature runs were only single experiments due to the long duration, but the observed trend in *TTN* vs. temperature was nonetheless very clear.

Table 5.3 *TTN* estimation from 37-57°C using the heuristic approach.

Temperature (K)	$k_{cat,obs}$ (s^{-1})	$k_{D,obs}$ (s^{-1})	half-life (h)	*TTN* (dimensionless)
37	1552	2.28e-06	84.3	6.81e+08
42	1560	4.09e-06	47.1	3.81e+08
45	1476	8.26e-06	23.3	1.79e+08
48	1417	3.84e-05	5.01	3.69e+07
51	1250	1.22e-04	1.58	1.02e+07
54	775	3.30e-04	0.58	2.35e+06
57	440	1.16e-03	0.17	3.79e+05

5.3.2 Accelerated TTN Estimation

All of the non-isothermal temperature ramp modeling results are contained in Appendix C, with representative examples shown in the body of this section for purposes of discussion. The effects of the temperature ramp rate and choice of stability model on the goodness of fit to experimental data are shown in Table 5.4. The values in the table are the average percentage by which the predicted model values of the reaction rate differ from the corresponding experimental values. The fit became slightly worse for all five models as the ramp rate increased to 12 K/h and above. This is due to the fact that at the high temperature portion of these ramps, the reactor effluent still contains product which was produced by enzyme that was still active one residence time before the measurement was taken.

As such, the guideline which was established in Table 5.1 - that the time needed for reactor temperature to increase by 1 K should not be less than one full residence time of the reactor - is manifested in the data. Figure 5.2 illustrates the difference (for model 3 only) between reaction data collected at 2 K/h and 16 K/h, and the corresponding fits to model 3. The deviations occur at the beginning and end of the ramp as expected when there is a delay between CSTR flow and observed deactivation, and notably the enzyme's apparent activity for the 16 K/h ramp is nowhere near zero at the end of the experiment when the reactor temperature is 60°C. Batch experiments confirmed that the enzyme should lose all activity on the order of one minute at 60°C.

Comparing the three- and four-state models at the ramp rate in the middle of the acceptable range (the 4 K/h ramp), it was found that neither of the three-state models

were able to match the experimental data with an accuracy better than 10%. All three of the four-state models 4 and 5, though they contain more parameters, consistently result in fits which are almost indistinguishable from those of model 3 (see Appendix C). The three-state models, on the other hand, are unable to match the rather shallow rate increase (i.e. non-Arrhenius behavior) observed in the low-temperature segment of the experiment. Manually lowering the T_m and the ΔH parameters for these models the four-state models were able to converge equally well such that the fitting error was only about 1%. Models 1 and 3 (at the 4 K/h ramp rate) are used as representative examples in the comparison shown in Figure 5.3.

Table 5.4 Average percentage error of fit for five models, all ramp rates.

Model	1 K/hr	2 K/hr	4 K/hr	8 K/hr	12 K/hr	16 K/hr
1	13.4	13.7	14.8	12.5	10.3	5.6
2	13.3	13.6	14.9	12.7	10.5	5.7
3	1.1	0.7	0.8	1.6	3.9	3.3
4	1.1	0.7	0.9	1.4	1.9	3.5
5	1.0	0.6	1.0	0.9	2.0	3.3

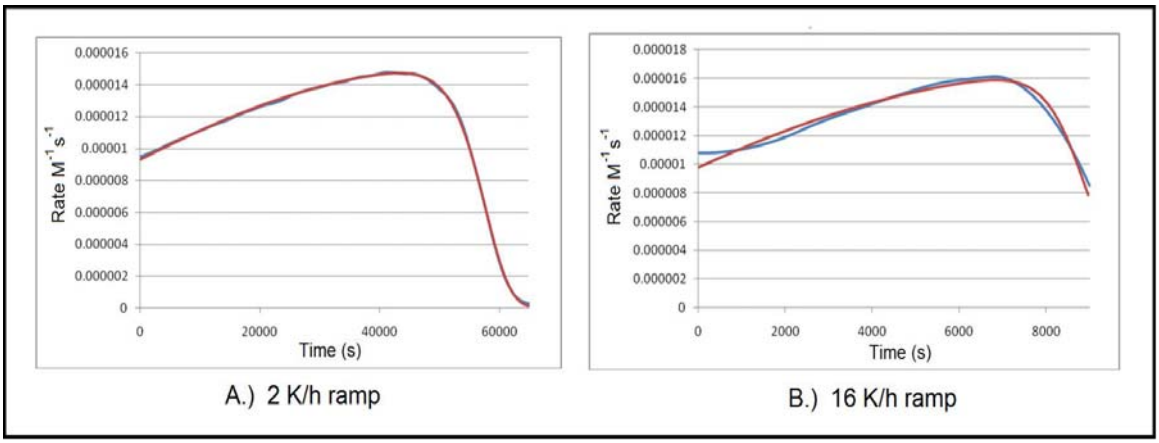

Figure 5.2 Comparison of slow and fast temperature ramp rates, model 3.

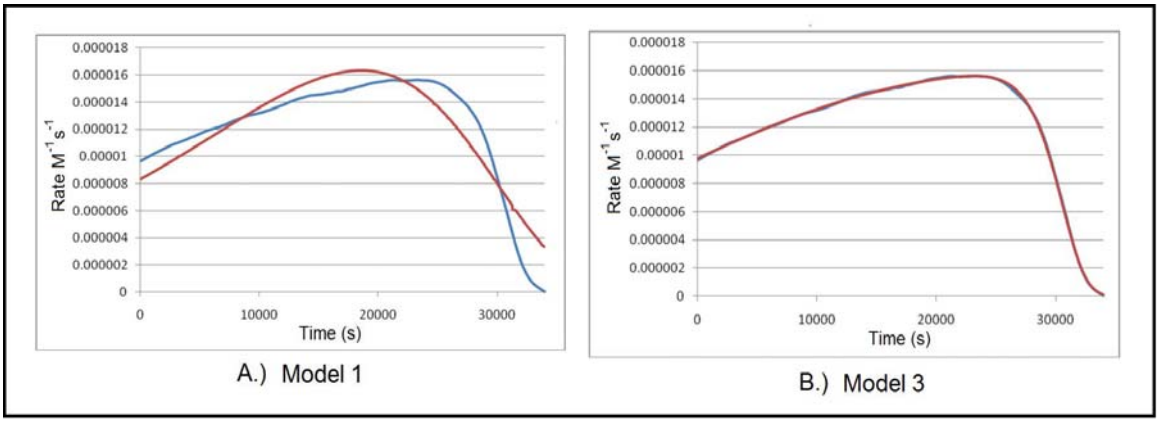

Figure 5.3 Comparison of selected three- and four-state models, 4 K/h ramp.

The four-state models 4 and 5, though they contain more parameters, consistently result in fits which are almost indistinguishable from those of model 3 (see Appendix C). The three-state models, on the other hand, are unable to match the rather shallow rate increase (i.e. non-Arrhenius behavior) observed in the low-temperature segment of the experiment. Manually lowering the T_m and the ΔH parameters for these models (essentially modeling "easier" unfolding) improves the fit of the model at low temperatures but then far underestimates the activity at higher temperatures. Similarly,

setting these parameters higher can bring the model closer to showing sudden deactivation at the end of the ramp, but then indicates almost no deactivation should happen until this transition is reached. These are the consequences of trying to use only one thermodynamic transition in the model when in reality there may be two: the gradual destabilization of the active site which keeps the activity profile flat at low temperatures, and the complete loss of secondary structure once the melting temperature is reached. The effects of the aforementioned manual changes to the fitting parameters are shown in Figure 5.4. This exercise was conducted with the 4 K/h ramp data, model 1.

The fitting parameters achieved by all five models at all scan rates are shown in Table 5.5. Worth noting is that models 1 and 2 resulted in a low level of consistency in the parameters ΔH_1 and $T_{m,1}$, at times even giving values which would indicate the enzyme is 50% thermodynamically unfolded at 234 K, a clearly incorrect result. The four-state models were rather consistent in predicting parameters at ramp rates 8 K/h and slower. There was a significant trend in $T_{m,1}$ - slightly decreasing as the ramp rate increased - which was accompanied by a corresponding decrease in the ΔG_{cat}. The correlation between these two parameters is expected; to match the observed reaction rate at the beginning of the ramp, a decrease in the energy barrier for the enzyme-catalyzed reaction can be offset by a decrease in the temperature at which thermodynamically-controlled inactivation begins. The most likely explanation for the variation between models is that the different scan rate experiments involve slightly different levels of cumulative denatured protein as the experiment progresses and therefore a slightly

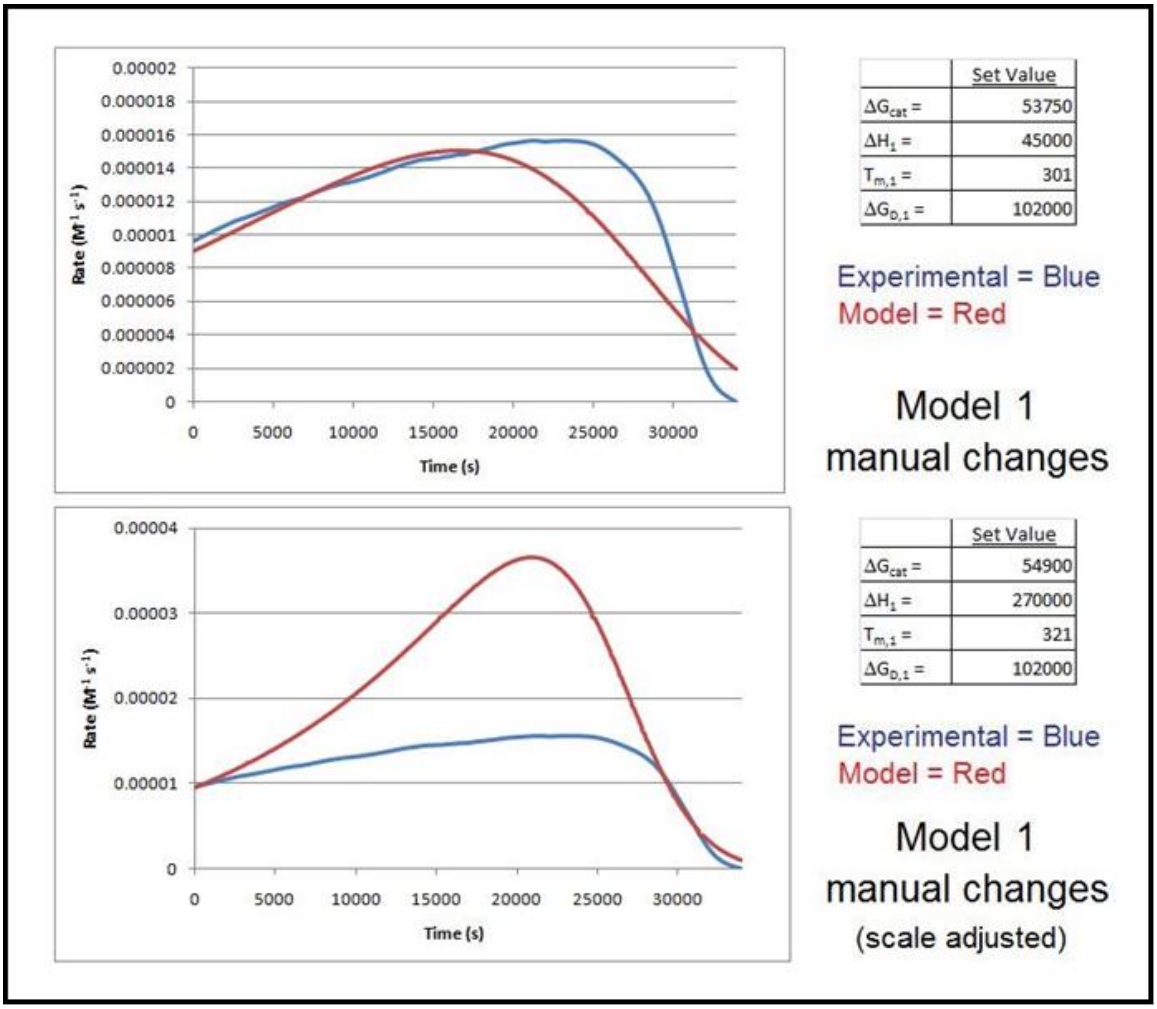

Figure 5.4 Relative inflexibility of model 1 in capturing two deactivation regimes.

different overall rate trajectory in the early part of the ramp before the effects of the second transition dominate. It should be noted that model 3 showed the least variation, predicting the $T_{m,1}$ within 6°C (or, ignoring the 1 K/h ramp, 2°C) at ramp rates 8 K/h and slower.

The agreement of parameter values between models 3, 4, and 5 is quite good, and it was apparent that the addition of denaturation paths from states other than *U* had only slight effect on the estimated parameter values - though these differences can become

Table 5.5 Fitting parameters obtained from five models, all ramp rates.

Model 1		1K	2K	4K	8K	12K	16K
	Gcat	55439.8	54674.94	54528.24	54037.44	47652.77	52003.66
	Hn-u	62690.28	50847.98	53139.68	52564.9	26211.04	41616.37
	Tn-u	319.8839	310.9482	310.1796	303.6407	234.0857	282.4326
	Gu-d	104696	103467.4	102262.9	101643.1	101392.9	101915.9

Model 2		1K	2K	4K	8K	12K	16K
	Gcat	55148.99	54549.72	54502.84	54095.03	50603.05	52323.27
	Hn-u	44361.39	46953.05	52318.41	52589.8	33021.79	43386.8
	Tn-u	319.5883	309.5931	310.0007	304.4645	266.6807	285.8048
	Gu-d	104493	103470.9	102316	101787.3	101363.1	101918.8
	Gn-d	207432.1	116387.1	110557.9	105546.1	116461.4	116398.9

Model 3		1K	2K	4K	8K	12K	16K
	Gcat	54213.65	53579.54	53413.89	53235.45	52792.48	52742.28
	Hn-m	61465.52	61034.18	60914.85	61029.71	61035.54	55789.18
	Tn-m	302.5149	297.8799	297.6601	296.2214	294.612	292.0764
	Hm-u	450109.7	450207.7	450264.9	450210	450203.3	449836.2
	Tm-u	325.6621	326.3339	327.9931	328.0955	328.3317	328.4008
	Gu-d	102838.1	99502.79	97134.55	98894.44	99622.27	103786.2

Model 4		1K	2K	4K	8K	12K	16K
	Gcat	54200.34	53296.55	53105.84	52828.67	50828.85	52825.26
	Hn-m	61154.95	56476.13	56480.43	56525.87	47970.38	56405.26
	Tn-m	302.384	295.1395	294.6866	292.5209	277.8109	292.8186
	Hm-u	450116.1	412759.7	412802.8	412758.1	412573.4	412741.4
	Tm-u	325.7319	327.7147	328.7695	328.688	327.2322	329.6412
	Gu-d	102715.2	97966.87	96515.36	98010.78	103743.8	98311.78
	Gm-d	120040.8	112248.9	112347.7	112240	113581.7	112221.9

Model 5		1K	2K	4K	8K	12K	16K
	Gcat	54137.45	53201.2	53024.18	52749.6	51120.54	52722.85
	Hn-m	60078.22	55806.5	55964.04	55492.87	49044.24	55470.68
	Tn-m	301.7524	294.2653	293.9748	291.7247	280.1408	291.8779
	Hm-u	450116.3	412808.3	412855.8	412688.3	412711	412729.7
	Tm-u	325.5994	327.6572	328.9035	327.8621	327.2967	329.2291
	Gu-d	102946.3	97998.82	96302.09	99548.56	103245.2	99423.16
	Gm-d	121217.4	113121.4	113127.4	113038.3	113971.5	113035.3
	Gn-d	120000.3	120010	120009.6	120010	120019.5	120009.6

magnified when estimating the *TTN* as seen later in this section. At least in the case of $\Delta G_{D,3}$ in model 5, the value did not significantly change from its initial guess (120 kJ/mol) and the same lack of sensitivity was observed when guesses between 100-160 kJ/mol were used. This is evidence that the effects of a direct path from *N* to *D* are unnecessary in model 5; including $\Delta G_{D,3}$ in the model amounts to overparameterization. The parameter $\Delta G_{D,2}$, from *M* to *D*, did vary somewhat from its initial guess (113 kJ/mol in all cases but the 1 K/h ramp which was 120 kJ/mol) but only by about 0.1% indicating the effects of this pathway are also eclisped by more dominant mechanisms. Once again, model 3 was demonstrated to be the model with the fewest parameters which can still produce the same degree of fit as models 4 and 5.

Table 5.6 shows a comparison of *TTN* predictions from all five models at various temperatures, along with calculated values of the thermodynamic and kinetic rate constants, using the data from one of the intermediate ramp speeds (4 K/h). It can be immediately seen that models 1 and 2 predict less than one order of magnitude change in *TTN* as the temperature is varied from 37°C to 54°C. This is an unrealistic result and is in sharp contrast to both the direct *TTN* measurements (presented in the next section) and the short-term batch observations. The *TTN* values predicted by models 3, 4, and 5 agree rather well at higher temperatures, but start to show significant differences at lower temperatures (factor of 40 difference at 37°C, factor of 4 difference at 42°C, factor of 2 or better at all higher temperatures). Model 3 predicts a 73000-fold higher *TTN* at 37°C than at 54°C, while models 4 and 5 both only predict about an 1800-fold increase. As the $k_{cat,obs}$ for all three models agree very closely at low temperatures, the source of this difference is the much smaller $k_{D,obs}$ predicted by model 3 as compared to models 4 and

5. The agreement between all three models and the batch-mode heuristic data worsens as the temperature decreases, again due to differences in $k_{D,obs}$.

To revisit the effects of temperature ramp rate, model 3 *TTN* predictions were examined for all six experimental ramps at six temperatures (Table 5.7). The ramps between 1 K/h and 8 K/h again produced similar results; a factor of 3 or better at all temperatures with best agreement at high temperatures. The 12 K/h ramp widened the error margin to a factor of 7, and the 16 K/h ramp to a factor of 15.

5.3.3 Comparison to Direct TTN Measurement

The actual product yield over the course of the enzyme lifetime was examined at five different tempeartures; the results are shown in Table 5.8 and are compared to the heuristic and accelerated methods. A direct isothermal experiment was attempted at 37°C but was terminated due to instrument failure after approximately 10 days, well before the residual activity of the enzyme was gone. This run was not pursued further due to the very long duration and inefficient use of substrate. Nonetheless, the directly measured *TTN* at 42°C shows that there is already a factor of 2200x change in *TTN* between 42°C and 54°C. This result indicates not only that the heuristic method begins to underestimate *TTN* as the operating temperature becomes more remote from the T_m of the enzyme, but also that the change in *TTN* over this range is better captured by model 3 than by models 4 and 5 (the data for model 3 is shown in Table 5.8).

In summary, both the heuristic batch method and the accelerated temperature ramp method, when used in conjuction with the appropriate model (model 3, at any intermediate scan rate), can be used to predict the actual *TTN* within a factor of 3 at any

Table 5.6 *TTN* prediction from 37-54°C for five models, 4 K/h ramp rate.

Model 1

Temp C	kcat	Kn-u	kinact	kcat,obs	kd.obs	TTN
37	4235	0.998	3.87E-05	2119.62	1.93206E-05	1.10E+08
42	6102	1.385	7.39E-05	2558.491	4.29089E-05	5.96E+07
45	7505	1.676	1.08E-04	2804.559	6.74534E-05	4.16E+07
48	9048	2.021	1.56E-04	2995.035	0.000104361	2.87E+07
51	11027	2.428	2.25E-04	3216.744	0.000159222	2.02E+07
54	13147	2.913	3.21E-04	3359.826	0.000238891	1.41E+07

Model 2

Temp C	kcat	Kn-u	ki n-d	ki u-d	kcat,obs	kd.obs	TTN
37	4277	1.009	1.55E-06	3.79E-05	2128.919861	1.97964E-05	1.08E+08
42	6084	1.394	3.12E-06	7.24E-05	2541.353383	4.34656E-05	5.85E+07
45	7469	1.682	4.68E-06	1.06E-04	2784.862043	6.79087E-05	4.10E+07
48	9135	2.022	6.97E-06	1.53E-04	3022.832561	0.000104478	2.89E+07
51	11132	2.423	1.03E-05	2.20E-04	3252.118025	0.000158458	2.05E+07
54	13543	2.899	1.52E-05	3.15E-04	3473.454732	0.000237888	1.46E+07

Model 3

Temp C	kcat	Kn-m	Km-u	kinact	kcat,obs	kd.obs	TTN
37	6524	2.693	7.46E-05	2.83E-04	1766.489323	1.53746E-08	1.15E+11
42	9219	3.922	0.001202	5.21E-04	1871.226855	4.98627E-07	3.75E+09
45	11273	4.88	0.00605	7.48E-04	1907.598649	3.73851E-06	5.10E+08
48	13734	6.048	0.02954	1.06E-03	1900.463555	2.62796E-05	7.23E+07
51	16674	7.466	0.1423	1.50E-03	1749.924368	0.000167472	1.04E+07
54	20211	9.2	0.6558	2.11E-03	1245.028756	0.000785698	1.58E+06

Model 4

Temp C	kcat	Kn-m	Km-u	ki m-d	ki u-d	kcat,obs	kd.obs	TTN
37	7352	3.154	0.000115	7.75E-07	3.59E-04	1769.705852	6.19372E-07	2.86E+09
42	10369	4.47	0.00147	1.57E-06	6.63E-04	1893.338037	2.07632E-06	9.12E+08
45	12665	5.475	0.00647	2.38E-06	9.46E-04	1945.342033	7.14566E-06	2.72E+08
48	15414	6.679	0.0277	3.57E-06	1.34E-03	1960.069142	3.45778E-05	5.67E+07
51	18693	8.12	0.1154	5.31E-06	1.89E-03	1858.696508	0.000180291	1.03E+07
54	22634	9.854	0.4751	7.88E-06	2.66E-03	1456.908547	0.000805074	1.81E+06

Model 5

Temp C	kcat	Kn-m	Km-u	ki n-d	ki m-d	ki u-d	kcat,obs	kd.obs	TTN
37	7588	3.299	0.000108	3.97E-08	5.72E-07	3.90E-04	1764.915234	4.8082E-07	3.67E+09
42	10697	4.66	0.001382	8.46E-08	1.17E-06	7.19E-04	1887.781354	1.793E-06	1.05E+09
45	13063	5.697	0.006082	1.31E-07	1.77E-06	1.03E-03	1940.534882	6.795E-06	2.86E+08
48	15893	6.938	0.026	2.02E-07	2.66E-06	1.45E-03	1957.654648	3.4565E-05	5.66E+07
51	19268	8.419	0.1085	3.09E-07	3.98E-06	2.05E-03	1864.802496	0.00018406	1.01E+07
54	23324	10.199	0.447	4.71E-07	5.91E-06	2.87E-03	1480.141488	0.00083447	1.77E+06

Table 5.7 *TTN* prediction from 37-54°C for all ramp rates, model 3.

1 K/hr

	kcat	Kn-m	Km-u	kinact	kcat,obs	kd.obs	TTN
37	4788	1.825	0.0002453	3.10E-05	1694.599	4.90857E-09	3.45E+11
42	6791	2.664	0.003912	5.93E-05	1848.182	1.68133E-07	1.10E+10
45	8330	3.325	0.01972	8.66E-05	1897.248	1.29314E-06	1.47E+09
48	10185	4.129	0.09681	1.26E-04	1842.196	9.08814E-06	2.03E+08
51	12402	5.108	0.4596	1.81E-04	1466.714	5.02809E-05	2.92E+07
54	15055	6.297	2.056	2.60E-04	743.6907	0.000165961	4.48E+06

2 K/hr

	kcat	Kn-m	Km-u	kinact	kcat,obs	kd.obs	TTN
37	6121	2.651	0.0001735	1.13E-04	1676.316	1.42212E-08	1.18E+11
42	8649	3.859	0.002771	2.12E-04	1776.087	4.64649E-07	3.82E+09
45	10586	4.806	0.01399	3.06E-04	1802.414	3.49732E-06	5.15E+08
48	12910	5.961	0.06851	4.38E-04	1751.842	2.42781E-05	7.22E+07
51	15688	7.372	0.3258	6.24E-04	1456.125	0.000139153	1.05E+07
54	19015	9.072	1.517	8.85E-04	797.8024	0.000511127	1.56E+06

4 K/hr

	kcat	Kn-m	Km-u	kinact	kcat,obs	kd.obs	TTN
37	6524	2.693	0.00007461	2.83E-04	1766.489	1.53746E-08	1.15E+11
42	9219	3.922	0.001202	5.21E-04	1871.227	4.98627E-07	3.75E+09
45	11273	4.88	0.00605	7.48E-04	1907.599	3.73851E-06	5.10E+08
48	13734	6.048	0.02954	1.06E-03	1900.464	2.62796E-05	7.23E+07
51	16674	7.466	0.1423	1.50E-03	1749.924	0.000167472	1.04E+07
54	20211	9.2	0.6558	2.11E-03	1245.029	0.000785698	1.58E+06

8 K/hr

	kcat	Kn-m	Km-u	kinact	kcat,obs	kd.obs	TTN
37	6997	3.044	0.00007144	1.43E-04	1730.125	7.68931E-09	2.25E+11
42	9866	4.431	0.00114	2.67E-04	1814.92	2.48197E-07	7.31E+09
45	12053	5.514	0.005723	3.84E-04	1841.402	1.85274E-06	9.94E+08
48	14730	6.865	0.0288	5.53E-04	1826.929	1.35679E-05	1.35E+08
51	17866	8.474	0.1362	7.86E-04	1681.006	8.53118E-05	1.97E+07
54	21594	10.421	0.626	1.11E-03	1203.374	0.000402801	2.99E+06

12 K/hr

	kcat	Kn-m	Km-u	kinact	kcat,obs	kd.obs	TTN
37	8291	3.22	0.00003538	1.07E-04	1964.639	2.8993E-09	6.78E+11
42	11668	5.067	0.001002	2.02E-04	1921.583	1.68734E-07	1.14E+10
45	14251	6.315	0.005084	2.92E-04	1939.675	1.27555E-06	1.52E+09
48	17342	7.838	0.02502	4.19E-04	1919.614	9.09973E-06	2.11E+08
51	21029	9.69	0.1196	5.98E-04	1774.76	5.8509E-05	3.03E+07
54	25411	11.933	0.5556	8.48E-04	1298.933	0.000287391	4.52E+06

16 K/hr

	kcat	Kn-m	Km-u	kinact	kcat,obs	kd.obs	TTN
37	8483	3.82	0.00006244	2.15E-05	1759.871	1.06438E-09	1.65E+12
42	11872	5.361	0.0009588	4.11E-05	1864.866	3.31444E-08	5.63E+10
45	14543	6.577	0.004985	6.06E-05	1911.092	2.61178E-07	7.32E+09
48	17748	7.976	0.02361	8.76E-05	1936.643	1.80005E-06	1.08E+09
51	21419	9.712	0.1155	1.28E-04	1809.995	1.20954E-05	1.50E+08
54	25955	11.783	0.5172	1.82E-04	1374.941	5.87233E-05	2.34E+07

temperature between 45-54°C (i.e., the uppermost 10°C of this enzyme's operable range). At lower temperatures, the continuous non-isothermal modeling approach appears to be more favorable than the heuristic method both in terms of *TTN* prediction accuracy and the length of the necessary experiments. Therefore, the heuristic method is an attractive option when the desired operating temperature is near the anticipated upper limit of the enzyme's thermal stability range since it involves relatively short experiments which require only common equipment, low amounts of substrate, and no reactor design concerns. When the enzyme is to be operated in the regime where it is expected to be stable for weeks or months, or when the required operating temperature is unspecified, the accelerated modeling approach should be used in every case.

Table 5.8 Comparison of heuristic and modeling *TTN* estimations to directly measured *TTN* values at selected temperatures.

Temp (°C)	Heuristic (batch)	Direct (EMR)	Modeling (ramps)[&]
37	6.81E+08	X	1.15E+11
42	3.81E+08	1.62E+09	3.75E+09
45	1.79E+08	4.18E+08	5.10E+08
48	3.69E+07	8.88E+07	7.23E+07
51	1.02E+07	1.39E+07	1.04E+07
54	2.35E+06	7.39E+05	1.58E+06

5.4 Conclusions

We have presented two approaches for circumventing the need to directly measure the total product yield of a biocatalyst over the entire duration of its lifetime. Both methods resulted in *TTN* estimations that were well within one order of magnitude of the results obtained through the direct measurements (which, especially at low temperatures, are exceedingly slow and potentially troublesome in terms of limited equipment reliability and high substrate consumption). This level of accuracy renders these methods useful for quick estimates of biocatalyst stability, including estimations of their costs, especially with regard to initial screening of libraries of enzymes which are potential candidates to be used as the biocatalyst in an industrial process.

The relative strengths of each of the two presented methods are apparent. The heuristic approach of collecting $k_{cat,obs}$ and $k_{D,obs}$ values is favored when the process temperature is approximately known (so that repeated experiments at multiple temperatures are not required) and when that temperature is near the anticipated upper limit of the enzyme's stability (so that the duration of the deactivation experiments are reasonably short). Even if the intended process temperature is low, the protein engineer can quickly obtain a *TTN* estimate for the enzyme if its specific activity and half-life data have already been obtained or are available in the literature.

The non-isothermal temperature ramp modeling approach is most useful when the enzyme is to be used at a process temperature well under its anticipated stability limit, or when the process temperature is unknown. By evaluating the intrinsic thermodynamic and kinetic parameters of the biocatalyst through modeling, one can then predict the *TTN*

at any desired temperature. An additional benefit of the modeling approach is that if the exact deactivation mechanism of an enzyme is not known, multiple stability models can be examined, as shown in this work, and the model which is able to accurately fit the data with the fewest parameters can be selected.

5.5 Publication Information

This work presented in Chapter 5 of this dissertation has been submitted as a manuscript to *Biotechnology and Bioengineering* with my thesis advisor, Andreas S. Bommarius, as co-author.

5.6 References

1. Rogers, T.A. and Bommarius, A.S., *Utilizing simple biochemical measurements to predict lifetime output of biocatalysts in continuous isothermal processes*. Chemical Engineering Science, 2010. **65**(6): 2118-2124.

2. Gardossi, L., Poulsen, P.B., Ballesteros, A., Hult, K., Svedas, V.K., Vasic-Racki, D., Carrea, G., Magnusson, A., Schmid, A., Wohlgemuth, R., and Halling, P.J., *Guidelines for reporting of biochemical reactions*. Trends in Biotechnology, 2010. **28**(4): 171-180.

3. Daniel, R.M., Danson, M.J., and Eisenthal, R., *The temperature optima of enzymes; a new perspective on an old phenomenon*. Trends in Biochemical Sciences, 2001. **26**: 223-225.

4. Gibbs, P.R., Uehara, C.S., Neunert, U., and Bommarius, A.S., *Accelerated Biocatalyst Stability Testing for Process Optimization.* Biotechnology Progress, 2005. **21**(3): 762–774.

5. Wojciechowski, B.W., *The temperature scanning reactor I: Reactor types and modes of operation.* Catalysis Today, 1997. **36**: 167-190.

6. van Tilburg, R. and Roels, J.A., *An improved productivity and stability test for immobilized enzymes with reference to glucose isomerase*. Starch, 1982. 34(4): 134-140.

7. Rachinskiy, K., Schultze, H., Boy, M., Bornscheuer, U., and Büchs, J., *"Enzyme Test Bench" a high-throughput enzyme characterization technique including the long-term stability.* Biotechnology and Bioengineering, 2009. 103(2): 305-322.

8. Fylstra, D., Lasdon, L., Watson, J., and Waren, A., *Design and Use of the Microsoft Excel Solver*. INTERFACES, 1998. 28(5): 29-55.

CHAPTER 6

CONCLUSION AND RECOMMENDATIONS

Highly stable biocatalysts, though they are ultimately very good news in the context of large-scale bioprocesses, can present certain challenges for the protein engineers who develop them. The very same quality that renders an enzyme desirable to use in a long-term process makes it expensive, time-consuming, and potentially difficult to directly measure and document the enzyme's lifetime productivity. We have presented two distinct methods for obtaining accurate estimates of a biocatalyst's total turnover number, both of which can potentially circumvent many hundreds of hours of stability characterization as compared to direct measurement.

The comparison of the isothermal batch-mode experimental techniques (fitted to the Equilibrium Model) to the non-isothermal continuous-mode experiments (fitted to the molten globule model) in Chapter 3 elucidated the importance of timescale in enzyme deactivation experiments. Effects which may not be easily observed during assays a few minutes in duration could manifest themselves in a much more significant way in an experiment lasting for hours or days. Despite a few differences in the numerical results, both methods showed conclusively that TEM-1 β-lactamase is an enzyme which does not obey the classical Lumry-Eyring model and provides contrary evidence to the widespread belief that enzymes should operate at temperatures just below their melting point for peak performance. In general, the collaboration with the Daniel lab has made us keenly aware

of the concept of temperature optima and that deactivation and unfolding are clearly not synonymous in all cases.

The development of the heuristic method in Chapter 4 begins with the most generalizable model of enzyme deactivation and mathematically reduces it to a very simple expression, with two terms that correspond to easily measurable experimental values, for estimating a biocatalyst total turnover number. We have demonstrated the applicability of this method in selecting the best candidate from a small assortment of similarly thermostable enzymes, and have verified the method through comparison to directly measured *TTN* values of the mesophilic TEM-1 β-lactamase. The heuristic method is still somewhat limited, as we demonstrate, when a catalyst is being tested at temperatures far below its upper stability limit. To obtain an accurate value of $k_{D,obs}$ through simple residual activity measurements, one should expose a biocatalyst to the denaturing condition for at least three half-lives to ensure a good fit to an exponential decay rate law. For highly stable catalysts, the required experiments become prohibitively long and the direct measurement option starts to appear more competitive.

Suggestions for future work related to the heuristic model are i.) perform the heuristic estimation vs. direct *TTN* measurement approach on a variety of different enzymes which exhibit overall first-order kinetic deactivation, to assess its generalizability and ii.) determine the magnitude of error that arises when non-first-order mechanisms such as aggregation or subunit interactions are present and, if necessary, develop analogous heuristic expressions which can be used when these mechanisms are confirmed or expected. While these multiple-mechanism heuristics will not be reducible

to such an elegant form as Equation 4-11 and will require additional enzyme-specific information about the non-thermal deactivation routes, they could nonetheless be useful.

The work presented in Chapter 5 is the capstone piece to our study of both accelerated non-isothermal methods and heuristic estimations from $k_{cat,obs}$ and $k_{D,obs}$. To our knowledge, it is the only study to date which subjects a soluble enzyme (not immobilized, as this can alter or obscure enzyme stability parameters) to an accelerated, continuous, non-isothermal deactivation experiment and then directly compares *TTN* predictions to the results of complete isothermal deactivation studies also performed in continuous mode. The examination of several stability models in conjunction with the temperature ramp studies, ranging from the simple three-state Lumry-Eyring model to the highly generalized four-state model with irreversible denaturation pathways available from each of the first three states, demonstrates how an assessment of the goodness of model fit can be used to select the model which will best predict the true *TTN*.

Aside from the logical recommendation that the continuous EMR temperature ramp method be tested on other soluble enzymes, especially ones which we suspect may have a temperature optimum far below their melting temperature (as indicated by an attenuated rise in specific activity through the temperature range preceding T_m), we would like to further investigate the mathematical model fitting techniques. The Euler-type numerical integration used in Chapter 5 should have a high degree of accuracy due to the small time step made possible by our novel in-line polarimetric assay. However, the experimental data to which the model must be fitted (here, reaction rate) is in reality the solution to a complex function involving the unobservable state [*N*]. Theoretically, the concentration of native enzyme remaining in the reactor could be directly measured

by absorbance or fluorescence, but this would require an extremely complicated experimental setup. One potential avenue for improving the models is to use nonlinear state estimation,[1,2] which has demonstrated utility in systems where the observable instrument output is governed by one or more nonlinear differential equations involving a non-observed system state that depends on system inputs (in our case, reactor temperature) and time. Again, while our current numerical fits are already very good (less than 1% error on the four-state models) it may be interesting to use the nonlinear estimation approach to independently follow the changes in activity and cumulative denaturation through the course of a temperature ramp.

The two rapid *TTN* estimation methods described in our work were shown to eliminate the need for the third method (direct measurement over entire enzyme lifetime) which should only be used in the very late stages of biocatalyst screening and selection to confirm the accuracy of the heuristic or modeling methods. The heuristic method is particularly useful when published half-life and specific activity data are already known, or when the *TTN* estimation only needs to be carried out at one temperature which is in the vicinity of the enzyme's upper stability limit. The modeling approach takes the results from a single experiment and generates an estimate for *TTN* for any desired temperature, avoiding the need for an array of isothermal deactivation experiments, and can even be used to gain information about the true deactivation mechanism that takes into account both thermodynamic and kinetic enzyme stability.

References

1. Tatiraju, S., Soroush, M., and Ogunnaike, B.A., *Multirate nonlinear state estimation with application to a polymerization reactor*. AIChE Journal, 2004. **45**(4): 769-780.

2. Alvarez, J., *Nonlinear state estimation with robust convergence*. Journal of Process Control, 2000. **10**(1), 59-71.

APPENDIX A

RIGOROUS MATHEMATICAL DERIVATION OF THE HEURISTIC TOTAL TURNOVER ESTIMATION METHOD

Demonstrated herein is the complete derivation for $[N](t)$, the concentration of native, active enzyme remaining at time t during an isothermal process, based on the multiple pathway deactivation model in Figure 4.5. Firstly, a mass balance is performed on all enzyme species that occupy any of the different conformations including a number n of stable intermediates. Assuming a closed system with constant volume, the mass balance takes the form of Equation A1, where $[E]_0$ is the initial concentration of enzyme in the system. Next, the definitions of the equilibrium constants are applied to the mass balance. The concentration of each of the intermediate states may then be written in terms of $[N]$. For example, since $K_1 = [I_1]/[N]$ such that $[I_1] = K_1[N]$ and furthermore $K_2 = [I_2]/[I_1]$ such that $[I_2] = K_2[I_1] = K_2K_1[N]$, the mass balance can be rewritten as Equation A2 and then factored as in Equation A3. The resulting expression is then condensed using summation notation according to Equation A4.

$$[E]_0 = [N] + [I_1] + [I_2] \ldots + [I_{n-1}] + [I_n] + [D] \qquad \text{[A1]}$$

$$[E]_0 = [N] + K_1[N] + K_1K_2[N] \ldots + \left(\prod_{i=1}^{n-1} K_i\right)[N] + \left(\prod_{i=1}^{n} K_i\right)[N] + [D] \qquad \text{[A2]}$$

$$[E]_0 = \left(1 + K_1 + K_1K_2 + \ldots \prod_{i=1}^{n-1} K_i + \prod_{i=1}^{n} K_i\right)[N] + [D] \qquad [A3]$$

$$[E]_0 = \left(1 + \sum_{j=1}^{n} \prod_{i=1}^{j} K_i\right)[N] + [D] \qquad [A4]$$

Each of the transition equilibria is treated as a van't Hoff relationship in which the equilibrium constant K_n depends on temperature as well as the parameters T_n (the temperature at which $[I_n]/[I_{n-1}]$ equals unity) and ΔH_n (the enthalpy change associated with the transition from I_{n-1} to I_n). The van't Hoff relationship is shown in Equation A5, where R is the gas constant. It is hereby assumed that at the initial time $t = 0$, the equilibria between the native and intermediate states are rapidly (essentially instantaneously) established and that none of the enzyme has yet decayed to a denatured state. This leads to the initial condition shown in Equation A6.

$$K_n = e^{\frac{\Delta H_n}{R}\left(\frac{1}{T_n} - \frac{1}{T}\right)} \qquad [A5]$$

$$[N]_{t=0} = \frac{[E]_0}{1 + \sum_{j=1}^{n} \prod_{i=1}^{j} K_i} \qquad [A6]$$

To establish the time dependence of $[N]$, Equation A4 is differentiated with respect to time as shown in Equation A7. Since all equilibrium constants are functions of temperature according to the van't Hoff relationship and should not vary with time in an isothermal process, they need not be differentiated.

$$0 = \left(1 + \sum_{j=1}^{n} \prod_{i=1}^{j} K_i\right) \frac{d[N]}{dt} + \frac{d[D]}{dt} \qquad [A7]$$

The rate of accumulation of denatured enzyme is then assumed to equal the sum of the contributions from all native and intermediate states (which is valid if all pathways to D in Figure 4.5 obey first-order kinetics). Each of the first-order decay processes is assumed to have a rate constant $k_{D,n}$ which may be modeled by thermodynamic transition state theory as in Equation A8. Here, k_B = Boltzmann constant, h = Planck's constant, R = gas constant, and ΔG_n is the Gibbs free enthalpy change upon I_n transitioning to a denatured state. These deactivation rate constants, which are functions of temperature, are assumed to remain constant for the duration of an isothermal process.

$$k_{D,n} = \frac{k_B T}{h} e^{-\frac{\Delta G_n}{RT}} \qquad [A8]$$

The total rate of accumulation is shown in Equation A9 which can be put in terms of [N] by again applying the definitions of the equilibrium constants, leading to Equation A10. Summation notation is then used to condense the expression according to Equation A12.

$$\frac{d[D]}{dt} = k_{D,0}[N] + k_{D,1}[I_1] + k_{D,2}[I_2] + \ldots k_{D,n-1}[I_{n-1}] + k_{D,n}[I_n] \qquad [A9]$$

$$\frac{d[D]}{dt} = k_{D,0}[N] + k_{D,1}K_1[N] + k_{D,2}K_1K_2[N] + \ldots k_{D,n-1}\left(\prod_{i=1}^{n-1} K_i\right)[N] + k_{D,n}\left(\prod_{i=1}^{n} K_i\right)[N] \qquad [A10]$$

$$\frac{d[D]}{dt} = \left(k_{D,0} + k_{D,1}K_1 + k_{D,2}K_1K_2 + \ldots k_{D,n-1}\prod_{i=1}^{n-1} K_i + k_{D,n}\prod_{i=1}^{n} K_i\right)[N] \qquad [A11]$$

$$\frac{d[D]}{dt} = \left(k_{D,0} + \sum_{j=1}^{n} k_{D,j} \prod_{i=1}^{j} K_i \right) [N] \qquad \text{[A12]}$$

Equations A7 and A12 are combined to form Equation A13, and rearrangement yields the first-order differential equation in Equation A14. Since the coefficient is a constant under isothermal conditions, the system may be solved via separation of variables using the initial condition already set forth in Equation A6. The particular solution is therefore given by Equation A15.

$$0 = \left(1 + \sum_{j=1}^{n} \prod_{i=1}^{j} K_i \right) \frac{d[N]}{dt} + \left(k_{D,0} + \sum_{j=1}^{n} k_{D,j} \prod_{i=1}^{j} K_i \right) [N] \qquad \text{[A13]}$$

$$\frac{d[N]}{dt} = -\left(\frac{k_{D,0} + \sum_{j=1}^{n} k_{D,j} \prod_{i=1}^{j} K_i}{1 + \sum_{j=1}^{n} \prod_{i=1}^{j} K_i} \right) [N] \qquad \text{[A14]}$$

$$[N](t) = \left(\frac{[E]_0}{1 + \sum_{j=1}^{n} \prod_{i=1}^{j} K_i} \right) e^{-\left(\frac{k_{D,0} + \sum_{j=1}^{n} k_{D,j} \prod_{i=1}^{j} K_i}{1 + \sum_{j=1}^{n} \prod_{i=1}^{j} K_i} \right) t} \qquad \text{[A15]}$$

APPENDIX B

SAMPLE CALCULATION: MICROSOFT EXCEL CODE

Shown below is the spreadsheet programming for Model 5 which uses the differential approximation listed in Table 5.2. The simpler models, 1-4, rely on the same method but blocks are deleted when the parameter does not exist within the particular model. The cells which contain adjustable parameter values are in bold and the objective cell of the built-in Generalized Reduced Gradient (GRG2) solver routine is underlined.

Fixed Value Cells

Z3 = 1.38065E-23 Boltzmann constant
Z4 = 6.62607E-34 Planck constant
Z5 = 8.31447 Gas constant
Z10 = 8.228E-9 Initial enzyme loading, M

Adjustable Cells

Z15 = Gcat, initial guess
Z16 = H1, initial guess
Z17 = Tm1, initial guess
Z18 = H2, initial guess
Z19 = Tm2, initial guess
Z20 = Gd1, initial guess
Z21 = Gd2, initial guess
Z22 = Gd3, initial guess

Objective Cell

Z27 = SUM(U:U) sum of residuals squared

Column Formulas

A: <time data, seconds>

B: <temp data, Kelvin>

C: <rate data, M^{-1} s^{-1}>

D: =($Z$3/$Z$4)*B1*EXP(-$Z$15/($Z$5*B1)) kcat value

E: =($Z$3/$Z$4)*((B2-B1)/(A2-A1))*EXP($Z$15/($Z$5*B1))
*(1+($Z$15/($Z$5*B1))) dkcat/dt value

F: =EXP(($Z$16/$Z$5)*((1/$Z$17)-(1/B1))) K1 value

G: =((B2-B1)/(A2-A1))*($Z$16/$Z$5)*(1/(B1^2))*EXP(($Z$16/$Z$5)
*((1/$Z$17)-(1/B1))) dK1/dt value

H: =EXP(($Z$18/$Z$5)*((1/$Z$19)-(1/B1))) K2 value

I: =((B2-B1)/(A2-A1))*($Z$18/$Z$5)*(1/(B1^2))*EXP(($Z$18/$Z$5)
*((1/$Z$19)-(1/B1))) dK2/dt value

J: =($Z$3/$Z$4)*B1*EXP(-$Z$20/($Z$5*B1)) kd1 value

K: =($Z$3/$Z$4)*B1*EXP(-$Z$21/($Z$5*B1)) kd2 value

L: =($Z$3/$Z$4)*B1*EXP(-$Z$22/($Z$5*B1)) kd3 value

M (first row): =$Z$10/(1+F1+(F1*H1)) initial condition N t=0

M (all other rows): =Q(n-1) where n = current row number, result for N after
previous time step

N: =M1*D1 rate before

O: =M1*(E1-D1*(G1+F1*I1+H1*G1+F1*H1*J1+K1*F1+L1)/(1+F1+F1*H1))
differential change

P: =N1+(A2-A1)*O1 rate after

Q: =P1/D2 native enzyme after, feed to cell M of next row

R: =Q1*F1 molten enzyme after

S: =Q1*F1*H1 unfolded enzyme after

T: =$Z$10-Q1-R1-S1 denatured enzyme after, from species balance

U: =(C1-N1)^2 exp - model residual squared

APPENDIX C

TEMPERATURE RAMP MODELING RESULTS: FIVE MODELS, ALL RAMP RATES

Appendix C.1 Model Fits for 1 K/h Temperature Ramp Experiments

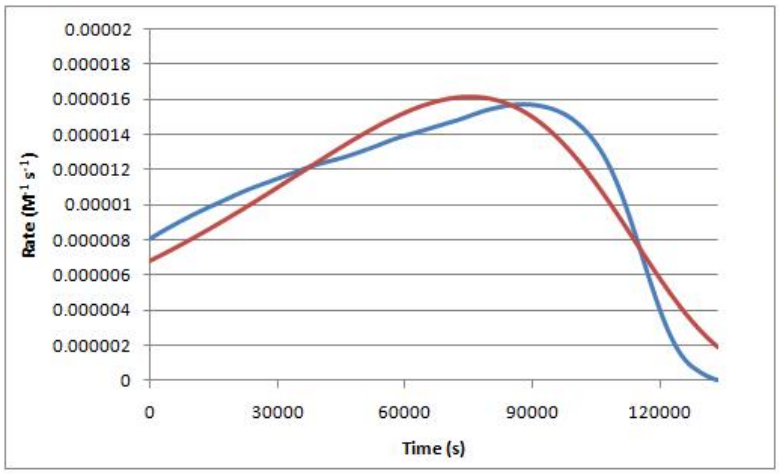

	Model	Guess
ΔG_{cat} =	55439.80	55000
ΔH_1 =	62690.28	70000
$T_{m,1}$ =	319.88	320
$\Delta G_{D,1}$ =	104695.98	100000

Experimental = Blue

Model = Red

Model 1

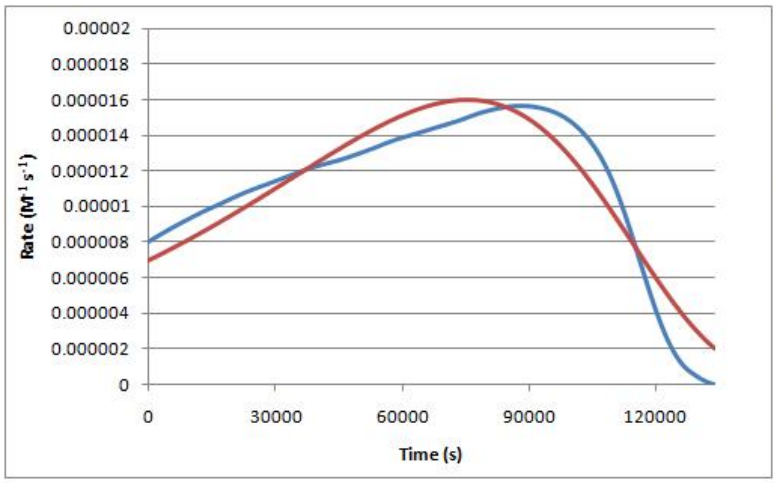

	Model	Guess
ΔG_{cat} =	55148.99	55000
ΔH_1 =	44361.39	70000
$T_{m,1}$ =	319.59	320
$\Delta G_{D,1}$ =	104492.99	100000
$\Delta G_{D,2}$ =	207432.06	200000

Experimental = Blue

Model = Red

Model 2

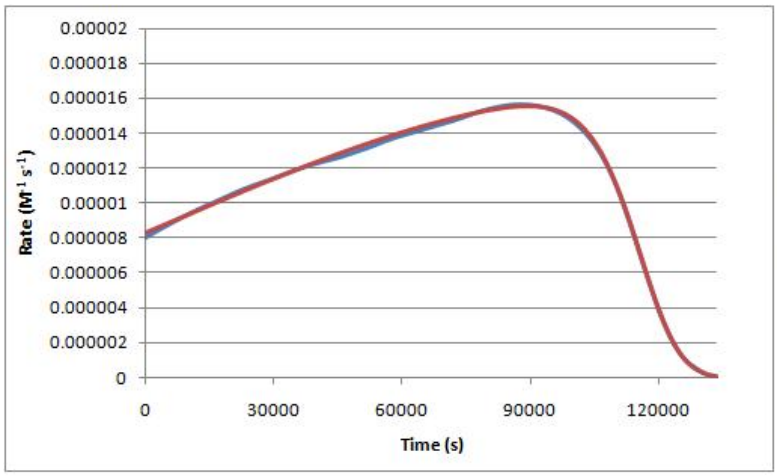

	Model	Guess
ΔG_{cat} =	54213.65	55000
ΔH_1 =	61465.52	70000
$T_{m,1}$ =	302.51	307
ΔH_2 =	450109.70	500000
$T_{m,2}$ =	325.66	325
$\Delta G_{D,1}$ =	102838.11	105000

Experimental = Blue

Model = Red

Model 3

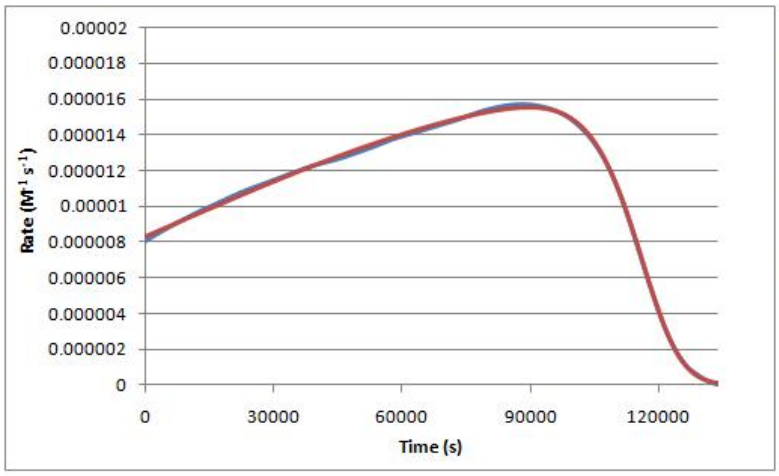

	Model	Guess
ΔG_{cat} =	54200.34	55000
ΔH_1 =	61154.95	70000
$T_{m,1}$ =	302.38	307
ΔH_2 =	450116.08	500000
$T_{m,2}$ =	325.73	325
$\Delta G_{D,1}$ =	102715.17	105000
$\Delta G_{D,2}$ =	120040.84	120000

Experimental = Blue

Model = Red

Model 4

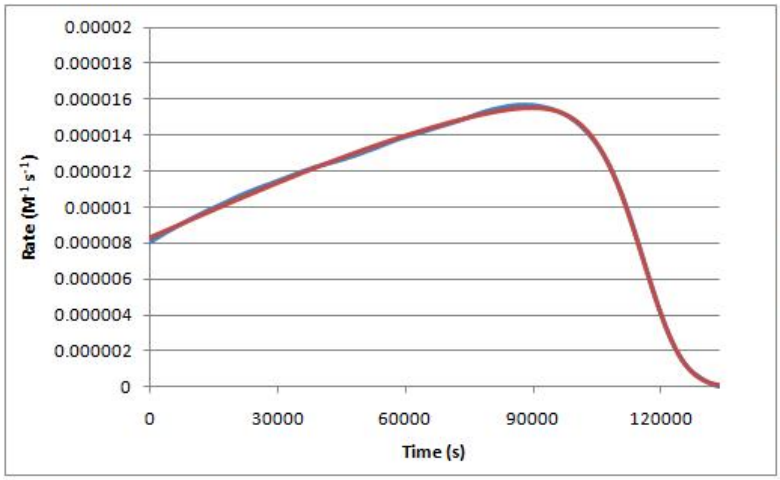

	Model	Guess
ΔG_{cat} =	54137.45	55000
ΔH_1 =	60078.22	70000
$T_{m,1}$ =	301.75	307
ΔH_2 =	450116.25	500000
$T_{m,2}$ =	325.60	325
$\Delta G_{D,1}$ =	102946.27	105000
$\Delta G_{D,2}$ =	121217.45	120000
$\Delta G_{D,3}$ =	140000.27	140000

Experimental = Blue

Model = Red

Model 5

Appendix C.2 Model Fits for 2 K/h Temperature Ramp Experiments

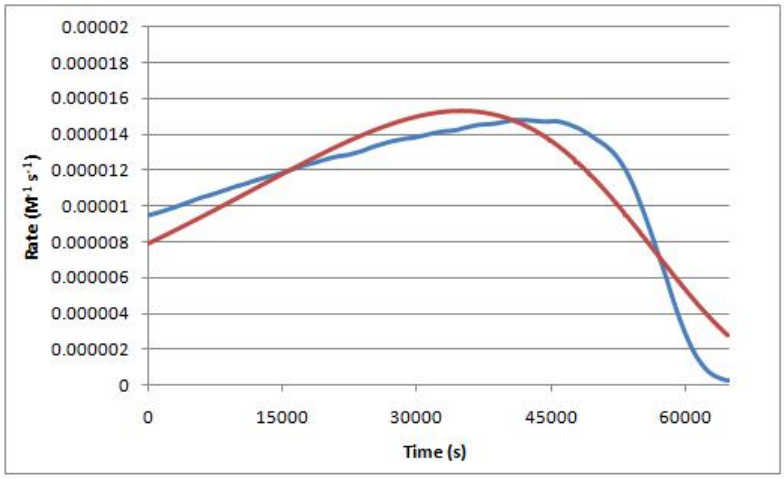

	Model	Guess
ΔG_{cat} =	54674.94	55000
ΔH_1 =	50847.98	70000
$T_{m,1}$ =	310.95	310
$\Delta G_{D,1}$ =	103467.43	100000

Experimental = Blue
Model = Red

Model 1

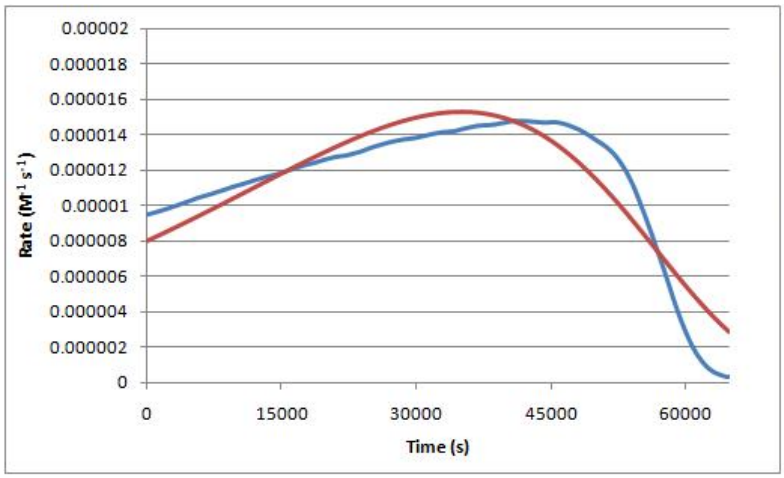

	Model	Guess
ΔG_{cat} =	54549.72	55000
ΔH_1 =	46953.05	70000
$T_{m,1}$ =	309.59	310
$\Delta G_{D,1}$ =	103470.86	100000
$\Delta G_{D,2}$ =	116387.07	120000

Experimental = Blue
Model = Red

Model 2

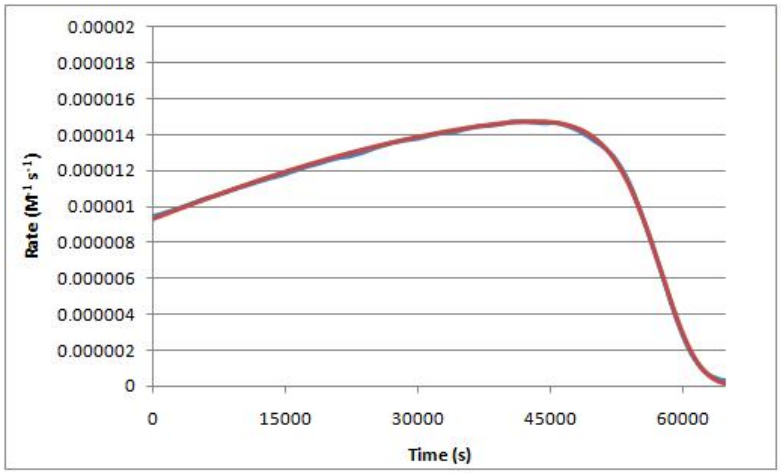

	Model	Guess
ΔG_{cat} =	53579.54	55000
ΔH_1 =	61034.18	70000
$T_{m,1}$ =	297.88	300
ΔH_2 =	450207.75	500000
$T_{m,2}$ =	326.33	325
$\Delta G_{D,1}$ =	99502.79	105000

Experimental = Blue
Model = Red

Model 3

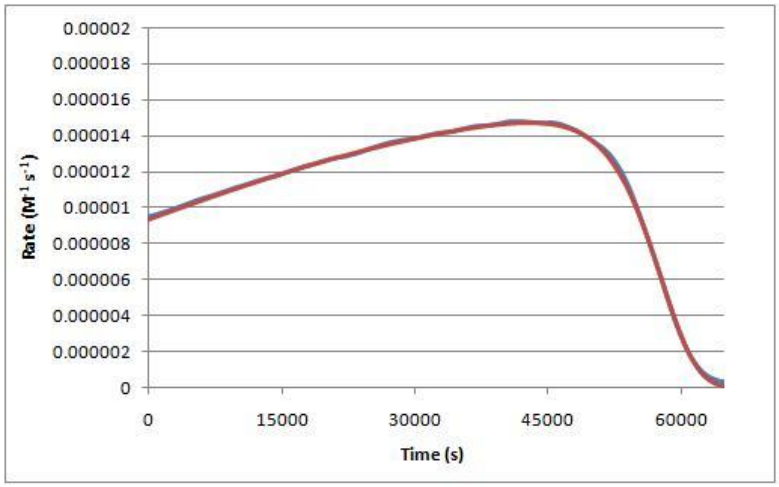

	Model	Guess
ΔG_{cat} =	53296.55	55000
ΔH_1 =	56476.13	70000
$T_{m,1}$ =	295.14	300
ΔH_2 =	412759.69	500000
$T_{m,2}$ =	327.71	325
$\Delta G_{D,1}$ =	97966.87	100000
$\Delta G_{D,2}$ =	112248.86	113000

Experimental = Blue
Model = Red

Model 4

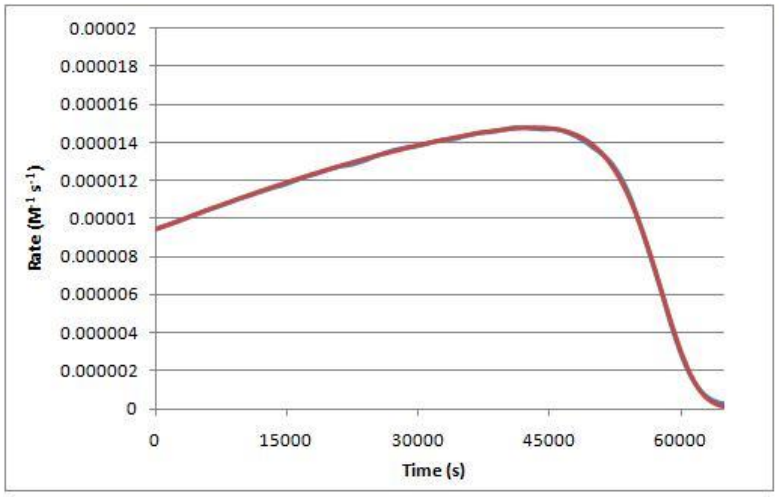

	Model	Guess
ΔG_{cat} =	53201.20	55000
ΔH_1 =	55806.50	70000
$T_{m,1}$ =	294.27	300
ΔH_2 =	412808.29	500000
$T_{m,2}$ =	327.66	325
$\Delta G_{D,1}$ =	97998.82	100000
$\Delta G_{D,2}$ =	113121.43	113000
$\Delta G_{D,3}$ =	120010.01	120000

Experimental = Blue
Model = Red

Model 5

Appendix C.3 Model Fits for 4 K/h Temperature Ramp Experiments

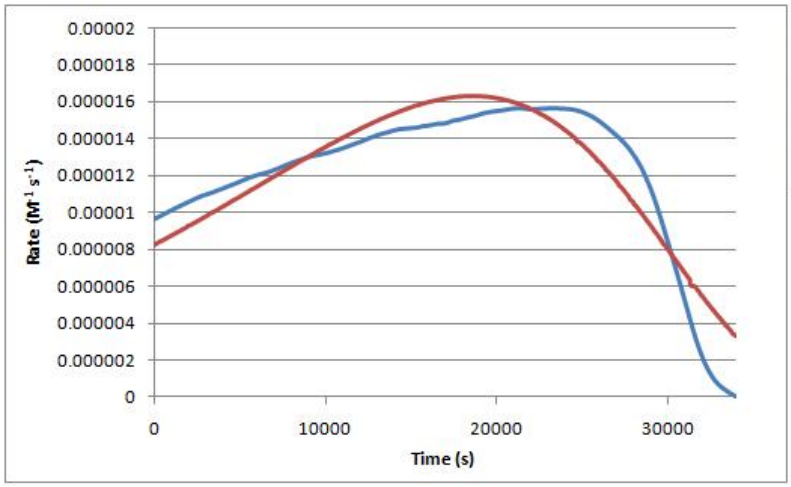

	Model	Guess
ΔG_{cat} =	54528.23682	55000
ΔH_1 =	53139.6811	70000
$T_{m,1}$ =	310.179645	310
$\Delta G_{D,1}$ =	102262.8943	100000

Experimental = Blue
Model = Red

Model 1

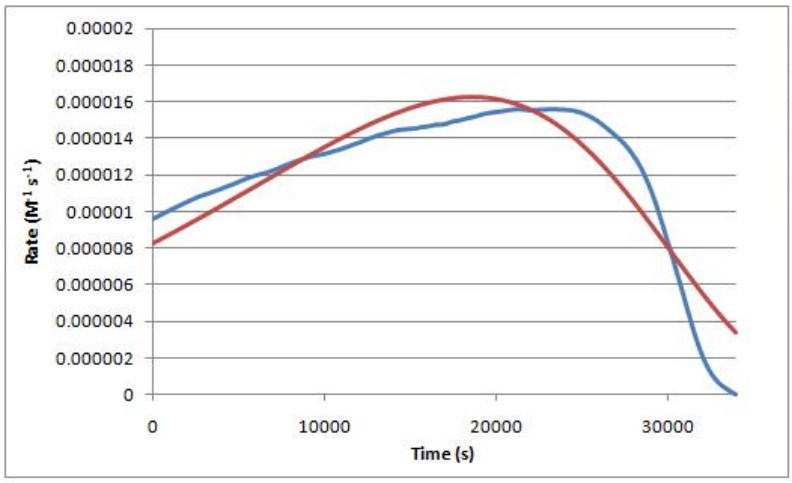

	Model	Guess
ΔG_{cat} =	54502.83598	55000
ΔH_1 =	52318.40957	70000
$T_{m,1}$ =	310.0006779	310
$\Delta G_{D,1}$ =	102316.0253	100000
$\Delta G_{D,2}$ =	110557.9197	120000

Experimental = Blue
Model = Red

Model 2

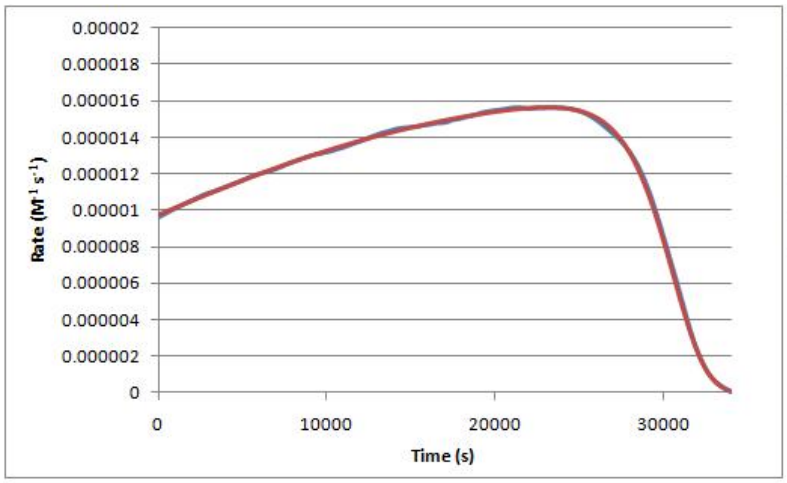

	Model	Guess
ΔG_{cat} =	53413.89193	55000
ΔH_1 =	60914.8519	70000
$T_{m,1}$ =	297.6600529	300
ΔH_2 =	450264.8769	500000
$T_{m,2}$ =	327.9931218	325
$\Delta G_{D,1}$ =	97134.54698	105000

Experimental = Blue
Model = Red

Model 3

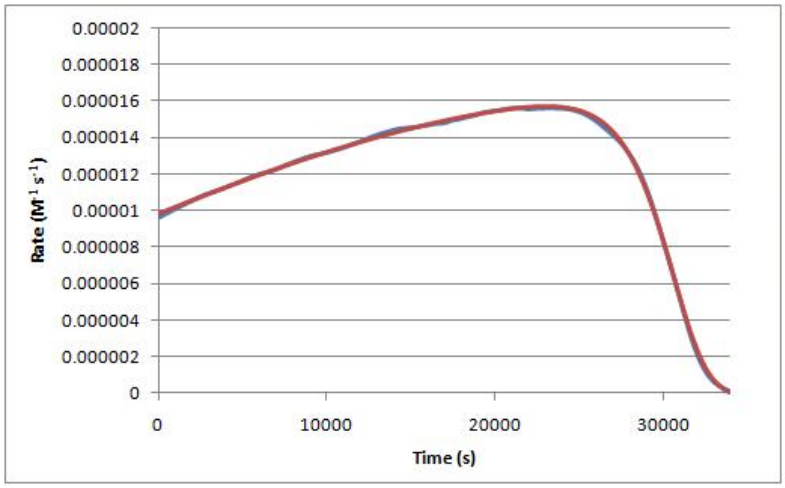

	Model	Guess
ΔG_{cat} =	53105.83952	55000
ΔH_1 =	56480.43138	70000
$T_{m,1}$ =	294.6866162	300
ΔH_2 =	412802.844	500000
$T_{m,2}$ =	328.7694524	325
$\Delta G_{D,1}$ =	96515.36307	100000
$\Delta G_{D,2}$ =	112347.6627	120000

Experimental = Blue
Model = Red

Model 4

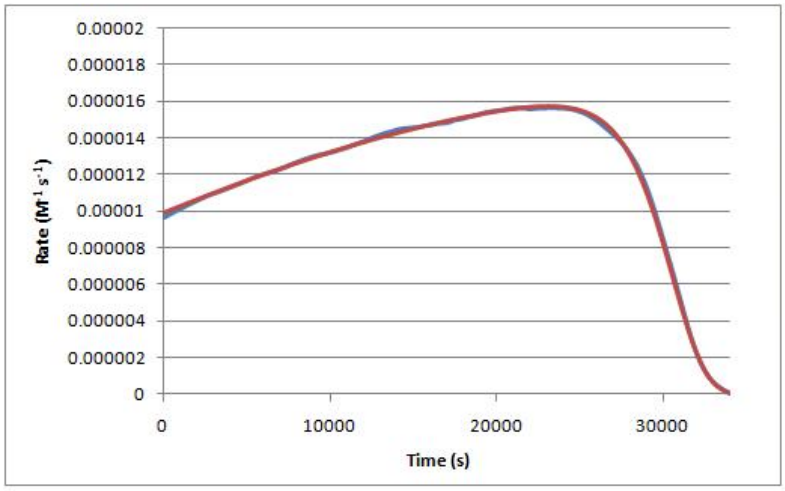

	Model	Guess
ΔG_{cat} =	53024.17898	55000
ΔH_1 =	55964.0443	70000
$T_{m,1}$ =	293.974803	300
ΔH_2 =	412855.8373	500000
$T_{m,2}$ =	328.9035167	325
$\Delta G_{D,1}$ =	96302.095	100000
$\Delta G_{D,2}$ =	113127.4081	115000
$\Delta G_{D,3}$ =	120009.5848	120000

Experimental = Blue
Model = Red

Model 5

Appendix C.4 Model Fits for 8 K/h Temperature Ramp Experiments

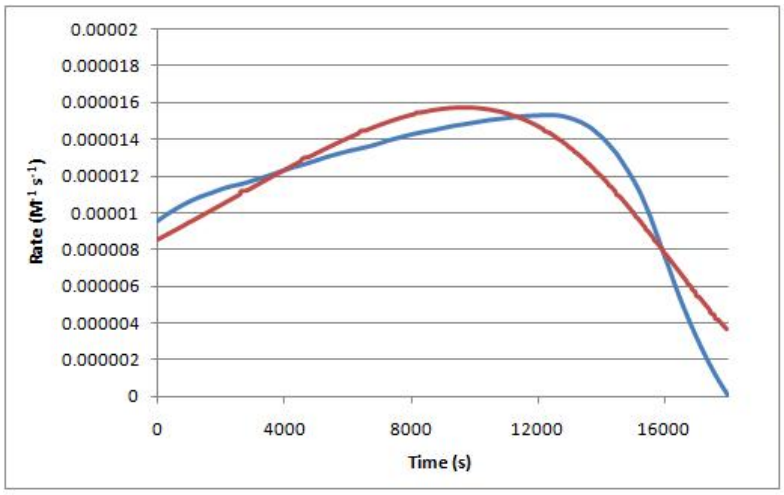

	Model	Guess
ΔG_{cat} =	54037.44391	55000
ΔH_1 =	52564.90454	70000
$T_{m,1}$ =	303.6406902	310
$\Delta G_{D,1}$ =	101643.0869	100000

Experimental = Blue
Model = Red

Model 1

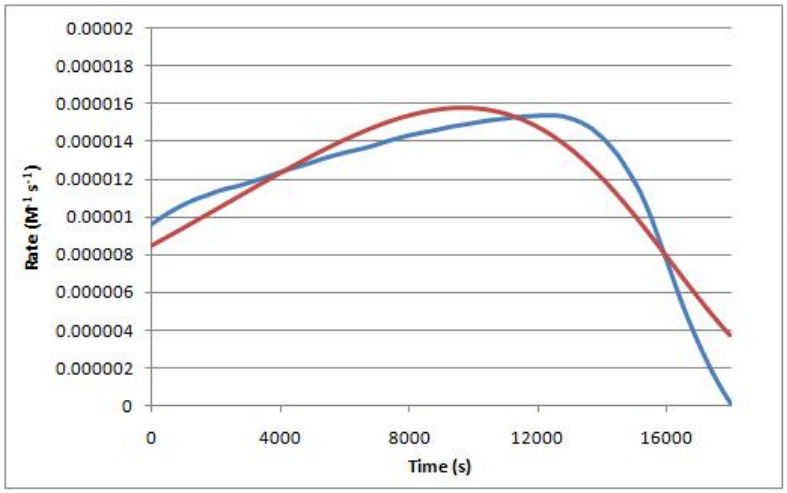

	Model	Guess
ΔG_{cat} =	54095.03345	55000
ΔH_1 =	52589.80147	70000
$T_{m,1}$ =	304.4645391	310
$\Delta G_{D,1}$ =	101787.2909	100000
$\Delta G_{D,2}$ =	105546.1079	120000

Experimental = Blue
Model = Red

Model 2

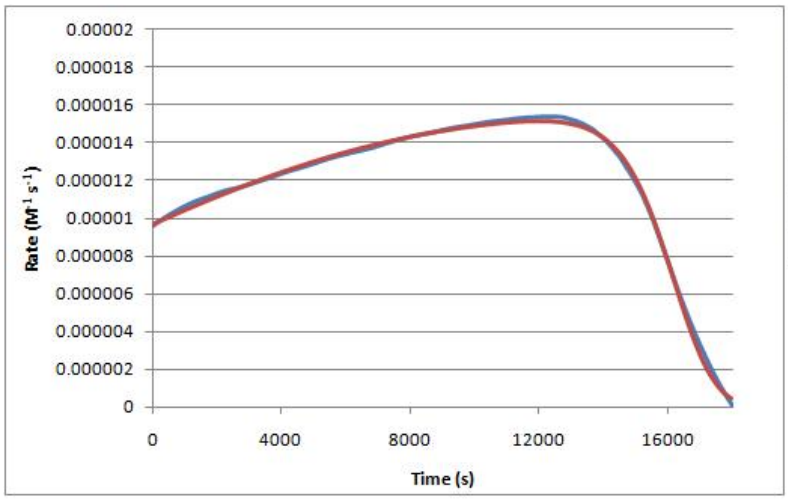

	Model	Guess
ΔG_{cat} =	53235.44532	55000
ΔH_1 =	61029.70605	70000
$T_{m,1}$ =	296.221352	300
ΔH_2 =	450210.0491	500000
$T_{m,2}$ =	328.0954975	325
$\Delta G_{D,1}$ =	98894.43618	105000

Experimental = Blue
Model = Red

Model 3

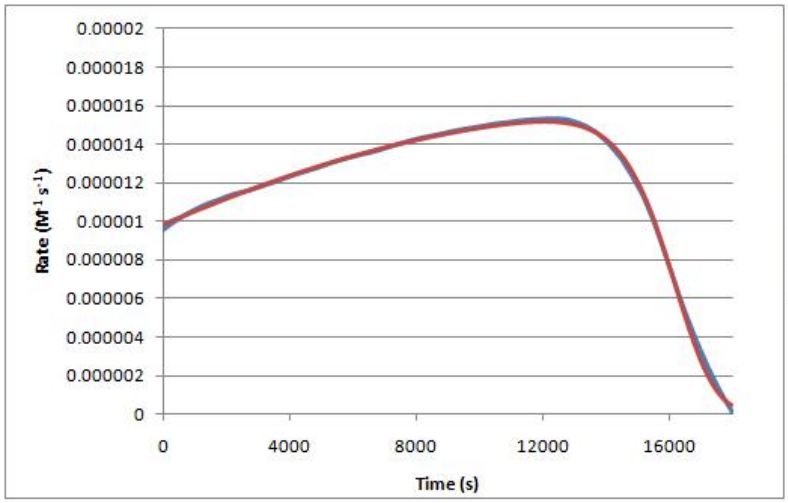

	Model	Guess
ΔG_{cat} =	52828.66521	55000
ΔH_1 =	56525.87254	70000
$T_{m,1}$ =	292.5209006	300
ΔH_2 =	412758.1277	500000
$T_{m,2}$ =	328.6879548	325
$\Delta G_{D,1}$ =	98010.77548	100000
$\Delta G_{D,2}$ =	112240.0486	120000

Experimental = Blue
Model = Red

Model 4

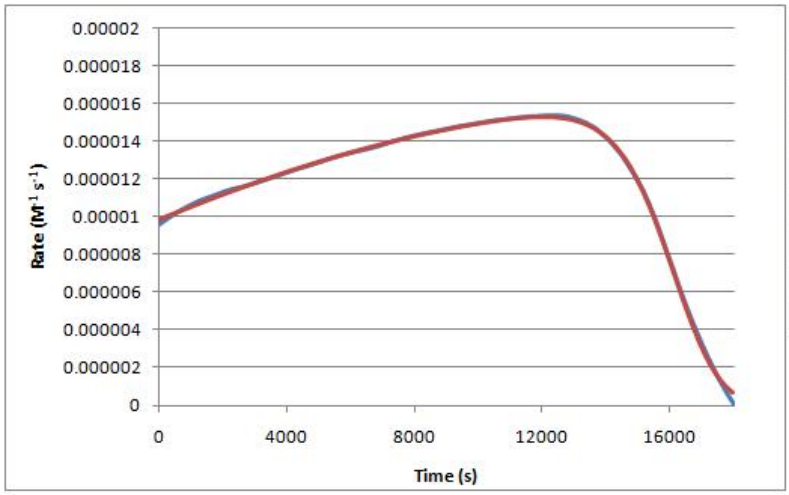

	Model	Guess
ΔG_{cat} =	52749.59921	55000
ΔH_1 =	55492.87083	70000
$T_{m,1}$ =	291.7246827	300
ΔH_2 =	412688.3412	500000
$T_{m,2}$ =	327.8621048	325
$\Delta G_{D,1}$ =	99548.56208	100000
$\Delta G_{D,2}$ =	113038.2637	115000
$\Delta G_{D,3}$ =	120009.9921	120000

Experimental = Blue
Model = Red

Model 5

Appendix C.5 Model Fits for 12 K/h Temperature Ramp Experiments

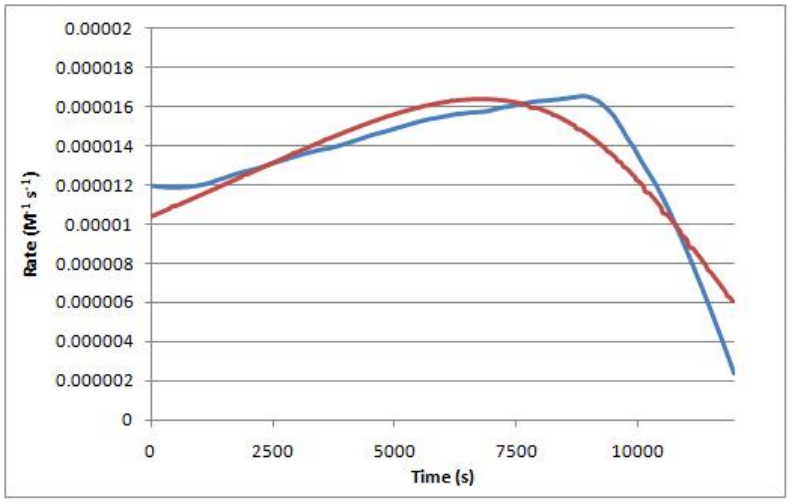

	Model	Guess
ΔG_{cat} =	47652.7748	55000
ΔH_1 =	26211.03842	70000
$T_{m,1}$ =	234.085679	310
$\Delta G_{D,1}$ =	101392.881	100000

Experimental = Blue
Model = Red

Model 1

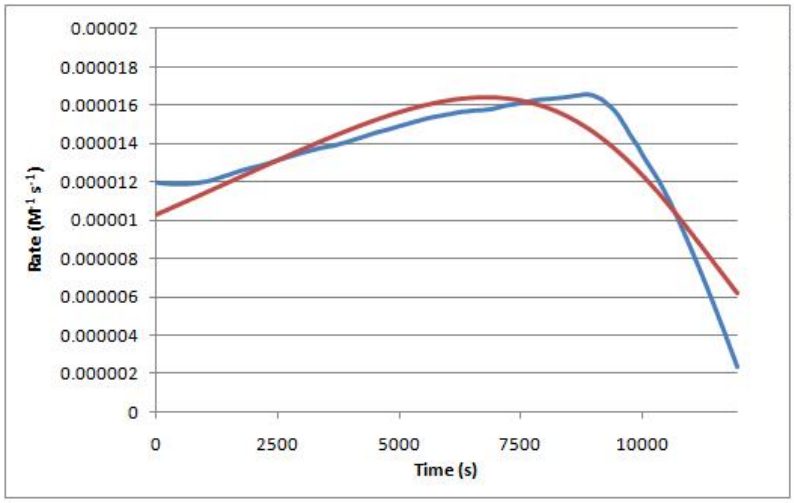

	Model	Guess
ΔG_{cat} =	50603.04829	55000
ΔH_1 =	33021.79251	70000
$T_{m,1}$ =	266.6807489	310
$\Delta G_{D,1}$ =	101363.0593	100000
$\Delta G_{D,2}$ =	116461.4283	120000

Experimental = Blue
Model = Red

Model 2

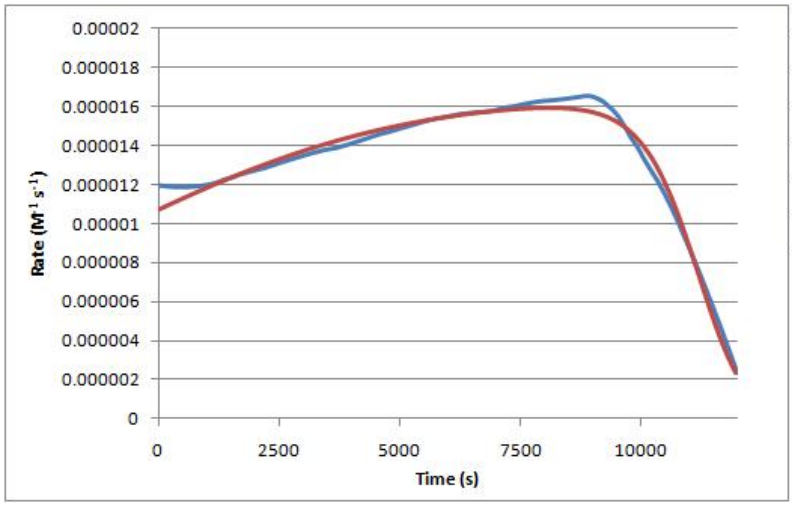

	Model	Guess
ΔG_{cat} =	52792.47949	55000
ΔH_1 =	61035.54036	70000
$T_{m,1}$ =	294.6120146	300
ΔH_2 =	450203.341	500000
$T_{m,2}$ =	328.3317318	325
$\Delta G_{D,1}$ =	99622.27228	105000

Experimental = Blue
Model = Red

Model 3

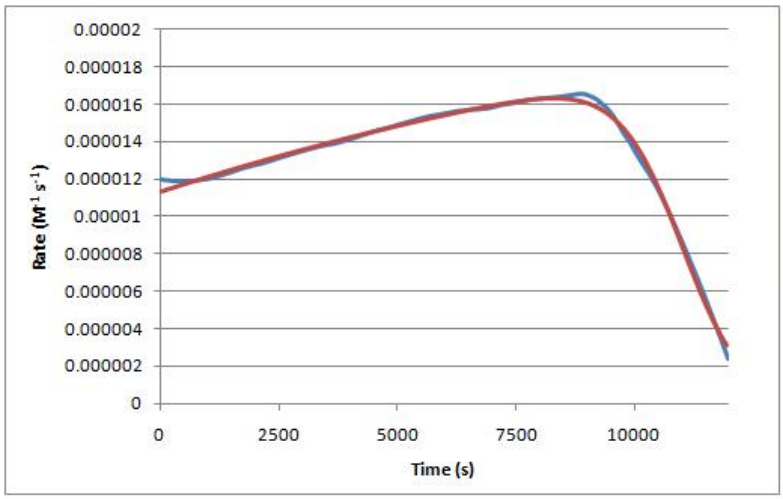

	Model	Guess
ΔG_{cat} =	50828.85396	55000
ΔH_1 =	47970.38272	70000
$T_{m,1}$ =	277.8109181	300
ΔH_2 =	412573.3762	500000
$T_{m,2}$ =	327.2321513	325
$\Delta G_{D,1}$ =	103743.8009	100000
$\Delta G_{D,2}$ =	113581.6996	113000

Experimental = Blue
Model = Red

Model 4

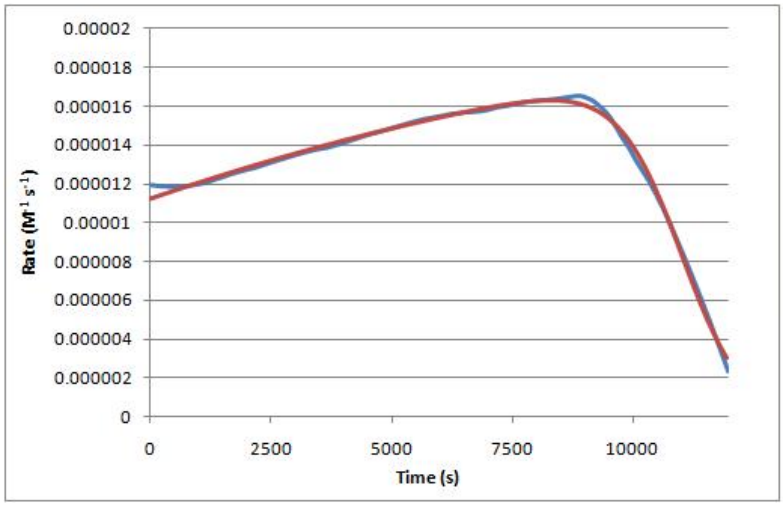

	Model	Guess
ΔG_{cat} =	51120.54305	55000
ΔH_1 =	49044.24086	70000
$T_{m,1}$ =	280.1408235	300
ΔH_2 =	412710.9562	500000
$T_{m,2}$ =	327.2967464	325
$\Delta G_{D,1}$ =	103245.2096	100000
$\Delta G_{D,2}$ =	113971.4701	115000
$\Delta G_{D,3}$ =	120019.5313	120000

Experimental = Blue
Model = Red

Model 5

Appendix C.6 Model Fits for 16 K/h Temperature Ramp Experiments

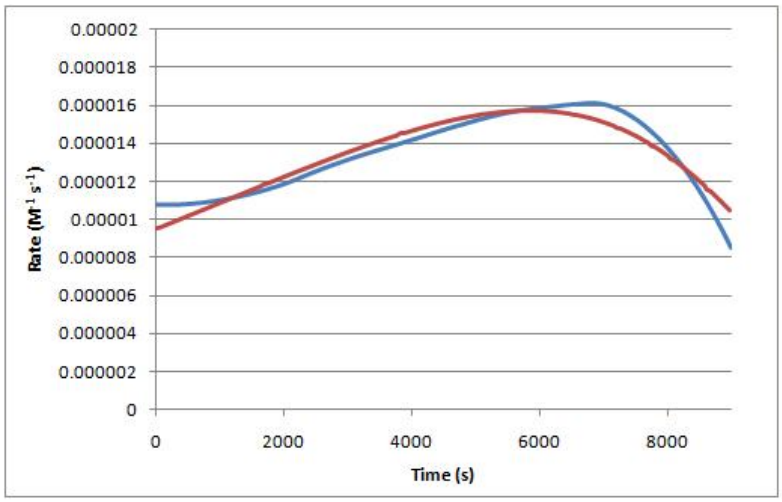

	Model	Guess
ΔG_{cat} =	52003.66251	55000
ΔH_1 =	41616.36505	70000
$T_{m,1}$ =	282.432615	310
$\Delta G_{D,1}$ =	101915.936	100000

Experimental = Blue
Model = Red

Model 1

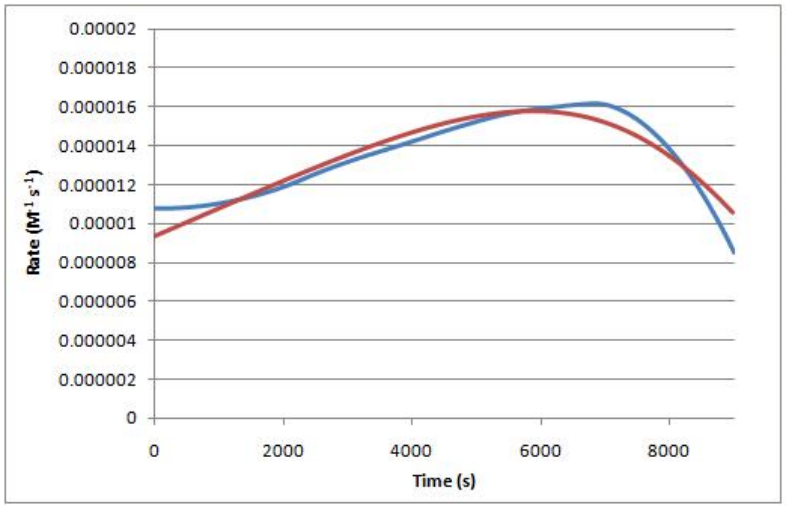

	Model	Guess
ΔG_{cat} =	52323.2707	55000
ΔH_1 =	43386.80396	70000
$T_{m,1}$ =	285.8048413	310
$\Delta G_{D,1}$ =	101918.7606	100000
$\Delta G_{D,2}$ =	116398.9245	120000

Experimental = Blue
Model = Red

Model 2

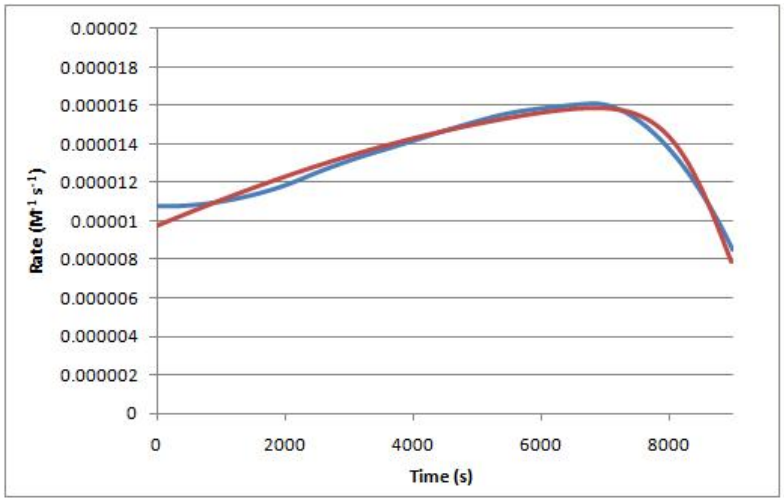

	Model	Guess
ΔG_{cat} =	52742.27569	55000
ΔH_1 =	55789.18239	70000
$T_{m,1}$ =	292.0763893	300
ΔH_2 =	449836.2237	500000
$T_{m,2}$ =	328.4008369	325
$\Delta G_{D,1}$ =	103786.1878	105000

Experimental = Blue
Model = Red

Model 3

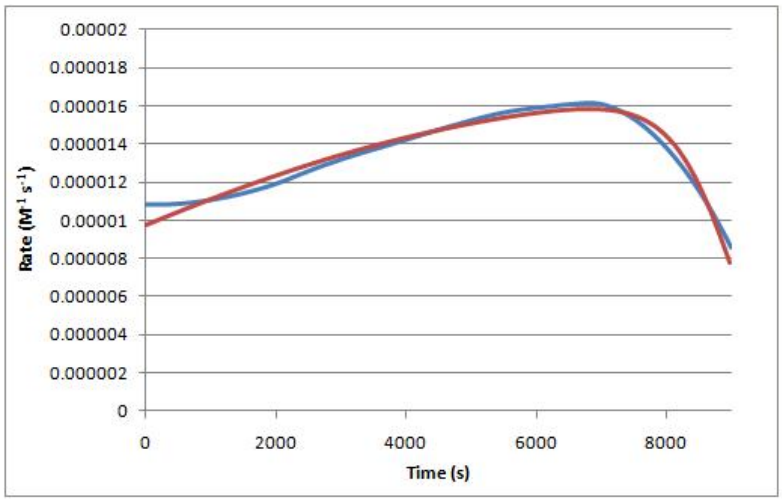

	Model	Guess
ΔG_{cat} =	52825.26144	55000
ΔH_1 =	56405.26231	70000
$T_{m,1}$ =	292.8186033	300
ΔH_2 =	412741.3695	500000
$T_{m,2}$ =	329.6411821	325
$\Delta G_{D,1}$ =	98311.77829	100000
$\Delta G_{D,2}$ =	112221.8921	113000

Experimental = Blue
Model = Red

Model 4

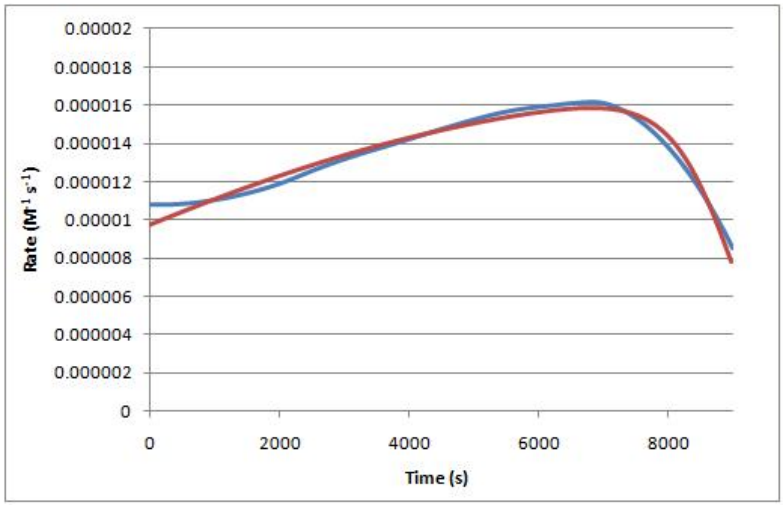

	Model	Guess
ΔG_{cat} =	52722.85277	55000
ΔH_1 =	55470.68449	70000
$T_{m,1}$ =	291.8778522	300
ΔH_2 =	412729.7411	500000
$T_{m,2}$ =	329.2290762	325
$\Delta G_{D,1}$ =	99423.15871	100000
$\Delta G_{D,2}$ =	113035.3159	115000
$\Delta G_{D,3}$ =	120009.6249	120000

Experimental = Blue
Model = Red

Model 5

VITA

THOMAS A. ROGERS

Thomas Rogers was born in Dover, NH in 1981. He graduated from public high school in Farmington, NH, as valedictorian, in 1999, and went on to earn a B.S. in Chemical Engineering, *cum laude*, from Worcester Polytechnic Institute in Worcester, MA in 2003. After being employed for two years as a process engineer at Tech-Etch, Inc. in Plymouth, MA, he came to Georgia Tech in the fall semester of 2005 to pursue his doctorate in Chemical and Biomolecular Engineering. Tom enjoys reading, traveling, skiing, and playing golf when he is not immersed in his research.